Bulletin of Geosciences, Vol. 79, No. 1, 1–40, 2004

Emerald mineralization in the Kafubu area, Zambia

Antonín V. Seifert [1] – Vladimír Žáček [1] – Stanislav Vrána [1] – Vratislav Pecina [1] – Jiří Zachariáš [2] – J. C. (Hanco) Zwaan [3]

[1] Czech Geological Survey, Klárov 3, 118 21 Praha 1, Czech Republic. E-mail: seifert@cgu.cz, zacek@cgu.cz,
[2] Charles University, Faculty of Science, Albertov 6, 128 43 Praha 2, Czech Republic. E-mail: zachar@natur.cuni.cz
[3] National Museum of Natural History Naturalis, 2300 RA Leiden, The Netherlands. E-mail: ZwaanJ@naturalis.nnm.nl

Abstract. This study provides the first quantitative geochemical, petrological, and mineralogical data on major rock types and minerals in the Kafubu area. Highly magnesian talc-chlorite ± actinolite ± magnetite metabasites hosting emerald mineralization are identified as metamorphosed komatiites. These rocks contain 3000–4000 ppm Cr, and provided the amount of this element necessary for the crystallization of emeralds. Associated amphibolites of andesitic and basaltic-andesitic composition are low in chromium. The estimated equilibration temperatures during regional metamorphism, using amphibole-plagioclase thermometry on several amphibolite samples, gave a narrow interval of 590–630 °C, assuming a pressure of 400–600 MPa. This metamorphic event pre-dates the emerald mineralization and the emplacement of pegmatite dikes. Emerald-bearing phlogopite schists are confined to the contacts of quartz-tourmaline veins and quartz-feldspar pegmatites with magnesian metabasites. The quartz-tourmaline veins and pegmatite dikes are genetically related to a hidden fertile granite pluton. The formation of phlogopite schists from metabasite was associated with the introduction of ca. 8–10 wt.% K_2O, 3–4 wt.% fluorine, 0.12–0.74 wt.% Li_2O, 1700–2900 ppm Rb, and spikes of beryllium. Quartz-feldspar pegmatites of the Kafubu area, often evolved as albite-dominated types, belong to the rare-element pegmatites of the LCT family (i.e., Li-Cs-Ta), with common beryllium enrichment. The identification of several Nb-Ta minerals (manganocolumbite-manganotantalite, niobian rutile, tantalian rutile, and plumbomicrolite) underlines the geochemical typology of pegmatites. High activities of fluorine (up to 4 wt.% F in phlogopite schists) and boron (in exceptionally abundant tourmaline) probably functioned as solidus/liquidus depressants during evolution of mineralizing fluids and their separation from the parent granite. These fluids deposited quartz-tourmaline veins, and altered the adjacent metabasites into emerald-bearing phlogopite schists. Thus, in the case of the Kafubu emerald area, the classical explanation for the origin of emeralds in schist-related deposits still stands. Data on pegmatite occurrences in active mines and exploration pits, and their extrapolation into the surrounding area, point to the existence of a single, major Kafubu pegmatite field that overlaps the extensive horizons of Cr-rich metabasite. $^{40}K/^{40}Ar$ dating of muscovite from a muscovite pegmatite and a quartz-tourmaline-muscovite vein accompanying the Be-mineralization records closure of the system within the interval of 452–447 Ma.

Emerald samples from the Kafubu area range in intensity of colour from light to dark green. The colour is unevenly distributed and often exhibits zoning. The emeralds have many inclusions and are moderately fractured. Electron microprobe analyses of Kafubu emeralds (n = 97) show the contents of 0.17–0.59 wt.% Cr_2O_3, 0.69–1.21 wt.% FeO^{tot}, 1.66–2.54 wt.% MgO, and 1.72–1.98 wt.% Na_2O, besides the major components. The emeralds exhibit a distinct dichroism, are inert to long- and short-wave ultraviolet radiation, and commonly show green under the Chelsea filter. UV-VIS spectra show peaks of both divalent and trivalent iron, besides chromium. Niobian rutile is newly identified as an inclusion in emeralds from the Mbuwa mine. For the first time, data on fluid inclusions in beryl/emerald, tourmaline and quartz are provided for these deposits. Three types of fluids were recognized: aqueous-only, aqueous-carbonic, and carbonic. Ambiguous primary inclusions were identified in some beryl/emerald crystals, scarce primary inclusions in tourmaline, and pseudosecondary inclusions in quartz. Several generations of secondary inclusions are common in all minerals considered here. The highest homogenization, i.e. minimum trapping conditions at 400–450 MPa and 360–390 °C, were recorded in the quartz of several samples. The majority of the quartz-tourmaline ± emerald veins was deposited at lower pressures around 200–400 MPa.

Key words: emerald, beryl, quartz-tourmaline veins, phlogopite schists, rare-element pegmatites, komatiite, Muva Supergroup, Kafubu area, Zambia

Introduction

In the past two decades Zambia has become a significant gem-producing country. The Kafubu area (Fig. 1) has supplied up to 20 per cent of the world's emerald production, and is believed to be second in value only to Colombia. Though many of the good-quality stones are taken from the country illegally, the total annual production is estimated to be worth between 100 and 200 million USD. The Kafubu area represents important economic potential for Zambia.

The fieldwork program in 2001 entailed research of the geological, structural, geochemical, and metamorphic conditions, as well as mineralogical features exposed in all significant open mines and pits. The major objectives were the study of the geological setting and the gathering of all key information and data regarding the origin and distribution of the emerald mineralization. During the fieldwork 36 of the main mines and open pits were visited and studied. All



Figure 1. Location of the Kafubu emerald area in Zambia.

field data, including the interpretation of a magnetic susceptibility survey, structural data on the quartz-tourmaline veins and pegmatites, and the exact GPS positioning of documented points, have been recorded on digitalized topographic map sheets at 1 : 50,000 and 1 : 25,000 scale. Altogether 146 rock and mineral samples, and 39 samples for the determination of heavy minerals in rock samples were studied. The results of the analyses of these samples and the interpretation of this data constitute the main parts of this paper.

The topographic materials used include map Sheet 1328 A1 at 1 : 50,000 scale, a geological map of the Luanshya area at 1 : 100,000 scale, Report no. 46 (Hickman 1973), an aeromagnetic survey map of Sheet 1328 A1 at 1 : 50,000 scale, and a Mining Rights Plot map issued by the Mining Department of the Ministry of Mines and Minerals Development in Zambia.

For many years the Kafubu area and the Ndola Rural Restricted area have been subdivided into a large number of prospecting plots as a result of the enormous interest in mineral exploration. This was done without the benefit of a thorough geological evaluation, the consideration of favourable indicators, or modern prospecting and exploration techniques. The main production is currently limited to the largest mechanized mines of Kagem, Kamakanga, and Grizzly.

Topography, drainage, and transportation

The present study area of some 200 square km is bound by latitudes 13° 02' and 13° 11' south and longitudes 28° 03' and 28° 11' east, as a part of Sheet 1328 A1 at 1 : 50,000 scale. The area is situated south of Zambian Copperbelt, 45 km southwest of Kitwe.

The Kafubu River, a right tributary of the Kafue River, drains the area together with small Pirala and Mitondo perennial streams. Except for the quartzite ridges in the south, there are no prominent topographic features and the whole area is typically flat. The average altitude is around 1200 m. The residual plateau clayey soils are yellow brown or red-brownish over much of the surface area, and support relatively thick Brachystegia-Isoberlinia types of woodland.

The area can be reached by 15 km of paved road from Kitwe to Kalulushi, and then by 30 km of poorly maintained gravel road. The accessibility of the main localities within the mining area is secured by many tracks which are passable throughout the year.

The population, composed mostly of miners and their families, is sparse. The small temporary settlements and camps are concentrated at some distance to individual mines.

History of mining

The first discovery of beryl mineralization in the Kafubu area was made by the Rhodesia Congo Border Concession Co. at the Miku locality in 1928. The very first stones were not found to be interesting as good-quality gems, but small exploration works were continued by the Rhokana Co. and the Rio Tinto Mineral Search of Africa Co. during the 1940s and '50s. In 1966 the claim was passed to Miku Enterprises Ltd., and in 1971 the rights to the Miku area were taken over by the Mindeco Limited, a government-owned company.

The whole Luanshya area (Degree Sheet 1328, NW Quarter) was mapped, and the Miku deposit verified by the Geological Survey Department (Hickman 1972, 1973). Since the 1970s, the Kafubu area has become a significant producer of good-quality emeralds with high economic potential. Because of new discoveries (such as at Kamakanga, Pirala, Mitondo, Fwaya-Fwaya, Kabashila, Dabwisa, Libwente, and Fibolele) and extensive illegal mining, the area has been declared by the government as a restricted zone.

During the 1980s a new government-controlled agency, the Reserved Minerals Corporation, took over the prospecting rights for the major deposits and their surroundings. Also during this time, Kagem Mining Ltd., a company of which 55 % is owned by the government's Reserved Mineral Corporation, was assigned to conduct exploration and mining in the Kafubu area on behalf of the state and in cooperation with other private companies.

At present, the mechanized mining activities for emeralds are mostly concentrated in the Kagem Mining Ltd., Kamakanga Corp., and Grizzly plots.

Opinions on the schist-hosted emerald occurrences in the literature

The mineralization in the Kafubu area is considered to be a typical example of schist-hosted emerald deposits, in which emeralds occur predominantly in phlogopitite or other types of schists (Sliwa and Nguluwe 1984, Milisenda et al. 1999).

The schist-hosted emerald deposits have been interpreted as the result of interactions between intruding granitic pegmatites and/or their accompanying fluids and pre-existing mafic or ultramafic rocks (Fersman 1929 and Lams et al. 1996), or the invasion of fluids related to fertile granite or pegmatite, producing metasomatism in ultramafic/mafic rocks (Barton and Young 2002). The emeralds then formed as a type of contact metamorphism or metasomatism at the borders of pegmatites or hydrothermal quartz ± feldspar ± mica veins and the surrounding (phlogopitized) mafic or ultramafic rocks. The fluids would provide the beryllium necessary to form beryl, while the ultramafic or mafic rocks supplied the chromium necessary for the green color of the emeralds.

Contrary to previous opinions, Morteani and Grundmann (1977), Grundmann and Morteani (1982, 1987, and 1989), and Nwe and Grundmann (1990) state that the Habachtal (Austria) and Leydsdorp (South Africa) deposits of schist-hosted emeralds were formed by the syn- to post-tectonic growth of beryl in metasomatic zones ("blackwall zones") during regional metamorphism. In

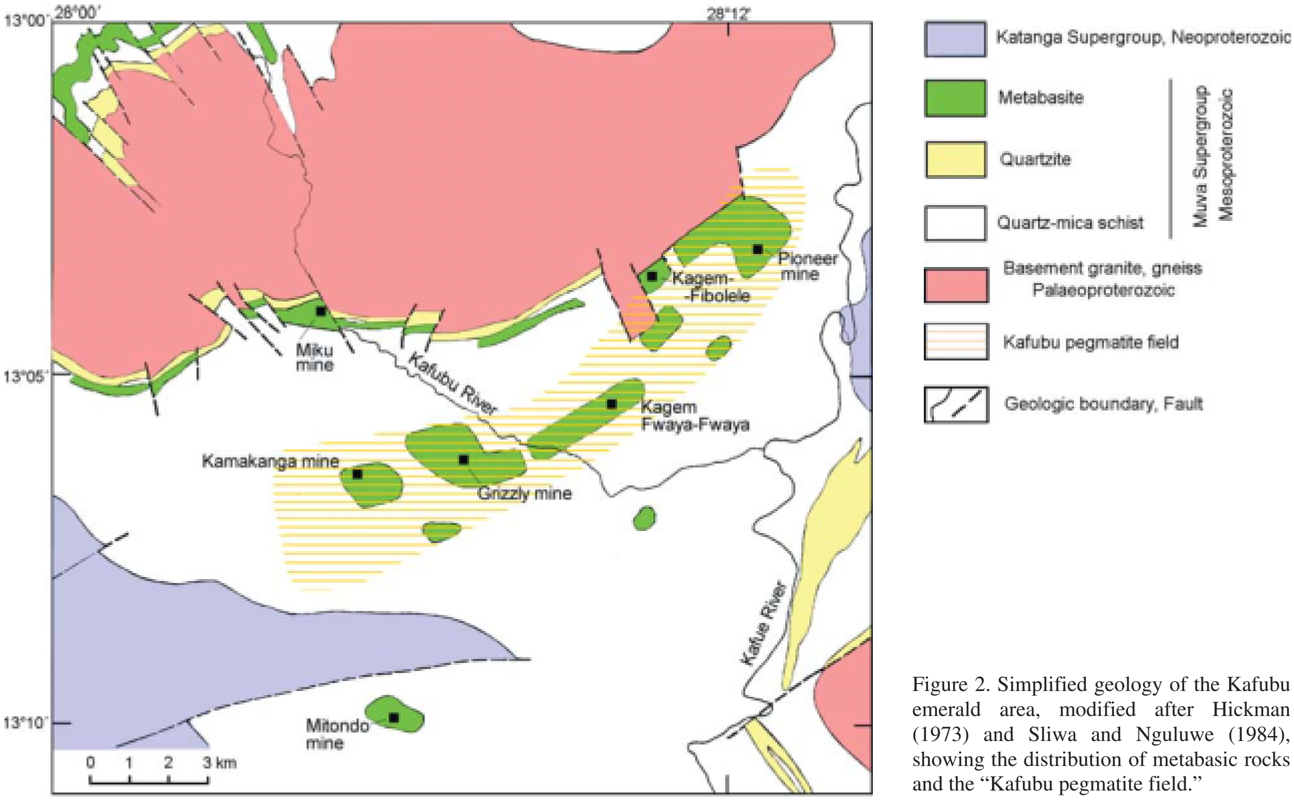


Figure 2. Simplified geology of the Kafubu emerald area, modified after Hickman (1973) and Sliwa and Nguluwe (1984), showing the distribution of metabasic rocks and the "Kafubu pegmatite field."

these zones reactions either occur at the contact of pre-existing beryl- and phenakite-bearing pegmatites (Leydsdorp), or else biotite, chlorite, or talc replace Be-rich Al-silicates such as muscovite in metasedimentary schist next to serpentinite. These reactions cause a release of the excess Be in muscovite to form beryllium-bearing phases (Habachtal). The original Be enrichment in muscovite schist is ascribed to submarine volcanic exhalation.

Zwaan and Touret (2000) have confirmed the syntectonic growth of emerald during regional metamorphism at Sandawana, Zimbabwe, thus advocating a multi-stage process leading to emerald growth in strongly deformed and metasomatized pegmatite/greenschist contact zones, as opposed to single-stage contact metamorphism at the border of intrusive pegmatite and ultramafic rocks. These examples show that the schist-hosted emerald deposits are not genetically uniform and that each deposit should be considered on an individual basis.

Milisenda et al. (1999) suggested for the Kafubu area a possible role for an evaporitic environment, mainly with reference to stratiform and finely banded quartz-tourmaline rocks (see also Slack et al. 1984; Plimer 1986; Bone 1988). They have also suggested that phlogopite rocks carrying beryl mineralization represent metamorphosed salt clays.

Geological setting

The oldest metamorphic rocks of the Kafubu area, comprising mainly quartz-feldspathic gneiss and granite gneiss, are exposed in structural elevations of basement domes (Hickman 1973). These Palaeoproterozoic rocks underwent polyphase deformation and high-grade metamorphism of Ubendian age (ca. 2000–1800 Ma) (Cahen and Snelling 1966; Cahen et al. 1970a, b). The Kafue anticlinorium and its marginal basement domes are rimmed by extensive outcrops of younger metasediments along its edges and in transversal structural depressions. The Muva Supergroup (Mesoproterozoic, Daly and Unrug 1983) overlays basement rocks with a distinct angular unconformity, marked by a regional ridge of basal quartzites (Fig. 2). These two units were jointly folded, which resulted in the sub-parallel trend of lithological boundaries. The Muva Supergroup comprises medium to coarse-grained sugary and friable metaquartzites showing banding of probable tectonic origin, fine-grained quartz-mica schists, and talc-chlorite-actinolite ± magnetite schists (Hickman 1973, Sliwa and Nguluwe 1984). Magnesian metabasic schists that host emerald mineralization have been interpreted as being derived from ultrabasic rocks (Hickman 1973).

The youngest stratigraphic unit, the Katanga Supergroup, is preserved in structural depressions in the northeast and southwest (Fig. 2). It consists of pebbly conglomerates, arkoses, quartzites, argillites, dolomites, quartz-carbonate rocks and carbonaceous shales, locally intruded by gabbro or meta-gabbro. The Muva and Katanga rocks appear to be conformable, though in places there is marked discordance between them, indicating that the Muva was deformed prior to the Katanga deposition (Hickman 1973).

According to Tembo et al. (2000), the rocks of the Kafubu area have been deformed by three orogenic events: the Ubendian, Irumide and Lufilian (Pan-African). The first event, which is the oldest (ca. 1.8 Ma), only affected

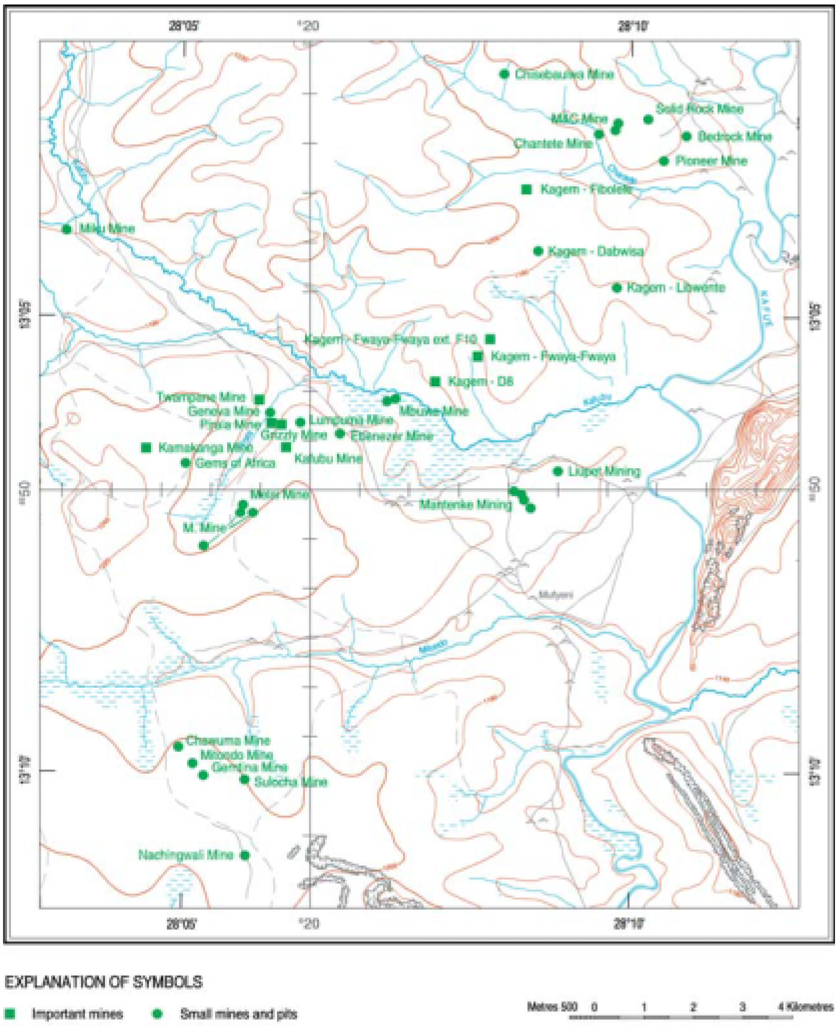


Figure 3. Location of mines and pits in the Kafubu area, based on GPS data.

The foliations measured in mines and pits show a predominantly shallow to moderate dip and a NE-SW to E-W trend which changes to a SE-NW trend in the southern part of the Kafubu area. Planar fabric exhibits a strong variation in strike at locations with flat-lying foliation. Fold axes trend E-W. In some areas, a strong cleavage obliterates older planar textures, e.g. in the old Kamakanga pit. Pegmatite dikes and steep quartz-tourmaline veins trend mainly N-S and NW-SE, while flat-lying quartz-tourmaline veins show variations in strike. All structural data documented in the field are presented in the final report (Seifert et al. 2002).

rocks of the basement complex and is poorly preserved due to overprinting by later events. The Irumide orogeny affected rocks of the basement complex and the Muva Supergroup. According to Hickman (1972, 1973), the Lufilian orogeny is represented by four deformation phases, which obliterated earlier structures and are responsible for the present structural configuration of the area. The D_3 event produced isoclinal to open folds on the northwest axes, and is responsible for the faulting accompanied by pegmatite intrusions in the area. The last deformation phase, D_4, produced NE-SW trending folds (Hickman 1973, Tembo et al. 2000).

Bedrock exposure in the Kafubu area is very scarce, and the total exposure resulting from the recent extensive mining represents about one percent of the entire area of potential emerald mineralization. Previous geologic mapping (Hickman 1973) has shown the main features of the Kafubu area, while Milisenda et al. (1999) have published a geologic sketch map with an idealized cross section, and Tembo et al. (2000) have studied the structural record in numerous mines, yet the documented data are not sufficient for the compilation of a detailed geologic map of the area.

Geochemistry, geology, and petrology of the main rock types

Whole-rock analyses

The major element analysis of whole-rock samples was performed by wet analysis in the laboratory of the Czech Geological Survey, Prague (chief chemist H. Vítková). The analytical uncertainties for oxide abundances similar to those of amphibolites (Table 1a) correspond to 0.30–0.42 % for CaO, MgO, SiO_2 and LOI; 0.07–0.20 % for TiO_2, Al_2O_3, Fe_2O_3, FeO; and 0.01–0.05 for MnO, Na_2O, K_2O, P_2O_5, CO_2, and F. Minor and trace element analyses were performed by X-ray fluorescence analysis (V, Cr, Ni, Cu, Zn, As, Rb, Sr, Y, Zr, Nb, Mo, Sn, Pb, U). The XRF analytical uncertainties are 1 % for abundances near 1000 ppm, 4 % around 100 ppm, and 10 % near 10–50 ppm. Rare earth elements were determined by the ICP-OES methods. Beryllium and Li were determined by optical absorption analysis. Platinum-group elements were analyzed in several samples using the ICP-MS analyser at the Institute of Geochemistry and Mineralogy, Charles University, Prague (analyst M. Mihaljevič). In all cases, aliquots from the same homogenized sample were used for various analyses. Totals significantly lower than 100 wt.%, reported for several samples, are due in particular to the absence of boron determination. Tourmalinite samples KF2 and LU1, containing about 95 vol.% tourmaline, should contain nearly 10 wt.% B_2O_3. Aside from this, there are several samples with between 10 to 40 vol.% tourmaline. Several minor elements, including Cr, Ni, Rb, Li, and sometimes also Be, attain rather high values which are not included in wet analysis totals.

The locations of the mines and pits, referred to in the text by their locality names, are shown in Fig. 3.

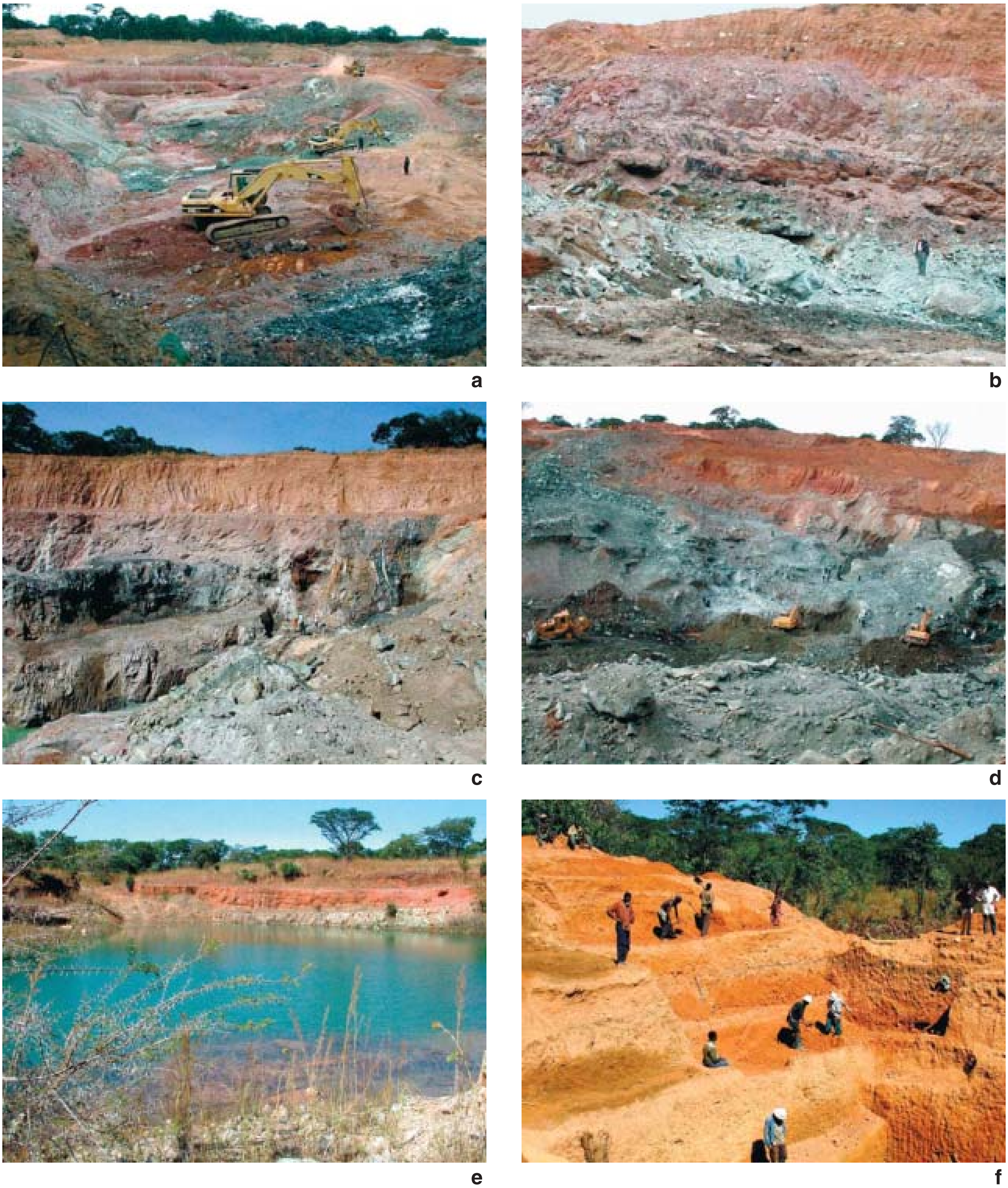


Figure 4. Selected operational and abandoned emerald mines in the Kafubu area (June 2001): a – Excavating operations in the Kafubu mine, a new open pit of the Kamakanga Co. Weathered muscovite-biotite schist (brown), underlying metabasite (grey-green) and quartz-tourmaline vein (black with white spots). b – Kafubu mine, detail of the wall with metabasite layer (grey with greenish tint) overlain by biotite-muscovite schist (weathered, red-brown). Flat-lying layer of banded quartz-tourmaline rock approximately follows the contact between the metabasite and the schist. c – Fibolele mine, Kagem Co. Emerald-bearing phlogopitite zone occurs at the contacts with several steep and flat-lying quartz-tourmaline veins. d – Grizzly mine, ca. 60 m deep, currently the deepest active mine in the Kafubu area, with good emerald production. The mining follows the contacts of a ca. 4 m wide, steep quartz-tourmaline vein with abundant offshoots. The colour contrast between the lateritized zone and the fresh metabasite is apparent. e – Miku mine, the oldest mine in the Kafubu area, abandoned and flooded. f – A new, small excavation in laterite close to the former Miku mine. The pit reached a depth of about 12 m in June 2001. Photos by V. Žáček.

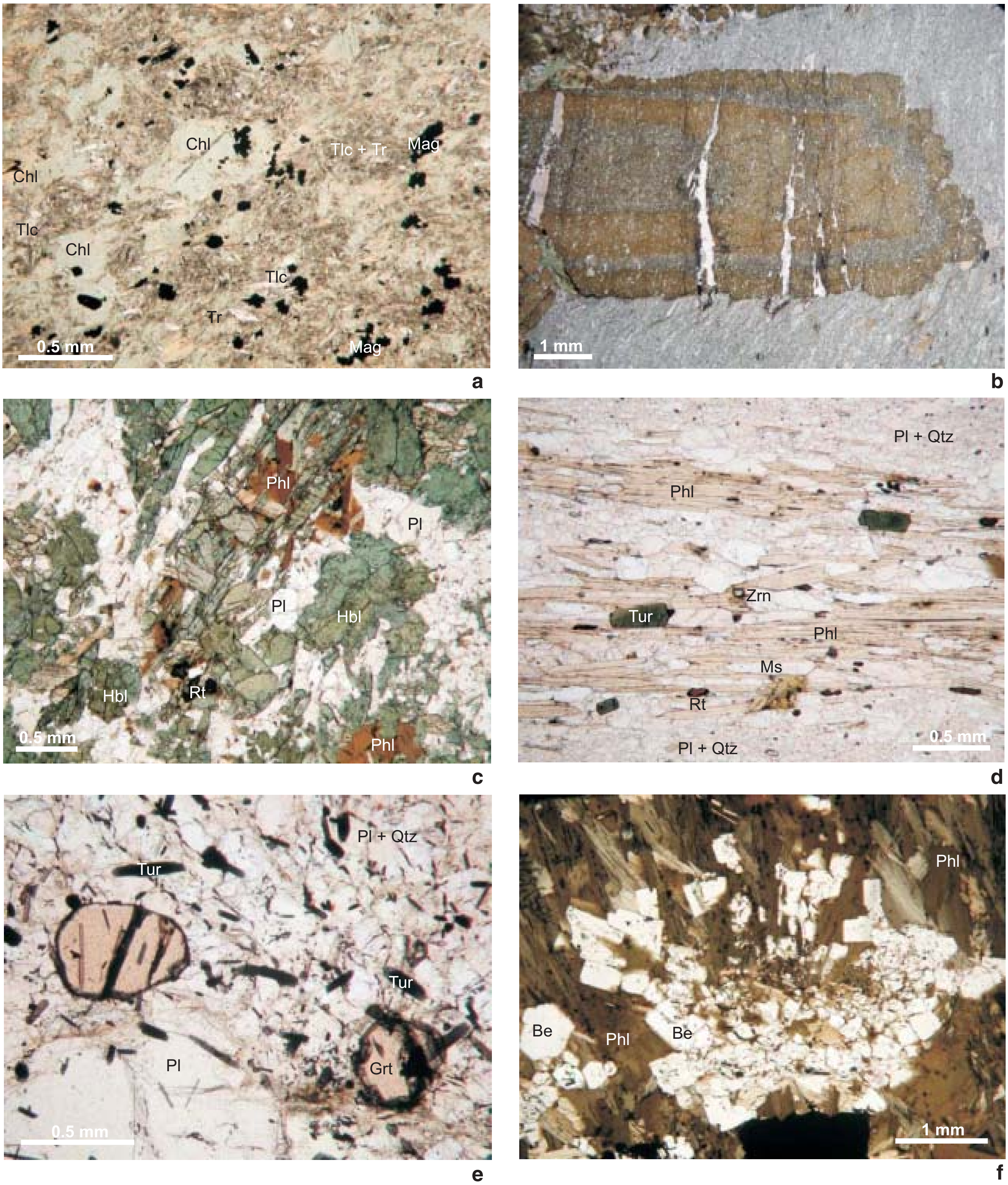


Figure 5. Photomicrographs of selected rock types from the Kafubu area: a – Metabasite from the Fwaya-Fwaya mine (sample FF4). The rock is composed of pleochroic chlorite, minor talc, tremolite, dolomite, and abundant Cr-magnetite. b – Metabasite with large tourmaline crystal from the Melai mine (sample ME4). Late-syntectonic crystals of tourmaline in fine-grained aggregate of talc, actinolite, and chlorite. Minor phlogopite and coarser green retrograde chlorite also occur. c – Amphibolite from the Grizzly mine (sample GR6). The rock is of uniform mineral assemblage (hornblende + quartz + plagioclase + rutile), and is partly phlogopitized. d – Phlogopite–muscovite schist from the Fwaya-Fwaya mine (sample FF3), composed of quartz, albite, phlogopite, sodic muscovite, and minor to accessory chlorite, tourmaline, rutile, and zircon. e – Pegmatite with abundant prismatic to acicular tourmaline (schorl) and spessartite-rich garnet from the Fwaya-Fwaya mine (sample FF2). Note that tourmaline is included both in quartz-albite matrix and in garnet. f – Euhedral crystals of beryl (emerald) in phlogopite rock from the Kafubu mine (sample KF7a). Photos by V. Žáček.

Metamorphosed basic rocks

The metamorphosed basic rocks occupy a stratiform position in a lower-middle part of the local Muva sequence. Since emerald mineralization is generally confined to the magnesium- and chromium-rich members of the metabasic sequence, these rocks are exposed in all productive mines and many exploration pits (Fig. 4). The folded and faulted basic rocks occur in a tectonically modified form, and a complete profile from footwall metasedimentary rocks to overlying quartz-muscovite-phlogopite schist was not observed in a continuous exposure. The integration of data from various mines and previous surface magnetic profiling (Lombe 1999–2000) indicates that the whole metabasic unit is around 20–140 m thick, with the probable occurrence of local tectonic repetitions.

Several major rock types constitute the metabasic unit:

1. Metabasic rocks: talc-chlorite ± actinolite ± magnetite rock/schist of ultramafic composition (Fig. 5a).
2. Amphibolite: corresponding in composition to andesite or basaltic andesite (Fig. 5c).
3. Actinolite/amphibole-rich metabasic rocks: the compositions of this group are transitional between types 1 and 2.

It is often difficult to identify individual types of metamorphosed basic rocks in the field. Our sampling indicates that amphibolites comprise less than 10 % of the volume of the basic rocks.

1. Metabasic rocks

Talc-chlorite ± actinolite ± magnetite rocks are frequently designated as TMS, an abbreviation for talc-magnetite schist, in reports on Kafubu. As many of these rocks are massive rather than schistose, and some samples contain no magnetite, we prefer to use the name metabasic rock in this description. These rocks (Table 1) are highly magnesian, typically with 18 to 28 wt.% MgO, and contain very low alkalis so that they plot outside the field of basaltic rocks in the TAS diagram ($Na_2O + K_2O$) vs. SiO_2 (Fig. 6). Low contents of Al_2O_3, CaO, and Na_2O indicate a strongly subdued role for plagioclase in the original igneous rocks. High Cr contents, typically 2800–4500 ppm, are of practical importance because Cr from this source became incorporated into the beryl and gives the green colour to emerald. The high magnesium contents favoured phlogopitization wherever fluids imported sufficient potassium and fluorine. Phlogopitites, typically hosting emeralds, have MgO, SiO_2 and FeO + Fe_2O_3 contents similar to those of the metabasites. MgO vs. Cr and Ni for the three major rock types of the metamorphosed basic unit are compared in Fig. 7.

The metabasic rocks are comprised of a a fine-grained aggregate (< 0.2 mm) of talc + chlorite, sometimes with actinolite, rarely tremolite (Fig. 5a). Few samples contain up to 10 vol.% of ferroan dolomite. Chromium-bearing magnetite reaches up to 4 vol.% in some samples, but is absent in others which contain minor ilmenite (MnO up to 22.5 wt.%) as the single opaque mineral. In samples without magnetite, chromium is contained mainly in chlorite and actinolite.

Alteration and metamorphism have obliterated diagnostic igneous textures. There are no unmetamorphosed equivalents of the volcanics in the region, and thus the conservative behaviour of some relatively stable elements (Grauch 1989) is considered as the remaining opportunity for interpreting the original composition. The identification of the original rock type thus depends on chemical analyses (Table 1a). After recalculation to an anhydrous basis, the chemical analyses correspond to the present criteria for komatiites: MgO > 18 wt.%, TiO_2 < 1 wt.%, and

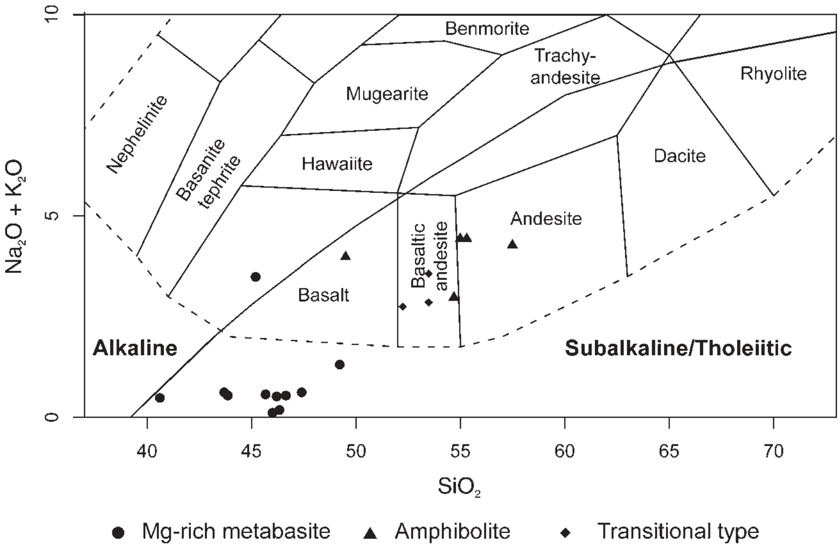


Figure 6. Plot of chemical analyses of metamorphosed volcanic rocks in the Kafubu area, Zambia, in the TAS diagram for magmatites (Cox et al. 1979, adapted by Wilson 1989; dividing line between alkaline and subalkaline series by Irvine and Barragar 1971).

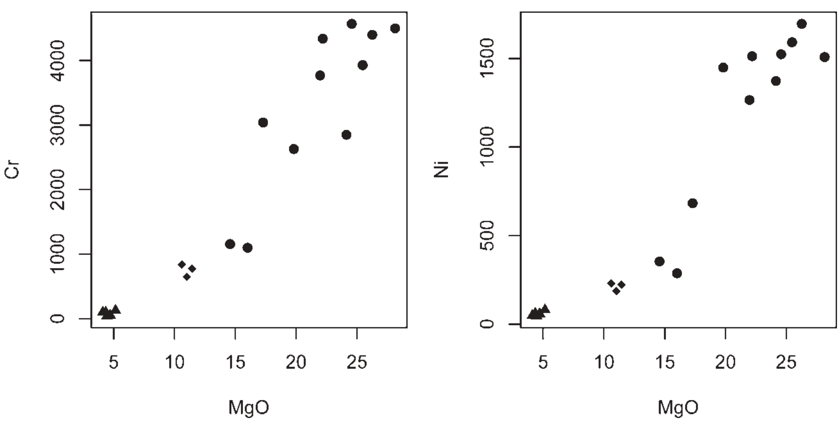


Figure 7. Plot of Cr and Ni vs. MgO. Solid circle – metabasic rocks, diamond – transitional rock types, triangle – amphibolites.

Table 1a. Chemical analyses of whole-rock samples

	Metabasic rocks														Amphibolites				
Sample	FF4	PI5	MB1	GR5	FB1	KF1	PN3	BD4	ME1	EB1	GR1	LU3	PI1	MK1	CH1	KA9	DW3	DW2	FF1
SiO_2	40.61	43.69	43.86	45.19	45.67	46.00	46.33	46.64	47.40	49.22	52.24	53.47	53.48	46.20	49.50	54.69	54.99	55.30	57.49
TiO_2	0.38	0.30	0.47	0.48	0.52	0.56	0.50	0.43	0.29	0.61	0.61	0.67	0.62	0.46	2.53	0.80	0.89	0.89	0.97
Al_2O_3	5.56	5.54	6.84	8.42	7.44	8.56	4.46	6.23	7.46	9.23	11.85	11.30	11.84	9.71	15.02	15.48	14.60	14.47	15.82
Fe_2O_3	4.59	8.37	4.88	5.05	3.14	3.26	2.82	2.83	2.50	3.46	3.06	2.22	2.53	3.28	3.55	1.86	3.97	4.23	2.35
FeO	5.58	3.39	5.41	6.90	6.98	5.99	6.49	5.71	7.78	6.45	6.55	6.98	6.44	6.42	8.19	7.23	5.54	5.16	4.72
MnO	0.19	0.118	0.165	0.185	0.183	0.083	0.13	0.15	0.13	0.212	0.174	0.173	0.161	0.274	0.278	0.216	0.103	0.095	0.153
MgO	28.14	26.26	25.47	17.29	22.19	24.14	21.97	24.57	19.81	16.01	11.45	10.60	11.02	14.57	4.46	4.11	5.15	4.35	4.71
CaO	1.87	1.22	1.93	4.50	6.21	0.19	4.04	4.57	5.47	5.72	4.44	6.10	4.72	4.55	7.96	8.48	6.56	6.42	8.57
Li_2O	0.001	0.004	0.003	0.104	0.007	0.025	0.013	0.003	0.017	0.023	0.089	0.065	0.081	0.013	0.005	0.009	0.043	0.038	0.017
Na_2O	0.39	0.51	0.50	0.26	0.48	0.07	0.16	0.44	0.54	0.59	0.59	1.27	1.01	0.04	3.26	2.51	3.74	3.76	3.84
K_2O	0.09	0.11	0.04	3.23	0.09	0.04	0.02	0.10	0.08	0.72	2.16	2.30	1.85	0.48	0.72	0.47	0.69	0.67	0.43
P_2O_5	0.025	0.032	0.042	0.018	0.043	0.042	0.044	0.037	0.047	0.04	0.062	0.068	0.056	0.031	0.41	0.089	0.087	0.097	0.107
CO_2	0.99	1.64	1.27	< 0.010	0.01	< 0.010	< 0.010	0.03	< 0.010	0.01	0.01	0.01	0.01	< 0.010	0.01	0.05	0.02	< 0.010	0.03
$C_{noncarb.}$	0.007	< 0.005	0.01	0.009	0.007	< 0.005	0.012	< 0.005	< 0.005	< 0.005	< 0.005	0.007	< 0.005	0.007	< 0.005	< 0.005	0.008	0.006	< 0.005
F	0.08	0.309	0.048	0.31	0.034	0.21	0.106	0.316	0.123	0.255	0.166	0.116	0.046	0.969	0.069	0.063	0.048	0.061	0.052
S	0.243	0.031	< 0.005	< 0.005	< 0.005	< 0.005	< 0.005	< 0.005	< 0.005	< 0.005	< 0.005	< 0.005	< 0.005	< 0.005	< 0.005	< 0.005	< 0.005	< 0.005	< 0.005
LOI	8.80	6.97	7.32	4.62	6.35	8.55	6.48	6.71	5.98	3.48	3.77	2.85	4.06	3.68	1.70	1.33	1.61	1.91	1.03
H_2O^-	0.06	0.04	0.08	0.38	0.14	0.61	0.13	0.21	0.38	0.26	0.46	0.22	0.83	0.26	0.14	0.12	0.28	0.48	0.11
Total	97.50	98.40	98.30	96.83	99.50	98.25	96.65	98.85	97.96	96.21	97.63	98.40	98.78	92.82	97.82	97.53	98.34	97.93	100.42
Minor- and trace-elements (ppm)																			
Be	2	4	2	16	2	6	1	4	4	15	4	11	1	17	2	1	2	2	2
V	76	72	107	123	109	101	124	106	113	119	135	152	111	124	220	172	195	165	196
Cr	4500	4400	3930	3040	4340	2850	3770	4570	2630	1098	774	838	650	1156	44	99	128	97	52
Ni	1508	1696	1592	683	1513	1373	1266	1524	1449	287	223	230	186	354	47	48	80	61	58
Cu	119	25	318	125	37	241	73	119	30	5	72	144	50	21	293	81	92	80	58
Zn	179	178	167	130	75	90	73	153	100	123	114	76	62	113	94	163	38	33	60
As	5	6	5	5	5	5	4	6	5	5	5	5	5	6	4	6	5	6	5
Rb	18	19	19	622	17	20	19	21	19	166	342	341	293	426	42	28	61	68	21
Sr	5	4	9	7	8	5	6	9	3	64	26	28	27	36	487	187	201	175	303
Y	5.5	5.1	6	12	14	7.6	10	11	23	16	14.5	18.8	14	44	27.7	23.4	23	25	21.7
Zr	30	26	32	45	46	54	41	36	41	69	69	80	67	46	131	123	105	106	131
Nb	1	1	3	3	3	2	4	3	2	3	3	4	4	6	20	6	5	5	6

Table 1a, continued

Sample	FF4	PI5	MB1	GR5	FB1	KF1	PN3	BD4	ME1	EB1	GR1	LU3	PI1	MK1	CH1	KA9	DW3	DW2	FF1
Mo	< 1	< 1	< 1	< 1	< 1	< 1	< 1	2	< 1	1	< 1	< 1	< 1	< 1	< 1	< 1	< 1	< 1	< 1
Sn	< 2	< 2	< 2	< 2	< 2	2	< 2	< 2	< 2	< 2	< 2	< 2	< 2	4	< 2	< 2	< 2	< 2	3
Ba	< 45	< 45	< 45	90	< 45	45	< 45	< 45	< 45	81	143	233	430	116	81	260	90	82	81
Pb	< 2	< 2	< 2	< 2	< 2	< 2	< 2	< 2	< 2	< 2	< 2	< 2	< 2	< 2	11	< 2	< 2	< 2	4
La	7.1	11.5				8.9					10.9	14.1			23.5	18.2	15.7		8.9
Ce	14.1	19.6				18.4					22.6	25.5			46.2	35.6	31.8		30.8
Pr	2.1	2				2.8					3.3	3.7			7.2	5.2	4.7		4.4
Nd	8.1	8.8				10.3					11.9	14.8			28.8	18.8	17.3		16.3
Sm	2.35	2.62				2.59					2.82	4.34			6.7	3.91	4.45		4.5
Eu	0.21	0.24				0.26					0.63	0.84			1.97	0.95	0.97		0.94
Gd	1.65	1.47				2.19					3.26	3.59			6.8	4.49	4.57		4.65
Tb	< 0.70	< 0.70				< 0.70					< 0.70	< 0.70			< 0.70	0.79	< 0.70		< 0.70
Dy	1.46	1.27				1.81					2.57	3.31			5.29	4.17	4.06		4.13
Ho	< 0.50	< 0.50				< 0.50					0.54	< 0.50			1.34	0.63	0.78		0.74
Er	0.58	< 0.40				0.73					1.44	1.68			2.46	2.52	2.21		2.03
Tm	< 0.30	< 0.30				< 0.30					< 0.30	< 0.30			0.47	0.36	0.34		0.36
Yb	0.70	0.74				1.09					1.79	2.20			2.97	2.86	2.57		2.36
Lu	0.11	0.11				0.16					0.24	0.31			0.44	0.39	0.37		0.36
U	< 2	< 2	< 2	< 2	< 2	< 2	< 2	< 2	< 2	< 2	< 2	< 2	< 2	3	< 2	4	3	3	< 2

$Na_2O + K_2O < 2$ wt.% (Le Bas 2000) (Fig. 6 and 7).

The rare earth element (REE) data (Table 1a, Fig. 8) show abundances and distribution patterns which are not compatible with the highly magnesian, "primitive" composition. The relatively high REE contents and their distribution patterns are due either to a somewhat anomalous enrichment in allanite (e.g. sample PN3, Pioneer mine) or probable hydrothermal alteration of the original volcanics.

Platinum-group element abundances in a metal/metal ratio diagram (Table 2, Fig. 9), following Barnes et al. (1988), indicate that the original compositions of the metabasic rocks lie within the range of komatiites to Mg-rich basalt.

2. Amphibolites

These rocks probably comprise less than 10 % of the total volume of metamorphosed volcanic rocks in the Kafubu area. The amphibolites are fine-grained, poorly to well-foliated rocks composed predominantly of green or blue-green amphibole (// Z), intermediate plagioclase, and quartz. A fine, laminar, streaky texture is observed at some localities, but in other instances the amphibolites can be safely distinguished from magnesian metabasites only in thin section. Accessory dark mica is often absent, and few samples contain up to 15 vol.% of mica. Microprobe analyses show mainly compositions of eastonitic phlogopite, $X_{Mg} = 0.65–0.71$, i.e. with Fe/Mg ratios somewhat higher than the phlogopite in phlogopitites. Examples of amphibole composition are presented in the mineralogy section of this article.

Minor Mg-chlorite is present in several samples, while titanite, rutile or ilmenite, apatite and tourmaline are accessory minerals. The rocks are free of garnet or clinozoisite--epidote and show an equilibrated mosaic texture. Five chemical analyses (Table 1a, Fig. 6) show that these amphibolites correspond in composition to andesite, marginally to basaltic andesite, and rarely to basalt (sample CH1). The REE of four analyzed samples give distribution patterns with limited variation, but their similarity to the pattern of metasedimentary quartz-muscovite-phlogopite ± albite schists may suggest that these REE abundances have been modified by a superimposed process, possibly by post-volcanic alteration. Widely dispersed accessory tourmaline has been identified in several amphibolite samples, in textures indicating

Table 1b. Chemical analyses of whole-rock samples

	Phlogopite schists, in part with tourmaline and beryl									Tourmalinites and pegmatites					Quartz-muscovite schists		
Sample	KF4b	MK1	CT1	GN3	KA12	KF4A	EB2	LU2	PN7	KF2	LU1	PN4	FF2	SR1	MB4b	FF3	MB4a
SiO_2	39.88	40.58	41.73	41.83	42.30	45.78	48.24	50.69	38.28	37.04	41.88	66.86	72.50	58.70	61.59	64.73	68.38
TiO_2	0.87	0.26	0.45	0.40	1.01	0.53	1.15	0.53	0.61	1.08	0.54	0.96	0.03	0.93	1.03	0.86	0.80
Al_2O_3	14.93	16.15	14.50	15.68	13.89	13.43	13.48	11.71	12.48	29.39	26.29	14.81	15.47	20.31	18.72	15.32	14.66
Fe_2O_3	2.79	2.80	1.47	3.04	2.32	1.90	2.69	1.65	2.08	6.49	4.77	3.85	0.816	2.74	1.08	1.28	1.06
FeO	6.20	3.81	5.00	6.98	6.62	5.98	6.17	4.93	6.29	1.44	1.26	0.84	0.481	0.66	3.19	2.46	2.55
MnO	0.155	0.185	0.397	0.297	0.404	0.101	0.443	0.212	0.171	0.12	0.124	0.047	0.753	0.016	0.029	0.022	0.023
MgO	16.61	18.48	18.42	12.24	16.28	12.89	11.61	14.18	18.18	6.24	7.47	3.81	0.11	2.76	3.20	4.46	3.34
CaO	0.32	0.16	0.03	0.25	0.01	0.07	0.30	0.04	2.89	0.95	1.03	0.60	0.42	0.59	0.23	0.83	0.26
Li_2O	0.218	0.312	0.739	0.542	0.715	0.473	0.338	0.386	0.289	0.016	0.041	0.003	0.008	0.002	0.059	0.047	0.05
Na_2O	0.31	0.46	0.12	0.35	0.21	0.25	0.30	0.25	0.22	1.94	1.68	0.93	7.17	5.59	2.60	4.72	2.24
K_2O	8.03	7.60	10.15	7.39	9.33	8.02	6.27	7.25	8.98	0.03	0.60	0.05	0.22	0.07	4.21	2.39	3.36
P_2O_5	0.035	0.008	0.008	0.006	0.016	0.008	0.032	0.006	1.92	0.031	0.029	0.013	0.138	0.027	0.084	0.156	0.076
CO_2	0.01	0.02	0.02	0.01	0.01	0.01	0.01	0.01	0.03	< 0.010	0.01	0.01	< 0.010	< 0.010	0.01	< 0.010	0.01
$C_{noncarb.}$	< 0.005	0.005	< 0.005	0.01	< 0.005	< 0.005	0.007	0.009	0.008	< 0.005	0.005	< 0.005	< 0.005	< 0.005	< 0.005	< 0.005	< 0.005
F	2.82	2.67	4.37	3.68	4.70	3.77	2.61	3.07	3.17	0.975	1.12	0.203	0.045	0.167	0.055	0.076	0.06
S	< 0.005	< 0.005	< 0.005	< 0.005	0.005	< 0.005	< 0.005	< 0.005	< 0.005	< 0.005	0.007	< 0.005	< 0.005	< 0.005	< 0.005	< 0.005	< 0.005
LOI	3.93	4.56	4.59	4.11	3.69	3.28	3.56	3.48	4.32	3.09	3.25	1.73	0.545	1.62	2.75	1.77	2.23
H_2O^-	0.10	0.11	0.12	0.06	0.13	0.05	0.10	0.11	0.11	0.04	0.12	0.11	0.11	0.16	0.12	0.27	0.12
Total	96.10	97.11	100.37	95.36	99.74	95.03	96.42	97.29	98.75	88.46	89.77	94.75	98.81	94.29	99.16	99.41	99.26
Minor- and trace-elements																	
Be	13	7	8	6	8	1249	10	1644	9	7	7	5	36	9	3	2	1
V	117	41	31	78	101	66	79	87	46	86	88	70	8	83	121	56	75
Cr	2270	203	4670	699	275	2250	350	2120	1201	95	1770	86	9	115	102	78	97
Ni	980	309	1266	401	983	368	177	1022	345	57	410	36	4	43	45	41	47
Cu	52	424	25	42	76	25	35	21	30	6	34	121	17	33	96	4	24
Zn	173	546	1197	467	590	99	633	331	176	655	828	33	135	23	34	27	34
As	5	5	4	18	5	4	4	4	5	6	6	5	5	5	5	5	5
Rb	1725	1730	~ 2800	1851	~ 2900	~ 2600	1909	2111	1098	18	171	19	29	19	149	103	149
Sr	31	56	8	24	15	14	25	21	23	70	157	89	5	140	54	46	43
Y	12	1	< 1	< 1	13	< 1	8	< 1	16	25	14	14	6.2	0.9	30.8	42.5	25.6
Zr	80	< 1	36	29	122	43	126	32	59	259	55	216	32	206	155	275	126
Nb	7	14	48	28	22	6	56	7	26	185	6	8	7	8	14	12	10

Table 1b, continued

Sample	KF4b	MK1	CT1	GN3	KA12	KF4A	EB2	LU2	PN7	KF2	LU1	PN4	FF2	SR1	MB4b	FF3	MB4a
Mo	< 1	< 1	< 1	< 1	< 1	< 1	< 1	1	< 1	< 1	< 1	< 1	2	< 1	1	< 1	< 1
Sn	< 2	< 2	< 2	< 2	< 2	< 2	< 2	< 2	< 2	< 2	< 2	< 2	< 2	3	< 2	< 2	< 2
Ba	681	466	761	358	833	663	1791	618	421	< 45	107	< 45	134	45	1944	385	475
Pb	9	< 2	11	7	6	3	4	3	< 2	15	17	< 2	5	< 2	< 2	< 2	< 2
La		< 0.2											2.9	1.6	49.0	38.9	34.6
Ce		< 0.7											6.1	3.3	91.9	89.2	68.7
Pr		1.0											1.2	1.2	11.4	10.8	8.5
Nd		< 2.0											2.9	3.4	46.2	42.3	34.0
Sm		2.18											1.61	3.29	8.74	9.23	7.9
Eu		< 0.08											0.09	0.10	1.76	1.81	1.18
Gd		< 0.30											1.09	< 0.30	6.72	8.63	6.30
Tb		< 0.70											< 0.70	< 0.70	< 0.70	1.00	< 0.70
Dy		0.20											1.44	0.21	5.47	7.87	4.65
Ho		< 0.50											< 0.50	< 0.50	1.17	1.73	1.01
Er		< 0.40											< 0.40	< 0.40	3.48	3.99	2.13
Tm		< 0.30											< 0.30	< 0.30	0.63	0.64	< 0.30
Yb		0.11											0.29	0.11	3.55	4.04	2.81
Lu		< 0.04											< 0.04	< 0.04	0.52	0.57	0.42
U	6	3	< 2	6	9	6	5	7	4	3	3	2	< 2	3	2	4	2

probable equilibrium crystallization with the primary amphibolite minerals, or the late introduction of tourmaline. A heavy mineral concentrate (density > 3.3) prepared from sample DW3 contains several vol.% of zircon, showing a predominantly abraded morphology and pitted surfaces typical of detrital zircon. This may indicate a detrital admixture to an original tuff-like parent rock.

Chromium contents of 44 to 128 ppm are substantially lower than those in magnesian metabasites (Fig. 7). Any beryl mineralization in amphibolites of this type is unlikely to produce emeralds of good colour.

The mineral assemblages correspond to amphibolite facies conditions. The estimation of amphibole-plagioclase thermometry undertaken on five different amphibolite samples according to Holland and Blundy (1994), gives a narrow equilibration temperature interval of 590–630 °C for pressure of 400–600 MPa (Table 3). These results give an approximation of the regional metamorphic P-T conditions of the Muva Supergroup in the Kafubu area during the regional metamorphism of the Neoproterozoic Lufilian orogeny.

3. Transitional actinolite/amphibole-rich metabasic rocks with compositions partly transitional between types 1 and 2

These rocks are represented by three samples in Table 1a (GR1, LU3, PI1). Their SiO_2 content is about 8 wt.% higher and their Al_2O_3 about 5 wt.% higher than the magnesian metabasites. Their MgO contents are near 11 wt.%. The chromium content (650–838 ppm Cr) of these rocks is much lower than that of the magnesian metabasites. In various diagrams (Figs. 6 through 8), these rocks show compositions corresponding to basaltic andesites, occupying an intermediate position between amphibolites and magnesian metabasites. Their potassium contents (ca. 2 wt.% K_2O), however, probably indicate the influence of K-metasomatism.

Metasedimentary quartz-muscovite-phlogopite-albite schists

Mica-rich, silvery to grey mica schists to phyllites represent the regionally widespread suite of metasediments that host the metamorphosed basic rocks with emerald mineralization. These rocks show distinct small-scale compositional layering (Fig. 5d). Three whole-rock analyses (Table 1b) apparently do not cover the total compositional range of these rocks, though they show some important

Table 1c. Mineralogical composition of the chemically analyzed rock samples

Sample No.	Locality	Rock-type	Main components (vol. %)
FF4	Fwaya-Fwaya east	Fine-grained chlorite-talc-tremolite-dolomite-Cr-magnetite schist	Chl 60, Tlc 20, Tr 10, Dol 5 Cr-magnetite 3
PI5	Pirala mine	Fine- to medium-grained talc-chlorite metabasite	Chl 45, Tlc 45, Dol 5, Mt 5, Ilm 1
MB1	Mbuwa mine	Fine-grained chlorite-talc metabasite	Chl 50, Tlc 40, Dol 5, Cr-magnetite 3, accessory monazite
GR5	Grizzly mine	Fine-grained phlogopite metabasite	Act 45, Phl 30, Tlc 10, Chl 10, Cr-magnetite 3
FB1	Fibolele mine	Fine-grained talc-actinolite-chlorite metabasite	Chl + Act 53, Tlc 45, Mn-ilmenite 2
KF1	Kafubu mine	Fine-grained talc-chlorite-actinolite metabasite	Tlc 55, Chl 27, Act 15, Ilm 2
PN3	Pioneer mine	Fine-grained chlorite-actinolite-talc metabasite	Chl 50, Act 30, Tlc 20, Accessory Ilm + Mt
BD4	Bedrock mine	Fine-grained actinolite-chlorite-talc schist	Act 40, Chl 30, Tlc 27, Cr-magnetite 3
ME1	Melai pit	Very fine-grained talc-actinolite-chlorite metabasite	Act 45, Tlc 30, Chl 23, Ilm 1, accessory Rt, Ap
EB1	Ebenezer mine	Medium-grained actinolite-tourmaline-chlorite schist	Act 55, Tur 30, Chl 5, Phl 5, Qtz 5, Rt 1
GR1	Grizzly mine	Medium-grained amphibolite with tourmaline	Hbl 40, Chl 25, Qtz + Pl 15, Phl 10, Tur 10
LU3	Lumpuma mine	Fine-grained biotite amphibolite	Hbl 55, Qtz 12, Pl 10, Bt 12, Chl 6, Tur 1, Rt 1
PI1	Pirala mine	Fine-grained foliated amphibolite	Hbl 50, Qtz + Pl 20, Phl 15, Chl 15, accessory Tur, Zrn + D2
MK1	Miku mine	Actinolite-phlogopite-tourmaline rock	Act 50, Phl 20, Tur 15, Tr 10
CH1	Chisebaulwa mine	Fine-grained amphibolite	Hbl 40, Qtz + Pl 30, Bt 25, opaque min. 4, accessory Tnt
KA9	Kamakanga Old Pit	Medium-grained amphibolite	Hbl 52, Pl 25, Qtz 20, Tnt 1, Ilm 1, accessory Ap. Bt
DW3	Dabwisa mine	Fine-grained amphibolite	Hbl 40, Pl 40, Qtz 15, Bt 3, accessory Ilm
DW2	Dabwisa mine	Fine-grained amphibolite	Hbl 45, Pl 35, Qtz 15, Bt 3
FF1	Fwaya-Fwaya east	Fine-grained amphibolite	Pl 40, Hbl 35, Qtz 25, Tnt 1
KF4b	Kafubu mine	Coarse-grained phlogopite-beryl-tourmaline rock; thin section rich in beryl	Be 60, Phl 25, Tur 12
MK1	Miku mine	Fine-grained phlogopitite with euhedral crystals of tourmaline	Phl 70, Tur 30
CT1	Chantete mine	Medium-grained phlogopitite	Phl 99, accessory Zn-bearing chromite
GN3	Gerntine mine	Fine-grained phlogopitite	Phl 95, Qtz 5
KA12	Kamakanga Old Pit	Fine- to medium-grained phlogopitite	Phl 98, Rt 2, accessory monazite
KF4A	Kafubu mine	Medium-grained phlogopite-tourmaline-beryl-quartz rock	Phl 65, Tur 12, Be 12, Qtz 10
EB2	Ebenezer mine	Medium-grained phlogopite-quartz-tourmaline schist	Phl 70, Qtz 20, Tur 8
LU2	Lumpuma mine	Medium-grained phlogopite-tourmaline-quartz schist with a band rich in beryl	Phl 65, Be 15, Tur 12, Qtz 8
PN7	Pioneer mine	Medium-grained foliated phlogopitite	Phl 94, Ap 5, Tur 1
KF2	Kafubu mine	Fine-grained tourmalinite with planar-parallel texture	Tur 94, Qtz 5, Nb-Ta rutile 1
LU1	Lumpuma mine	Medium-grained tourmaline-quartz rock	Tur 95, Qtz 5
PN4	Pioneer mine	Fine-grained banded quartz-tourmaline rock with 3–5 mm wide bands	Qtz 53, Tur 47, accessory Ilm
FF2	Fwaya-Fwaya east	Medium-grained pegmatite with tourmaline and garnet	Ab 48, Qtz 40, Tur 7, Grt 3, Ms 2, accessory Zrn
SR1	Solid Rock mine	Medium-grained gneissic albite-quartz-tourmaline rock	Ab 40, Qtz 40, Tur 20
MB4b	Mbuwa mine	Fine-grained schist	Qtz + Ab 45, Bt 30, Ms 20, Chl 3, Tur 1, Rt 1, accessory Zrn
FF3	Fwaya-Fwaya east	Fine-grained schist	Ab 35, Bt 30, Qtz 28, Ms 5, Rt 0.5, accessory Tur, Ap
MB4a	Mbuwa mine	Fine-grained schist	Qtz + Ab 45, Ms 40, Bt 10, Chl 5, Rt 0.5, accessory Ap

Percentages of minerals are based on semiquantitative estimates in thin sections.
Abbreviations for minerals: Ab – albite, Act – actinolite, Ap – apatite, Be – beryl, Bt – biotite, Chl – chlorite, Dol – dolomite, Grt – garnet, Hbl – hornblende, Ilm – ilmenite, Ms – muscovite, Mt – magnetite, Phl – phlogopite, Pl – plagioclase, Qtz – quartz, Rt – rutile, Tlc – talc, Tnt – titanite, Tr – tremolite, Tur – tourmaline, Zrn – zircon.

Table 2. Analyses of platinum-group elements in metabasic rocks and phlogopitite, Kafubu area; mg/kg (= ppm) units

Sample No.	KF1	PI5	FF4	GR1	LU2	Estimate of Earth's mantle composition*
Locality	Kafubu pit	Pirala mine	Fwaya-Fwaya east	Grizzly mine	Lumpuma mine	
Rock type	metabasite	metabasite	metabasite	metabasite	phlogopitite	
Ir	0.0013	0.0014	0.0018	0.0005	0.0003	0.0044
Ru	0.0022	0.0040	0.0039	< 0.001	< 0.001	0.006
Rh	0.00092	0.0006	0.00066	0.00055	0.00056	0.002
Pt	0.0067	0.0035	0.0039	0.0162	0.007	0.0092
Pd	0.0093	0.0048	0.0066	0.0060	0.0083	0.0044
Ni	1373	1696	1508	223	1022	2000
Cu	241	25	119	72	21	28

* data by Barnes et al. (1988)

compositional features. In the diagram by Herron (1988) the samples plot within the fields of shale and wacke. Magnesium (MgO molar ratio) predominates above total iron (FeO), while the relatively high Na_2O contents are bound in fine-grained albite which is not visible in hand samples, and in paragonite molecule in muscovite. These rocks carry accessory tourmaline, probably derived in part from recrystallized detrital tourmaline(?), minor zircon, and apatite ± ilmenite or rutile. The REE patterns (Fig. 8) correspond to the derivation of detrital material from geochemically evolved crustal sources, such as granite- or gneiss-rich older terrain.

Quartz-tourmaline rocks and veins

The wide variability in texture and composition of these rocks necessitates the integration of observations from numerous localities. The importance of these rocks and veins follows from the fact that emerald mineralization at Kafubu is directly linked to phlogopitite exocontact of quartz-tourmaline veins. Also, the abundance of tourmaline makes Kafubu a major boron anomaly, which coincides with beryllium enrichment. This feature is not seen at most world-class emerald deposits, which typically show lesser quantities of tourmaline.

Type 1. Quartz-tourmaline rocks (ca 20–90 % tourmaline) with strongly defined, banded-planar texture

The layers of these rocks are conformable with the regional lithological layering. Quartz and tourmaline bands, largely 1 to 5 mm thick, alternate in a regular manner. On a microscopic scale, tourmaline shows a prominent orientation with its long axis lying in the foliation plane. The quartz bands show a fine-grained granular mosaic texture similar to that of quartzite. Chemical analysis of this rock type from the Pioneer mine (sample PN4), and a tourmaline-dominated sample KF2 from the Kafubu mine, are presented in Table 1b. The Kafubu mine presents the most well-exposed example, with a 1–2 m thick layer of quartz-tourmaline banded rock positioned on top of a thick metabasite body and overlain by quartz-muscovite-phlogopite mica schist. An emerald-bearing phlogopitite zone up to 2 m thick is developed at the base of the quartz-tourmaline layer, but as this layer is accompanied here by abundant confor-

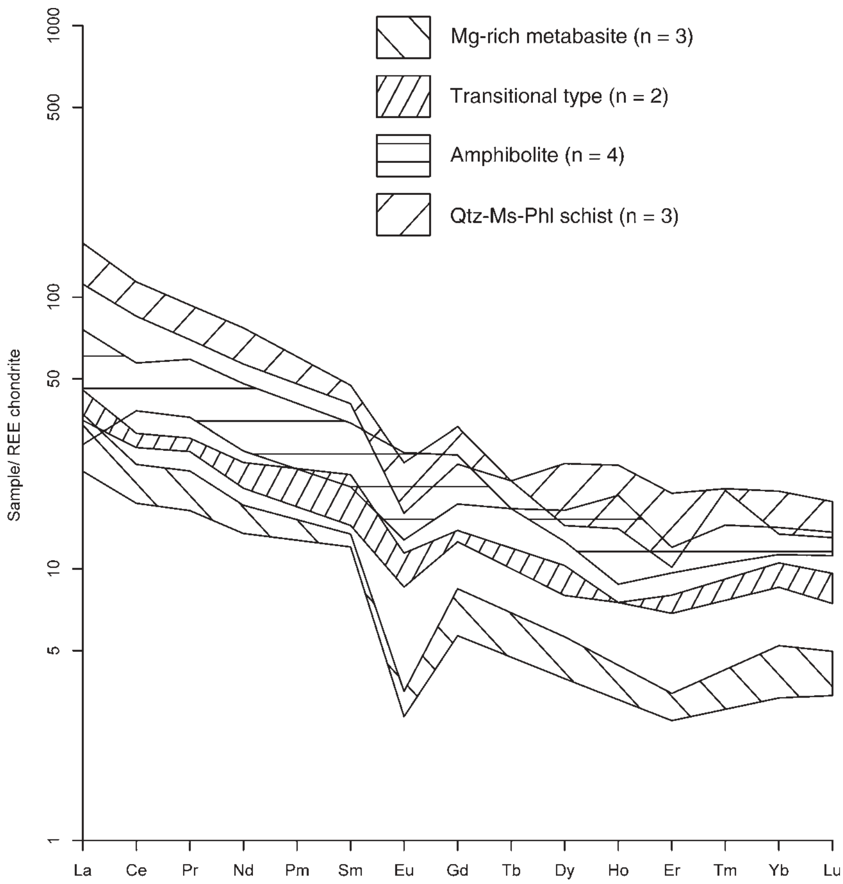


Figure 8. Chondrite-normalized REE patterns for Mg-rich metabasites, transitional basic rocks, amphibolites, and metasedimentary quartz-muscovite-phlogopite schists. The composition of the CI chondrite used for normalization is from Boynton (1984).

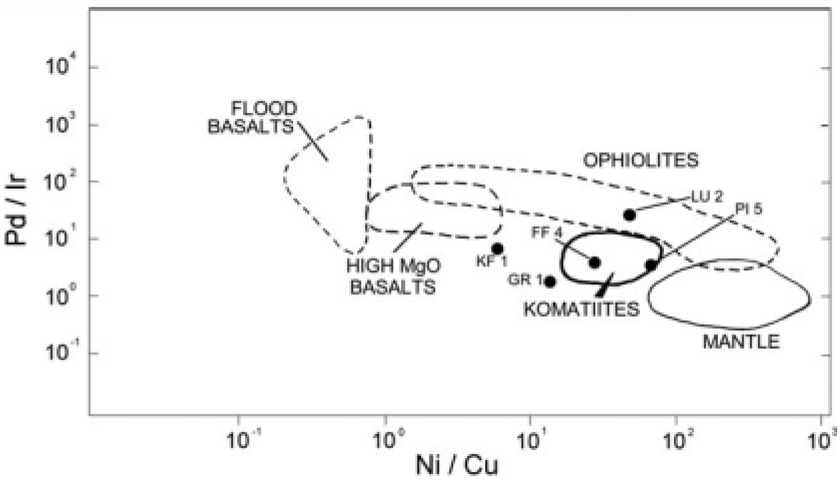


Figure 9. Plot of Pd/Ir vs. Ni/Cu ratio for the metamorphosed basic rocks of the Kafubu area, compared with selected compositional fields for basic magmatites after Barnes et al. (1988). Mg-rich metabasites: FF 4, PI 5, KF 1; transitional type of basic rock: GR 1; phlogopitite: LU 2 (note that the metabasites altered to phlogopitites experienced gross compositional alteration in the process of phlogopitization). Whole-rock analyses of these samples are presented in Tables 1a and 1b.

mable and discordant quartz-tourmaline veins (type 2), it is somewhat uncertain which type of tourmaline-rich rock is the most closely associated with phlogopitization and emerald mineralization in this particular place.

The banded quartz-tourmaline rocks contain some extreme compositions, with tourmaline increasing up to 90 vol.% (sample KF2 – Kafubu mine, Table 1b) and a variety containing about 12 vol.% of muscovite. The sample KF2 contains 185 ppm of niobium, which is considered as a geochemical signature of pegmatite-related mineralization. Niobium and tantalum are concentrated in the outer parts of Nb/Ta rutile lobate grains. Because of these relations, as well as the indications of inheritance of the banded texture from quartz-muscovite schists, and the similarity of tourmaline composition in these rocks and quartz-tourmaline veins, we interpret the banded quartz-tourmaline rocks as a product of metasomatism associated with the formation of phlogopitites bearing the emerald mineralization.

Type 2. Quartz-tourmaline veins

These veins show both conformable and discordant orientations to the lithological layering and a wide variation in quartz/tourmaline ratio. The veins are usually less than 3 m wide. Black Fe-dravite tourmaline occurs in prismatic crystals 1 mm to 10 cm long, with local tendencies to form radiating (3-D) aggregates. The quartz is milky white to semi-transparent and often coarse-grained, with single grains larger than 1–2 cm. Field observations and microscope studies indicate that the quartz-tourmaline veins postdate the phase of regional penetrative deformation and metamorphic recrystallization. Examples of discordant or vertical veins with some flat-lying offshoots penetrating the country rock parallel to foliation were documented by Sliwa and Nguluwe (1984). Examples of vertical veins of similar composition but emplaced across flat lying veins parallel to foliation also occur. Vertical veins, accompanied by a strong phlogopitization + beryl/emerald mineralization in zones up to 3 m wide, are best exemplified at the Grizzly mine, but are also documented at several other pits. The relations described in this section may suggest that a temporary sequence in the emplacement of veins with various orientations can be determined. In fact, field observations gave no reliable data in this respect. The only group of veins which, on the basis of textural and mineralogical criteria, are safely recognized as a later set, postdating the emerald mineralization, are the late, vug-filling veins, described below as Type 3. The fluid inclusion data indicate three P-T stages in the supposed evolution of quartz-tourmaline veins.

Based on observations made at more than 30 localities, it seems that the quartz-tourmaline veins are completely free of feldspars, and there is no indication that transitional types between quartz-tourmaline veins and true quartz-feldspar pegmatites occur. The description by Sliwa and Nguluwe (1984), indicating the potential presence of such transitional veins, may relate to quartz- and tourmaline-rich pegmatites with kaolinized feldspar.

The veins rarely carry additional mineral besides quartz and tourmaline. Examples include sporadic, light-coloured

Table 3. Amphibole-plagioclase thermometry for Kafubu amphibolites (Holland and Blundy 1994)

Sample No.	amphibole				plagioclase	P = 400 MPa		P = 600 MPa		P = 800 MPa	
Analysis No.	Si (pfu)	$(Na + K)_A$ pfu	Fe^{2+}_{calc}	Fe^{3+}_{calc}	X_{Ab}	T 1 (°C)	T 2 (°C)	T 1 (°C)	T 2 (°C)	T 1 (°C)	T 2 (°C)
MB3/467	6.888	0.170	1.062	0.368	0.730	592	581	596	600	601	620
MB3/467	6.888	0.170	1.062	0.368	0.691	598	596	603	616	607	636
MB3/468	6.896	0.175	1.027	0.414	0.691	609	610	612	629	615	648
LU3/352	6.755	0.262	1.048	0.391	0.664	632	616	639	638	647	659
LU3/352	6.755	0.262	1.048	0.391	0.708	620	594	627	615	635	636
LU3/353	7.057	0.185	1.001	0.294	0.664	608	609	610	628	612	647
LU3/353	7.057	0.185	1.001	0.294	0.708	601	593	603	612	605	630
GR6/422	6.555	0.288	1.242	0.345	0.655	615	591	631	617	648	643
GR6/422	6.555	0.288	1.242	0.345	0.698	607	577	623	603	640	628

emerald (at Kamakanga and several other localities), and muscovite sampled at four localities. Muscovite books up to 7 cm long, constituting aggregates up to 20 cm in diametre, is confined to a few quartz-dominated veins with minor tourmaline along their walls.

Type 3. The youngest generation of quartz-tourmaline veins

The youngest veins fill extension fractures occurring in the main type (type 2) of quartz-tourmaline veins, as observed in the Old Kamakanga pit. They feature tourmaline crystals of a tabular/bladed habit, typically arranged in a herringbone pattern. Such veins, only about 3 cm wide, consist predominantly of tourmaline. Nonetheless, they are related to the wider veins. Some of them contain drusy cavities carrying freely grown rock crystal associated with the tourmaline in platy crystals, or with acicular tourmaline piercing rock crystal.

Quartz-feldspar-muscovite pegmatites

During the fieldwork about 20 granitic pegmatite dikes were examined, and several mainly kaolinized dikes were sampled. Given the very limited exposure of the area, with the exception of active mines and pits, it is only possible to give an estimate of the number of pegmatite bodies in the area on the order of hundreds (possibly > 1000). Most of these dikes are within the range of 2 to 10 m in width (one 100 m wide dike, exposed in the Fwaya-Fwaya mine, appears to be exceptional). We must therefore consider the possibility of the existence of a major pegmatite field (an area with a large number of pegmatite dikes), largely coinciding with the Kafubu emerald area. In this "Kafubu pegmatite field" the pegmatites extend from the Kamakanga, Twampane, and Pirala mines in the southwest, through Pit D8, Fwaya-Fwaya, Fwaya-Fwaya Ext. 10, and the Fibolele mines in the middle, up to the Pioneer and Solid Rock mines in the northeast.

The mineral assemblage of these pegmatites contains K-feldspar, albite, quartz, muscovite, with lesser amounts of biotite and Mn-rich garnet (Fig. 5e). Their minor minerals are schorl tourmaline or Fe-dravite, and ilmenite. Zircon, rutile, amphibole, monazite, aquamarine, Zn-spinel, magnetite, chalcopyrite, Fe-oxide (hematite) and Ta-Nb minerals are present as accessory minerals.

The emplacement and shape of these vertical to sub-vertical, fracture-filling pegmatites was controlled by fracturing that post-dated the regional metamorphism of the country rocks. The width of the dikes varies from dm to 15 m. They may be only several metres long, but lengths of hundreds of metres are not exceptional. At the Fwaya-Fwaya deposit one pegmatite was traced over 850 m in length. The prevailing strike of the main pegmatite bodies in the central Kafubu area is north-south.

Some granitic pegmatites show well developed, sometimes asymmetrical, structures (Fwaya-Fwaya mine). At the contact with the surrounding metabasic rocks there is a metasomatic external border zone up to two metres wide, formed by phlogopite. The 1–2 m wide inner wall zone is composed of K-feldspar, quartz, muscovite, and tourmaline, with a general grain size of 1–5 cm. Biotite or biotite-tourmaline "schlieren" (either vertical or horizontal) are found in some places. The 0.4–1 m wide intermediate zone is comprised of K-feldspar, quartz, muscovite, garnet, and ± cleavelandite. The grain size in this zone varies from 5–10 cm (e.g. muscovite flakes). The typical core zone (with block texture) is not commonly developed. Sometimes blocks of K-feldspar, quartz, and even beryl up to 0.5 m long (Fwaya-Fwaya Ext. 10) may be found, but usually only hints of coarse-grained quartz and feldspar are recognizable. Vertical asymmetry in the dikes is locally evident, as expressed by the widely variable widths of the pegmatite bodies themselves, as well as that of their internal zones and the surrounding foot- and hanging-walls. Some pegmatite dikes are medium-grained and free of any notable zonal structure. Albite is the dominant feldspar in some cases (e.g. sample FF2-Fwaya-Fwaya), but K-feldspar in 2 to 10 cm long crystals appears as the major component in some dikes at the Fwaya-Fwaya deposit. For technical reasons, we were unable to collect samples in detailed profiles across fresh pegmatite dikes at Fwaya-Fwaya. Kaolinization of these pegmatites is widespread and of variable intensity; it has obliterated the primary structure of many of these pegmatite dikes. No miarolitic textures have been observed in these pegmatite bodies.

Two analyses of a quartz-albite-muscovite-tourmaline pegmatite appear in Table 1b. Sample FF2 of the Fwaya-Fwaya mine is a particularly representative and fresh sample, which also contains accessory Mn-rich garnet; sample SR1 is from the Solid Rock mine.

In poorly exposed areas, pegmatite types can be reliably estimated from the geochemical signature of their rock forming minerals (Černý 1991). The data on spessartine-rich garnet, manganotantalite and some other accessory minerals separated from heavy mineral concentrates, including samples of kaolinized pegmatite dikes, are presented below. The compositional information shows a well-defined preference for the rare-element albite pegmatite class of the LCT family (Černý 1991). The abbreviation LCT stands for the elements Li, Cs and Ta, with the relation Ta > Nb. The enrichment in tantalum and niobium is evident from the occurrence of accessory manganotantalite (rather than columbite), tantalian rutile (strüverite), and rare plumbomicrolite. The last mineral from the Pirala mine pegmatite is a complex oxide of tantalum, lead, uranium, and titanium ± Ca and Na. The rare Ta minerals have been identified by microprobe analyses and X-ray powder diffraction. A high content of beryllium (beryl, emerald) is also an important feature of the LCT pegmatite family.

There is no information bearing directly on the presence of major lithium minerals, such as petalite, spodumene, eucryptite, lepidolite or lithium tourmalines, in these pegmatites. Petalite and spodumene may have disappeared during the process of kaolinisation in some of the altered dikes. Green elbaitic manganoan tourmaline from plot

No. 20 (Mantenke Mining Co.) in the southern part of the area appears to be an exception. On the other hand, our pegmatite sampling was not designed to recover low-density Li-minerals sensitive to weathering.

Muscovite in 5 cm long crystals from a pegmatite in the Fwaya-Fwaya mine contains 0.149 wt.% Li_2O, 32 ppm Be, 2450 ppm Rb, and 318 ppm Nb.

Phlogopitites

Phlogopite-rich rocks are typically formed as reaction zones along the contacts of quartz-tourmaline veins and quartz-feldspar pegmatites with metabasic rocks. These zones are several cm to several m wide. The simplest type of these rocks is dominated by phlogopite, amounting to 90–100 vol.%. Textural varieties include foliated types with perfect grain-shape orientation of the phlogopite crystals, and types with random orientation. Also widespread are phlogopitites with euhedral porphyroblasts of tourmaline or actinolite several mm up to 10 cm long. Individual crystals and clusters of beryl or emerald occur in a similar manner. Quartz, chlorite, or talc are occasionally present in phlogopitites as small size components.

Nine chemical analyses of phlogopitites and phlogopite-rich rocks are presented in Table 1b. These data are compared with oxide/element abundances in the Mg-rich metabasic rocks in Fig. 10. This comparison shows that the transformation of metabasic rocks into phlogopitite involves a major influx of K, Al, F, Li, Rb, pronounced localized concentration of beryllium, and the removal of Ca, Si, and water. The phlogopitization thus shows enrichment in pegmatitic components. Cr and Ni concentrations become somewhat diluted during the alteration of the metabasite protolith into phlogopitite.

The magnetic susceptibility of the rocks

Magnetic susceptibility was measured at 23 outcrops of the main rock types at different open pits. We used the pocket-sized SM-20 magnetic susceptibility metre (version 2.0 of Canadian patent), with a sensitivity of 10^{-6} SI and a range of 0–999 × 10^{-3} SI. The effective depth of measured signal is 2.5 cm. Measurements were carried out on flat surfaces of fresh outcrops at recently operated mines. Our method was to take 10–15 readings within a maximum area of 2 square metres. The final value for each documented point is the arithmetic mean of the individual measurements.

The survey of 17 documented localities of metabasic rocks revealed major variability in magnetic susceptibility (Table 4, Fig. 11). The average values in 10^{-3} SI units range from 0.31 at the Pirala mine to 90.7 at the Fwaya-Fwaya mine. The metabasic rocks present in the Kafubu area can be thus subdivided into two main types: one of low magnetic susceptibility, ranging between 0.31 to 0.88; and a second type with high magnetic susceptibility, ranging from 5.2 to 90.7 (Table 4).

In reference to exploration, it is important to note that a single locality (such as the Grizzly and and Pirala mines) may contain metabasic rocks of both low and high magnetic susceptibility (Fig. 11). This means that magnetic anomalies ascertained by ground-based magnetic surveys may be composed of the combined effect of both types, regardless of beryl potential. The absence of magnetite in some metabasite samples is probably due to the differences in iron distribution among the newly formed silicates.

These results have been verified by the study of heavy mineral concentrates from these metabasic rocks, and by the microscopic study of thin sections. Some samples show absolutely no ferromagnetic components (e.g. Fwaya-Fwaya Ext. 10, sample no. FE4 HM), while others show magnetite contents totalling 15–20 vol.% of the heavy mineral fraction (e.g. Kamakanga Old Extension, sample KA8 HM). Nearly half of the studied metabasic rock samples contain only accessory magnetite.

Table 4. Magnetic susceptibility of rocks in the Kafubu area

Locality	Rock	n	Average	Minimum	Maximum
Kafubu mine	metabasite	4	0.433	0.366	0.521
	tourmalinite	3	0.381		
	muscovite schist (violet)	10	0.139	0.087	0.210
	phlogopite-tourmaline schist	15	0.295	0.200	0.505
Grizzly mine	metabasite with phlogopite	12	0.427	0.218	1.380
	metabasite with phlogopite	12	5.26	2.80	11.10
Lumpuma mine	metabasite with phlogopite	13	0.407	0.329	0.476
	metabasite	13	0.890	0.526	1.13
	quartz-tourmaline rock	13	0.258	0.182	0.546
Pirala mine	metabasite	13	69.7	53.9	85.5
	metabasite 2 m from pegm.	12	0.312	0.232	0.420
Ebenezer mine	metabasite with phlogopite	15	0.344	0.243	0.467
	muscovite-biotite schist	6	0.085	0.062	0.118
Miku mine	metabasite	13	28.18	7.37	49.5
Pit No. D8	metabasite	14	0.416	0.318	0.510
Dabwisa	metabasite	15	0.496	0.293	1.05
Chantete mine	metabasite	16	6.73	1.84	14.1
Solid Rock mine	metabasite	14	14.25	7.40	28.2
Fwaya-Fwaya E.	metabasite	15	90.7	59.7	135.0
	amphibolite	10	0.506	0.251	0.970
Fwaya-Fwaya 10	phlogopite-chlorite schist	10	0.439	0.375	0.512
Fibolele mine	metabasite	11	0.469	0.358	0.548
	metabasite	9	28.1	15.5	38.9
Mbuwa mine	metabasite	15	30.2	19.8	43.0

n – number of measured points; values in 10^{-3} SI units

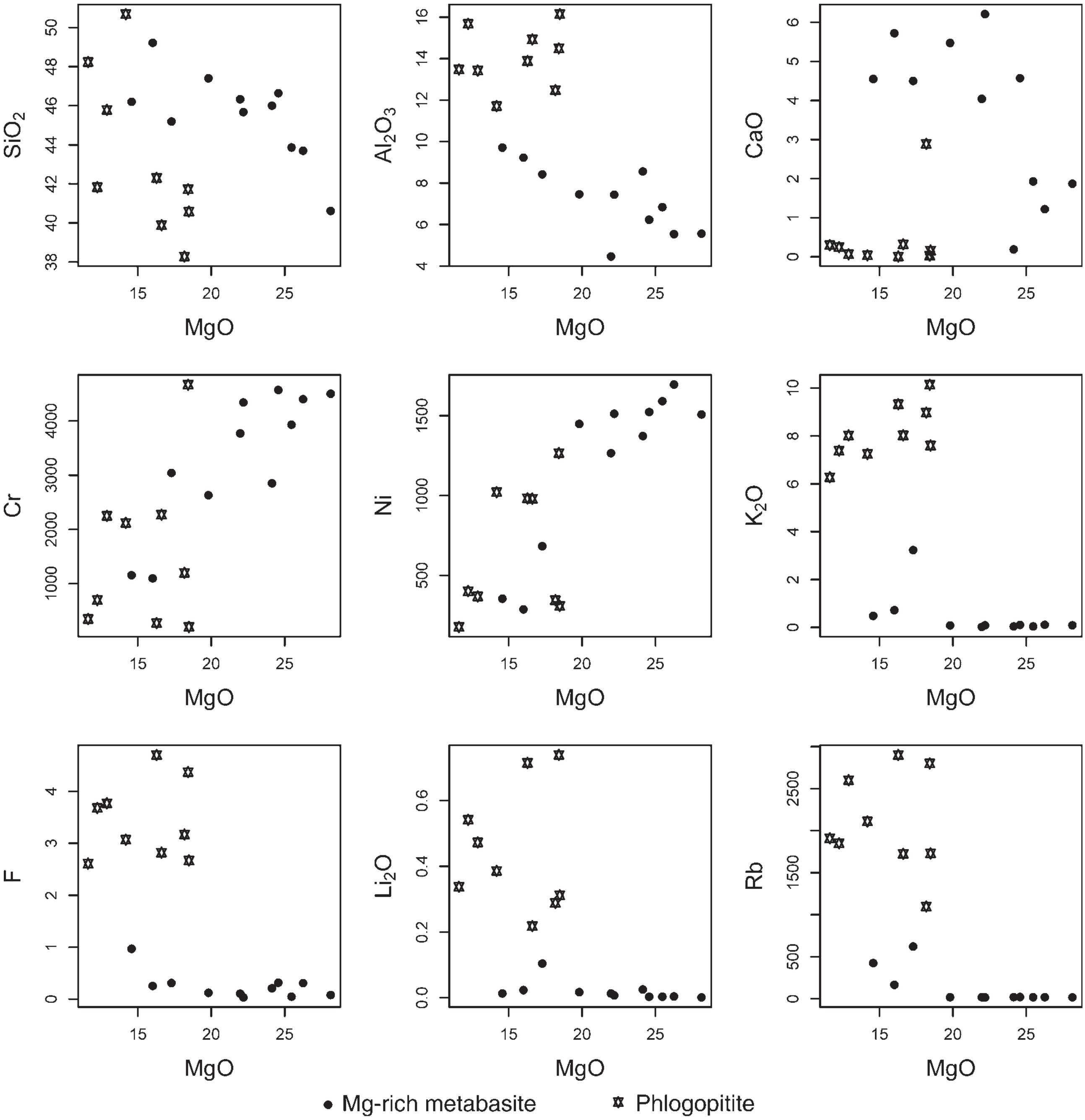


Figure 10. Comparison of metabasite and phlogopitite composition in oxide (element) vs. MgO diagrams.

Phlogopite schist (and some of the phlogopite-bearing metabasic rocks), quartz-tourmaline rocks, and phlogopite-tourmaline schists are among the rocks of low magnetic susceptibility (0.258–0.427). Amphibolite shows a value of 0.506, while the lowest value, 0.085, was measured in quartz-muscovite schist.

Mineralogy of the Kafubu emerald area

Mineral composition was analyzed by EMPA in the laboratories of the Czech Geological Survey, supervised by I. Vavřín, using an electron microprobe CamScan 4-90DV equipped with Link-ISIS Oxford Instruments (EDX). An accelerating voltage of 15 kV, a beam current of 3 nA, and a counting time of 80 seconds were used. Natural minerals were used as standards for Si (quartz), Al (corundum), Ca (wollastonite), Ti (rutile), K (adularia; orthoclase – MAC registered standard No. 2726), and Na (albite-MAC registered standard No. 2726), while synthetic olivines were used for Mg, Fe, and Mn (forsterite, fayalite and tephroite). The ZAF correction program was used. The analytical uncertainties (2 sigma) for oxide abundances similar to those of hornblende (Table 8) are 0.3–0.4 for SiO_2, Al_2O_3 and Na_2O, and 0.2 % for TiO_2, FeO, MgO, CaO and K_2O.

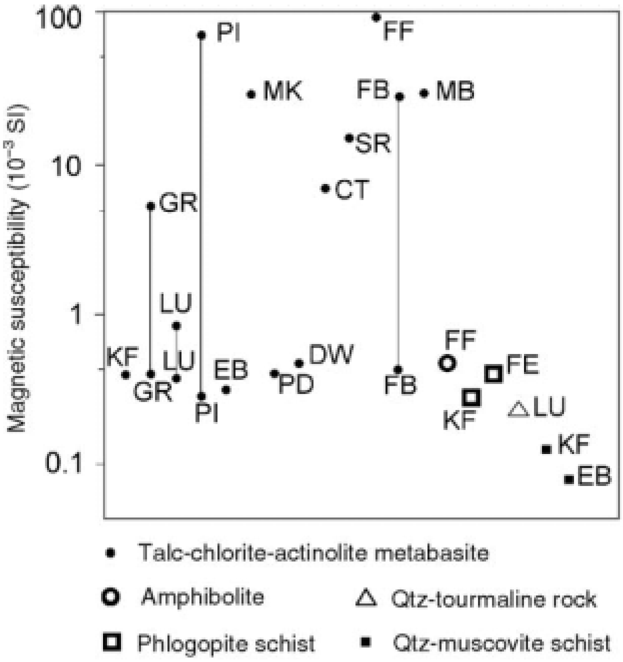


Figure 11. The magnetic susceptibility values of the main rock types from the Kafubu area. Data for various rock types from individual mines are plotted along the horizontal axis. Note two contrasting populations of metamorphosed basic rocks, which differ in their magnetite content and in their magnetic susceptibility. Explanation of the symbols: CT – Chantete mine, DW – Dabwisa, EB – Ebenezer mine, FB – Fibolele mine, FE – Fwaya-Fwaya Ext.10, FF – Fwaya-Fwaya, GR – Grizzly mine, KF – Kafubu mine, LU – Lumpuma mine, MB – Mbuwa mine, MK – Miku mine, PD – Pit No. D8, PI – Pirala mine, SR – Solid Rock mine.

Chemical composition of the major minerals

Besides beryl, which is of primary interest, we have analyzed number of major minerals from the rocks hosting the emerald mineralization. The knowledge of their crystal chemistry is important for understanding the mineralization processes and for planning exploration activities.

Tourmaline

Black tourmaline is a ubiquitous mineral in the Kafubu emerald area. It is a major constituent of the banded quartz-tourmaline rocks and the quartz-tourmaline veins (Figs. 12, 13f); in other rock types (pegmatites, phlogopite schists, amphibolites, muscovite-biotite-quartz schists) it occurs only as a minor or accessory component.

With the exception of pegmatite tourmaline and one exceptional Li-tourmaline, the tourmalines of this area have similar compositions with a relatively narrow range in Mg/Fe ratios and moderate variations in Al contents (Fig. 14, Table 5). Tourmalines have Mg > Fe (Mg = 1.54–2.54 apfu, Fe = 0.71–1.26 apfu), highly variable Ca (0.05–0.48 apfu), and low to moderate X-site vacancy (up to 34 %, but mostly 0–25 %). K_2O concentration is negligible, reaching up to 0.13 wt.%, but mostly ranging between 0.0–0.05 wt.%. Contents of TiO_2 are usually low to moderate (0.0–1.23 wt.%, typically 0.30–0.70 wt.%). MnO is very low; its concentrations go up to 0.26 wt.%, but are usually below the detection limit. Cr_2O_3 is low to relatively high (0.0–2.83 wt.%), but mostly ranging between 0.10–0.50 wt.%, the maximum values being found in the tourmalines of emerald-bearing phlogopite schists. Zoning (see below) is characterized by step-growth in Ca (Ti) and a decrease in Na, X-site vacancy, and Al. Core compositions mostly correspond to Fe-rich, slightly X-site vacant dravite, while the rims are Ca-Fe-rich dravite. Concerning the *V-* and *W-sites,* moderate to high F contents are indicated from several wet analyses, the rest being OH; the substitution of O for OH is probably rather limited.

Tourmalines will be described from the following mineral assemblages:

1. Banded tourmalinite and quartz-tourmaline rock (samples ME3 – Melai mine, KF2, KF5, Kafubu mine).
2. Quartz-tourmaline (beryl) veins (samples BD1a – Bedrock mine, MB2 – Mbuwa mine, KA3b – Kamakanga mine, MA3b – Mantenke mining, ME5 – Melai mine, GR4 – Grizzly mine, PI4 – Pirala mine).
3. Phlogopite schist, tourmaline-beryl-phlogopite rocks (samples KF4a, KF4b, KF7B, Kafubu mine, MK1 – Miku mine).
4. Amphibolite (samples GR1 – Grizzly mine, PI1 – Pirala mine, LU3 – Lumpuma mine, KF10 – Kafubu mine).
5. Talc-actinolite-chlorite metabasite (sample ME4 – Melai mine).
6. Muscovite-biotite-quartz schist (samples MB4a, MB4b – Mbuwa mine).
7. Late extension tourmaline vein (sample KA14 – Kamakanga mine).
8. Pegmatite (sample FF2 – Fwaya-Fwaya).
9. Cr-muscovite-tourmaline-quartz rock (sample CA1 – Chawuma pit).
10. Li-tourmaline (sample MA1 – Mantenke mining).

1. Banded tourmalinite and quartz-tourmaline rock

This tourmaline is prismatic to acicular, euhedral to subhedral, about 1–2 mm long. Pleochroism is pronounced, ε-smoky or pale brown, ω-deep olive green, cores are lighter. These tourmalines are on average slightly more ferroan than those in amphibolites, phlogopite schists, and the majority of quartz-tourmaline veins, although they also correspond to (Ca-) Fe-rich dravite. They display moderate to relatively high X-Ca (0.10–0.42 apfu), highly variable X-site vacancy (0–36 %), and optical and compositional zoning characterized by an increase in Ca and a decrease in Al and X-site vacancy from center to rim. They contain increased TiO_2 (0.35–1.39 wt.%) but very low Cr_2O_3 (up to 0.14 wt.%, mostly below detection limit).

2 and 3. Quartz-tourmaline (beryl) veins and phlogopite schist

The tourmaline from both quartz-tourmaline ± beryl veins and phlogopite schist is characterized by significant compositional variations in Ca-Na-Al-X_{Mg} and very conspicuous, principally two-step discontinuous zoning. Tourmaline I (core) is bluish, slightly to moderately pleochroic, ε-colourless to pinkish, ω-pale blue to bluish gray. Tour-

Table 5. Chemical composition of tourmaline.

Sample	GR4	GR4	KF4a	KF4a	KF4a	KA14	KF5	KF5	GR1	ME4	FF2	MA1	MA1	CA1
Rock	1(c)	1(r)	2(c)	2	2(r)	3	4(c)	4(r)	5	6	7	8(c)	8(r)	9
SiO_2	36.55	36.68	37.67	36.85	36.82	35.68	36.48	35.88	36.49	35.40	33.92	37.15	37.16	33.69
TiO_2	0.00	0.35	0.00	0.79	0.25	0.49	0.35	0.45	0.90	0.84	0.19	0.18	0.38	0.47
Cr_2O_3	0.15	0.00	1.30	2.76	1.45	0.00	0.00	0.00	0.21	1.07	0.00	0.00	0.00	1.43
Al_2O_3	31.25	27.96	30.78	27.46	28.64	27.65	32.41	28.99	30.12	29.29	31.50	36.63	36.66	29.72
FeO_{tot}	6.90	6.83	5.41	7.12	5.89	8.57	6.96	8.05	5.92	4.53	14.78	2.07	4.25	16.36
MnO	0.00	0.00	0.19	0.00	0.00	0.00	0.00	0.12	0.00	0.00	0.78	4.11	2.03	0.32
MgO	7.20	9.63	8.55	8.74	9.33	8.95	6.48	7.78	8.52	9.14	0.56	0.09	0.52	1.67
CaO	0.91	2.48	0.83	1.60	1.88	2.44	0.32	1.80	1.62	2.00	0.08	0.28	0.37	1.11
Na_2O	1.97	1.70	2.00	1.88	1.97	1.49	1.81	1.96	1.81	1.62	2.25	2.50	2.59	2.04
K_2O	0.00	0.00	0.10	0.00	0.09	0.04	0.00	0.07	0.04	0.00	0.06	0.00	0.00	0.04
H_2O_{calc}	3.62	3.61	3.71	3.65	3.65	3.56	3.63	3.57	3.65	3.58	3.43	3.61	3.64	3.47
$B_2O_{3\ calc}$	10.49	10.48	10.76	10.59	10.58	10.33	10.52	10.35	10.57	10.38	9.93	10.46	10.56	10.07
total	99.04	99.72	101.30	101.44	100.55	99.20	98.96	99.01	99.84	97.85	97.49	97.08	98.17	100.39
Si	6.054	6.085	6.086	6.050	6.048	6.005	6.025	6.022	6.000	5.930	5.937	6.175	6.122	5.815
Ti	0.000	0.043	0.000	0.097	0.031	0.062	0.043	0.057	0.111	0.106	0.025	0.023	0.047	0.061
Cr	0.020	0.000	0.166	0.358	0.188	0.000	0.000	0.000	0.027	0.142	0.000	0.000	0.000	0.196
Al	6.100	5.467	5.862	5.313	5.544	5.485	6.309	5.735	5.837	5.784	6.498	7.175	7.119	6.045
Fe^{2+}	0.956	0.947	0.732	0.977	0.809	1.206	0.961	1.130	0.814	0.634	2.163	0.288	0.586	2.362
Mn	0.000	0.000	0.025	0.000	0.000	0.000	0.000	0.017	0.000	0.000	0.116	0.579	0.284	0.047
Mg	1.779	2.382	2.060	2.140	2.283	2.246	1.596	1.946	2.088	2.284	0.145	0.021	0.129	0.429
Ca	0.162	0.441	0.144	0.282	0.330	0.440	0.057	0.324	0.285	0.358	0.015	0.049	0.066	0.205
Na	0.632	0.548	0.626	0.599	0.628	0.486	0.579	0.638	0.578	0.526	0.764	0.805	0.827	0.683
K	0.000	0.000	0.020	0.000	0.019	0.009	0.000	0.014	0.008	0.000	0.014	0.000	0.000	0.009
OH	4.000	3.995	3.999	3.997	3.999	3.997	3.999	3.997	4.004	4.000	4.004	4.002	4.001	3.995
B	2.999	3.001	3.001	3.001	2.999	3.001	2.999	2.999	3.000	3.001	3.000	3.001	3.003	3.000
total	22.702	22.909	22.721	22.815	22.879	22.936	22.567	22.878	22.751	22.765	22.680	22.118	22.184	22.847

(c) – centre, (r) – rim, 1 – quartz-tourmaline vein, 2 – phlogopite schist, 3 – tourmaline extensional vein, 4 – banded quartz-tourmaline rock, 5 – amphibolite, 6 – metabasite, 7 – pegmatite, 8 – yellow tourmaline from Li-pegmatite, 9 – Cr-muscovite-tourmaline rock
Numbers of ions were calculated on the basis of 27 O and 4 OH assuming stoichiometric amount of B

maline II (rim) is strongly pleochroic, ε-pale brown, brown-green, ω-deep brown or olive green, displaying a concentric oscillatory arrangement of multicoloured bands of variable thickness (brown, green, yellow-green). Compositionally, tourmaline I corresponds to Ti-Cr-poor (X-site slightly vacant) Fe-rich dravite with Al > 6 apfu and very low Ca. The multicoloured tourmaline II is Ca-Fe-rich dravite. It has mostly Al < 6 apfu, very low X-site vacancy and 0.20–0.47 Ca apfu. It frequently contains increased TiO_2 (up to 1.8 wt.%) and Cr_2O_3 (up to 2.83 wt.%).

4. Amphibolite

These tourmaline crystals are mostly euhedral, prismatic, of sizes from several mm up to about 1 cm long, weakly to strongly pleochroic, ε-pink pale brown, ω-light to deep olive green. They display relatively uniform chemical compositions, being on average richer in Mg than tourmalines from other rocks at relatively high X-Ca (0.17–0.35 apfu) and low to moderate X-site vacancy (5–23 %). Compositional zoning is insignificant. Elevated TiO_2 (0.4–1.0 wt.%) and Cr_2O_3 (up to 0.9 wt.%) were observed. These tourmalines are Ca-Fe-rich dravite.

5. Talc-actinolite-chlorite metabasite

The tourmaline of these rocks occurs as black prismatic crystals up to several cm long. They display weak pleochroism, ε-pink, ω-pale brown, and small compositional variations. They have Al < 6, high X_{Mg}, high Ca (0.31–0.42 apfu), and low to moderate X-site vacancy (5–19 %). They contain elevated Cr_2O_3 (0.14–1.1 wt.%). These tourmalines are Ca-Fe-rich dravite, similar to those in the amphibolites, but somewhat richer in Mg and Ca.

6. Muscovite-biotite-quartz schist

Accessory tourmaline in this rock type forms prismatic crystals up to 0.5 mm long. It is often zoned with darker cores, the colour is pale brown to olive green. Tourmaline from muscovite-biotite-quartz schists shows moderate X-site vacancy (20–25 %), and low Ca (0.04–0.11 apfu). Compositional zoning was observed (increase in Ca toward

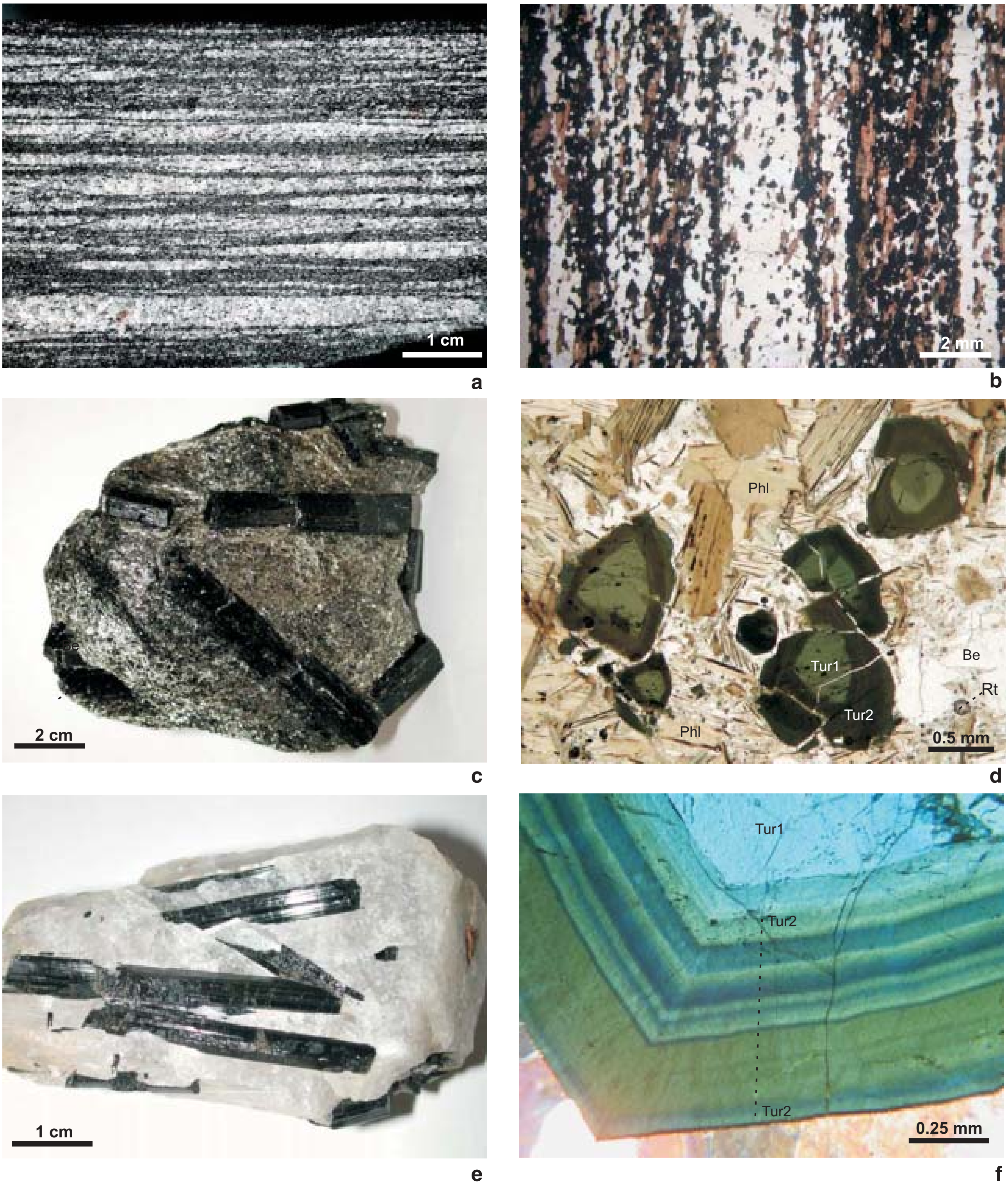


Figure 12. Various tourmaline samples from the Kafubu area: a, b – Characteristic texture of quartz-tourmaline banded rock, Kafubu mine, sample KF5. b – Microscopic image of the same rock. Accessory rutile, significantly enriched in Nb and Ta in its rims, is intergrown with dominant quartz and tourmaline. c – Phlogopite schist with prismatic tourmaline crystals from the Chantete mine. The crystals are black, euhedral, partly fractured, up to 10 cm long. d – Thin section of phlogopite rock with tourmaline and beryl from the Kafubu mine (sample KF7a). Two-step discontinuous zoning of tourmaline is characteristic for majority of tourmaline crystals from phlogopite schists and quartz-tourmaline veins. The lighter core corresponds to Fe-rich dravite, the darker rim is Ca- and Fe-rich dravite with increased concentration of Ti and Cr. e, f – Sample from the main quartz-tourmaline vein at the Grizzly mine; microscopic image of tourmaline crystal shows a uniform unzoned core (tourmaline 1) and complicated oscillatory zoning of tourmaline 2 (sample GR4, crossed polaroids). Photos by V. Žáček.

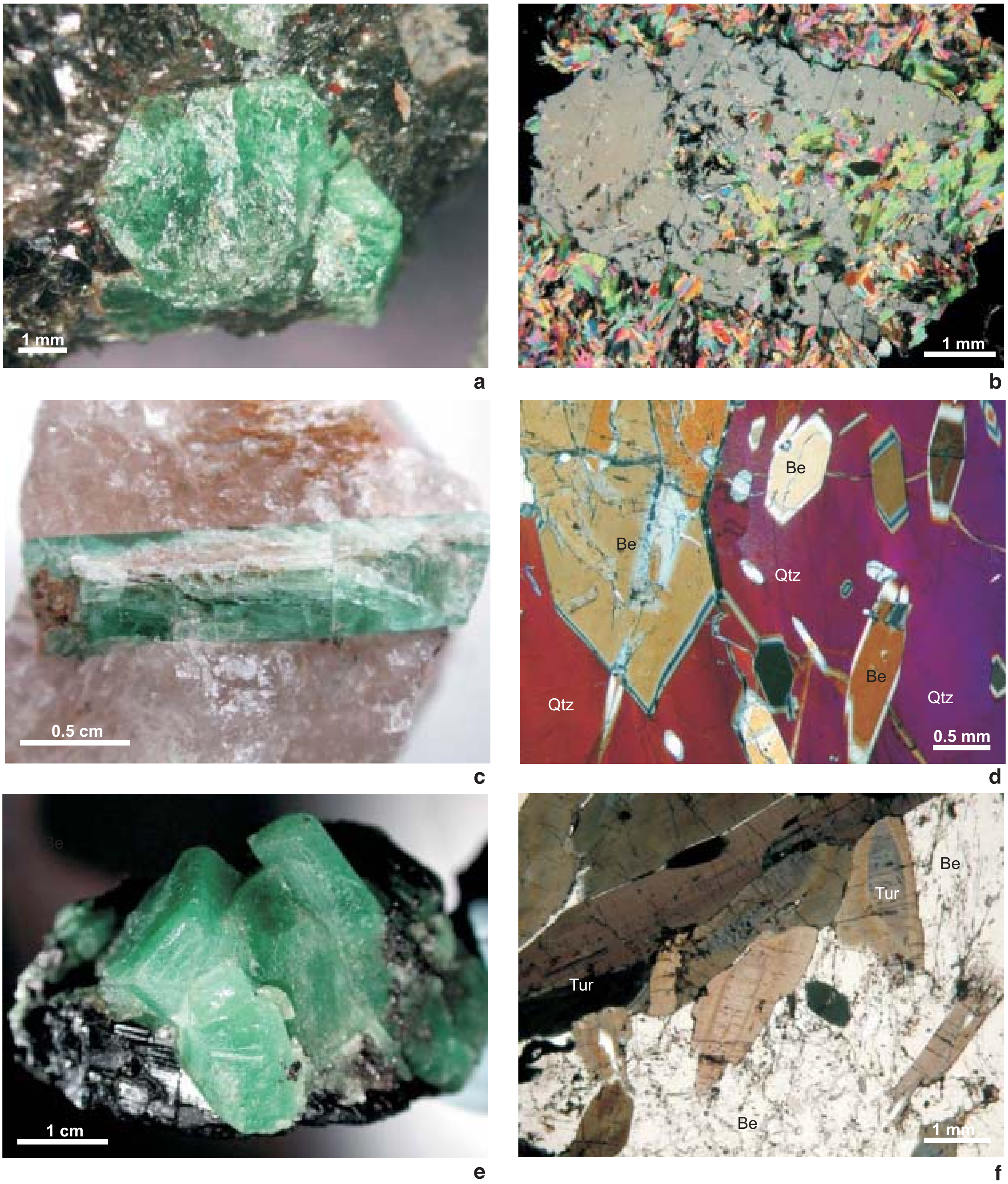


Figure 13. Various emerald samples from the Kafubu area: a – Emerald crystal in phlogopite rock. The specimen was sampled at the recently abandoned Kamakanga Old Pit-extension. The emerald crystals in phlogopite rocks represent the majority of gem-quality stones obtained. b – Thin section of emerald crystal with abundant phlogopite inclusions, Miku mine, sample MK6b, crossed polaroids. The photo shows the step-growth crystal faces and partial fracturing of emerald crystal. c – Prismatic crystal of blue-green beryl grown in quartz. The sample comes from vertical quartz-tourmaline vein from the Kafubu mine. d – Euhedral crystals of green beryl grown in quartz, Kamakanga Old Pit-extension, sample KA1, crossed polaroids. e – Emerald-tourmaline aggregate from the Kafubu area with well developed hexagonal prismatic crystals. f – Thin section of beryl (emerald)-tourmaline aggregate from Kamakanga mine, sample KA3a. Textures indicate that beryl crystallization post-dates tourmaline. Fluid and mineral inclusions and dense fracturing in beryl are frequent. Photos by V. Žáček.

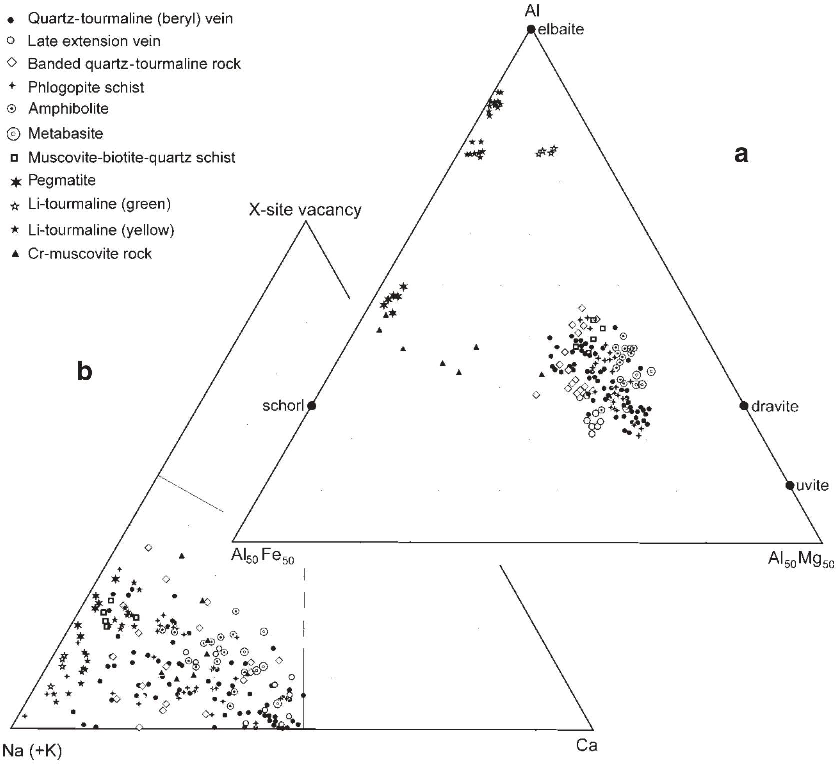


Figure 14. a – Al–Fe^{tot}–Mg diagram for tourmaline from Kafubu. b – Na-Ca-X-site vacancy diagram for tourmaline from Kafubu.

rim), but the differences are small. This tourmaline corresponds to Fe-rich dravite.

7. Late extensional veins

The tourmaline of late extensional veins forms crystals of unusual platy to tabular/platy habit, arranged in a herringbone pattern. It is Ca-Fe-rich dravite characterized by Al < 6 apfu, very low vacancies in the X-site (less than 16 % but mainly 3–10 %), high Ca, 0.22–0.46 apfu, and elevated TiO_2 (0.34–0.58 wt.%).

8. Pegmatite tourmaline

The tourmaline from the pegmatites is quite different from that in the other rocks. Tiny, euhedral, prismatic to acicular crystals from the Fwaya-Fwaya garnet-bearing pegmatite display strong pleochroism, ε-pale pink grey, ω-black. This tourmaline corresponds compositionally to nearly pure schorl, with Al > 6, Mg = 0.13–0.16 apfu and Fe = 2.07–2.23. It is also characterized by a relatively high X-site vacancy of 18–30%, and extremely low Ca (0.014–0.03 apfu). In contrast to other Kafubu tourmalines it contains increased MnO (0.44–1.23 wt.%). This schorl is similar to schorl-dominated tourmalines from the border zone of the zoned petalite Tanco pegmatite (Selway et al. 2000). The nearly complete absence of coloured (elbaitic) tourmaline, which characterizes various zones in the Tanco pegmatite, indicates that the pegmatites in the Kafubu area are less evolved. Large, stubby euhedral crystals of black tourmaline up to 10 cm long have been found in some Fwaya-Fwaya pegmatite dikes, though none were observed by the present authors.

9. Cr-muscovite-tourmaline-quartz rock

Black prismatic tourmaline associated with chromian muscovite in the quartz-tourmaline-muscovite veins (Chawuma pit) displays increased MnO (0.16–0.53 wt.%), highly variable Mg (0.18–1.40 apfu), increased Ca (0.12–0.26 apfu), X-site vacancis of 10–34%, and increased Cr_2O_3 (0.20–2.04 wt.%).

10. Li-tourmaline

Li-tourmaline is very rare in the Kafubu area. Yellow and green tourmaline occurs at Pit No. 1 in the Mantenke Mining Co. as loose crystals in the lateritic soil. This tourmaline contains increased Al_2O_3 (35.4–40.2 wt. %) and very low FeO (0.34–5.39 wt.%), MgO (0.09–2.80 wt.%), but strongly increased MnO (0.81–4.44 wt.%). This tourmaline is Na-dominant, Mn-rich elbaite, poor in Ca (0.02–0.11 apfu). The green tourmaline is richer in Fe and Mg and poorer in Mn than the yellow variety. Compositional zoning (from center to rim) is characterized by a decrease in Al and Mn, and an increase in Fe and Mg.

Beryl and emerald

Beryl occurs in phlogopite schist, and in pegmatite and quartz-tourmaline veins (Fig. 13). White, yellowish to bluish “common” beryl forms well developed hexagonal prismatic to short prismatic crystals up to 30 cm long, mainly in the pegmatite of the Fwaya-Fwaya mine. The most important mode of green beryl and emerald occurrence is confined to the peripheral zones of the pegmatite, and to the phlogopite reaction zones developed between the quartz-tourmaline veins and metabasite.

Beryl and emerald occur as euhedral to subhedral hexagonal crystals composing aggregates of several to tens of individuals. Step-growth crystal surfaces are frequently observed. The crystal size varies from less than 1 mm to several cm, though we have seen crystals about 10 cm long in the Kagem mines. Exceptionally large emerald crystals up to 60 cm long were found in the phlogopite schist at the Kamakanga Old Pit during the 1980s, as reported by a local mine manager. The colour of the beryl strongly varies, depending on Cr-content, from bluish or white-yellowish (rarely colorless) through bluish pale green, and medium to deep green. The irregular colouration of crystals is frequent; larger crystals commonly have a lighter core of yellow to pale blue beryl and a well-coloured deep green rim. Besides fluid inclusions of mostly equant or prismatic negative crystal shape, beryl frequently includes platy, euhedral to subhedral, slightly pleochroic (pale brown to nearly colourless) phlogopite. Milisenda et al. (1999) also reported rod-like actinolite-tremolite inclusions. Examples of other

Table 6. Chemical composition of light to dark green beryl and emerald from quartz-tourmaline veins and from phlogopite rocks

Sample	MA3b	KA1	GN6	KA3b	MB2	KA-8	MK6b	BD1a	LU2	MK6b	KF4a	FB4	FB4	KF4a
Rock	vein	vein	vein	vein	vein	vein	phlog.	vein	phlog.	phlog.	phlog.	phlog.	phlog.	phlog.
Colour	light	medium	light	medium	light	medium	medium	medium	medium	medium	dark	dark	dark	dark
SiO_2	66.23	64.86	65.24	65.15	64.84	64.28	64.05	64.65	65.93	64.83	65.10	65.29	64.82	65.40
TiO_2	0.00	0.00	0.00	0.00	0.00	0.00	0.00	0.00	0.00	0.00	0.00	0.00	0.00	0.00
Cr_2O_3	0.11	0.13	0.15	0.20	0.21	0.24	0.30	0.40	0.41	0.44	0.54	0.66	0.76	0.77
Al_2O_3	14.94	14.85	15.37	13.60	14.67	13.96	15.36	14.32	14.30	15.17	13.96	14.67	14.82	14.33
FeO_{tot}	1.40	0.88	0.90	1.88	0.93	1.77	0.76	0.84	1.18	0.79	1.29	1.13	1.18	1.36
MnO	0.00	0.00	0.00	0.00	0.00	0.00	0.00	0.23	0.16	0.00	0.12	0.00	0.00	0.00
MgO	2.49	2.22	1.86	2.64	2.39	2.29	1.55	2.42	2.31	1.76	2.30	2.07	2.17	2.31
CaO	0.00	0.00	0.00	0.14	0.00	0.00	0.00	0.00	0.08	0.00	0.00	0.00	0.00	0.00
Na_2O	2.19	1.80	1.73	2.04	2.10	2.22	1.84	2.16	2.09	1.79	2.02	1.84	1.72	1.90
K_2O	0.09	0.00	0.06	0.00	0.00	0.16	0.00	0.00	0.04	0.00	0.00	0.00	0.00	0.00
BeO_{calc}	13.83	13.48	13.58	13.51	13.51	13.38	13.36	13.47	13.68	13.50	13.50	13.58	13.55	13.61
Total	101.28	98.22	98.87	99.16	98.65	98.28	97.23	98.49	100.18	98.30	98.82	99.23	99.03	99.66
Si	5.982	6.009	6.001	6.024	5.995	6.002	5.991	5.997	6.018	6.001	6.025	6.004	5.978	6.002
Ti	0.000	0.000	0.000	0.000	0.000	0.000	0.000	0.000	0.000	0.000	0.000	0.000	0.000	0.000
Cr	0.008	0.010	0.011	0.015	0.015	0.017	0.022	0.030	0.030	0.032	0.039	0.048	0.055	0.056
Al	1.591	1.622	1.666	1.482	1.598	1.536	1.694	1.565	1.539	1.655	1.522	1.591	1.610	1.549
Fe^{2+}	0.106	0.068	0.069	0.146	0.072	0.138	0.059	0.065	0.090	0.061	0.100	0.087	0.091	0.104
Mn	0.000	0.000	0.000	0.000	0.000	0.000	0.000	0.018	0.012	0.000	0.010	0.000	0.000	0.000
Mg	0.336	0.307	0.254	0.363	0.329	0.318	0.216	0.335	0.314	0.244	0.317	0.283	0.299	0.316
Ca	0.000	0.000	0.000	0.014	0.000	0.000	0.000	0.000	0.008	0.000	0.000	0.000	0.000	0.000
Na	0.384	0.323	0.309	0.366	0.377	0.401	0.334	0.389	0.370	0.321	0.362	0.327	0.308	0.337
Be	3.000	2.999	3.001	3.000	3.000	3.001	3.001	3.001	2.999	3.001	3.001	3.000	3.001	3.000
Total	11.416	11.337	11.318	11.410	11.387	11.432	11.318	11.400	11.385	11.316	11.376	11.340	11.343	11.364

(vein) – vein samples, (phlog.) – phlogopite rock samples
Number of atoms (pfu) were calculated on the basis of 18 oxygen atoms assuming stoichiometric amount of 3 Be.

rare inclusions are euhedral apatite, euhedral to subhedral niobian rutile, anhedral quartz, and relic anhedral phenakite in a single sample (PN 9 from the Pioneer mine). Textural criteria in samples containing beryl in association with tourmaline indicate that beryl post-dates tourmaline; in some cases the tourmaline was fractured prior to beryl crystallization, and fragments of tourmaline crystals are enclosed in beryl. Euhedral tourmaline inclusions in beryl have not been found.

More than 100 microprobe analyses of beryl and emerald in 17 samples included in this study show Cr_2O_3 and FeO_{tot} concentrations ranging from less than 0.08 to 0.78 wt.% and 0.36 to 2.21 wt. %, respectively, with elevated MgO (1.09–2.69 wt.%) and Na_2O (1.25–2.22 wt. %) (Table 6). Rare alkali metal elements (Li, Rb, Cs) and H_2O analysis in emerald would require special micro-beam techniques, because of abundant mineral inclusions and small-scale compositional variation. This specialized topic was beyond the scope of our project.

Figure 15 shows the composition of 14 Kafubu emerald and beryl samples in terms of the sum of mainly divalent ions entering octahedral position versus Na + K + Ca contained in structural cavities (Černý 2002). Symbols for individual samples represent averages of several (3 to 11) spot analyses. Though the ratios are near unity, several samples showing the most extensive substitution indicate a steeper trend possibly corresponding to a partial substitution of Fe^{3+} for Al, as cited by Barton and Young (2002) for some emeralds from metamorphic phlogopite schists. This would correspond to the indications of ferric iron in polarised spectra.

Calligaro et al. (2000) analyzed 11 emerald samples from Zambia by PIXE/PIGE, using an external 3 MeV proton micro-beam. They determined average values for several trace elements, including the highest average content of cesium (1150 ppm) relative to other world-wide emerald localities, a high lithium content (> 500 ppm), and increased rubidium (> 100 ppm) and vanadium (180 ppm), which they consider as distinct trace element fingerprints for Zambian emeralds.

We have subdivided our beryl specimens as follows:

1. Medium to dark green emerald from phlogopite schists (samples KF4a, KF4b, and KF7b from the Kafubu mine; FB4 from the Fibolele mine; and MK6 from the Miku mine). These contain 0.12–0.76 wt.% Cr_2O_3 (mostly 0.40–0.60 wt.%; the mean of 33 analyses is 0.47 wt.%), 13.60–16.02 Al_2O_3 (mean = 14.74 wt.%), 0.36–1.47 FeO_{tot}

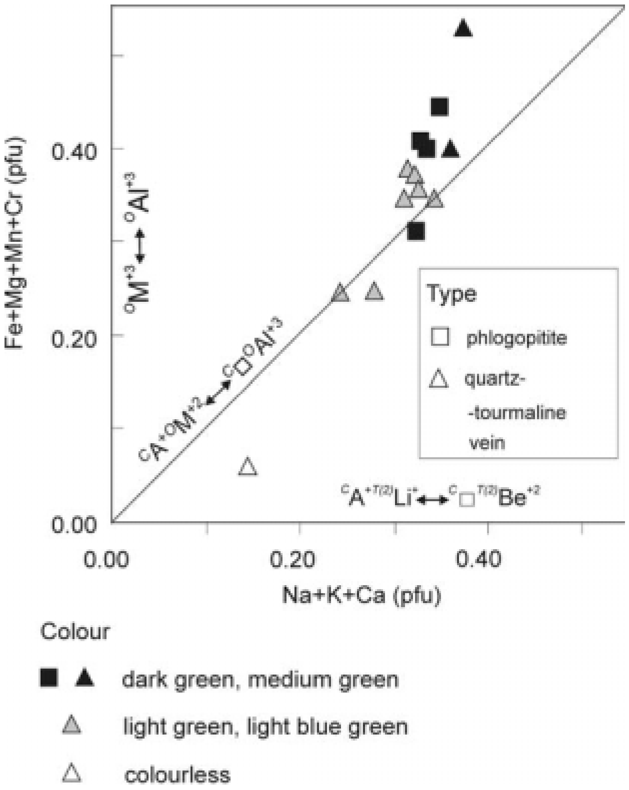


Figure 15. Beryl and emerald composition plotted in terms of transition metal and alkali elements (except Li) per formula unit (18 O). This corresponds mainly to octahedral and channel substitutions (following Barton and Young 2002). Fe is total iron. The frequency of phlogopitite vs. vein emerald types does not correspond to the actual proportion in the Kafubu area.

(mean = 1.03 wt.%), 1.46–2.53 MgO (mean = 2.06 wt.%), and 1.59–2.09 Na_2O (mean = 1.83 wt.%). The majority of gemstone-quality emeralds comes from the phlogopite schists.

2. Medium green emerald from quartz-tourmaline veins (samples KA1, KA3b, and KA8 from the Kamakanga mine, and BD1a of the Bedrock mine). These contain 0.15–0.55 wt.% Cr_2O_3 (mostly 0.20–30 wt.%; the mean value from 25 analyses is 0.23 wt.%), 13.22–15.19 Al_2O_3 (mean = 14.25 wt.%), 0.75–2.21 FeO_{tot} (mean = 1.03 wt.%), 1.87–2.64 MgO (mean = 2.21 wt.%), and 1.63–2.22 Na_2O (mean = 1.90 wt.%).

3. Light green to light blue green beryl from quartz–tourmaline veins (samples KA3b of the Kamakanga mine, BD1a of the Bedrock mine, MB2 of the Mbuwa mine, GN6 of the Gerntina mine, MA3b of the Mantenke mine, and ME5 of the Melai mine). These samples contain 0.0–0.27 wt.% Cr_2O_3 (mostly below 0.1 wt.%), 14.34–16.64 Al_2O_3 (the mean of 40 analyses is 15.44 wt.%), 0.43–1.81 FeO_{tot} (mean = 0.95 wt.%), 1.09–2.49 MgO (mean = 1.78 wt.%), and 1.18–2.19 Na_2O (mean = 1.69 wt.%).

4. Colourless (bluish) beryl as a single sample from the MR1 pit, taken from a quartz vein cutting the muscovite schist. This type of beryl displayed a markedly different composition than all other samples. It contains Cr_2O_3 below detection limit, low FeO_{tot} (0.37–0.65 wt.%), MgO (0.10–0.14 wt.%), and Na_2O (0.79–0.91 wt.%), and therefore high Al_2O_3 (17.60–18.03 wt.%).

Phlogopite

The dark mica in the phlogopite zones, partly phlogopitized metabasic rocks, amphibolite, and metasedimentary quartz-muscovite-phlogopite schist has been variously designated as biotite or phlogopite in published papers and unpublished reports. We have obtained more than 80 microprobe analyses of these dark micas from a number of samples (Table 7, Fig. 16). In the calculation of crystallochemical formulas, a uniform fluorine content of 4.7 wt.% was assumed for the phlogopite in phlogopitites. This is based on the results of fluorine determination by whole-rock wet analyses (Table 1b). We likewise assumed

Table 7. Chemical composition of phlogopite, biotite, muscovite, garnet, magnetite, and ilmenite

Sample	MK6b	KF4a	PI1	GR5	MB4a	CA1	MB4b	PN1hm	FE8hm	FF4	MB1	BD4	KF1	KF5
Rock	1	1	2	3	4	5	4	6	6	3	3	3	3	7
Mineral	Phl	Phl	Phl	Phl	Bt	Ms	Ms	Grt	Grt	Mgn	Mgn	Mgn	Ilm	Ilm
SiO_2	42.96	42.55	38.68	40.43	36.94	46.46	45.63	35.18	35.90	0.25	0.17	0.24	0.24	0.27
TiO_2	0.14	0.72	1.90	1.07	1.59	0.50	0.68	0.10	0.11	0.00	0.00	0.12	50.53	50.45
Cr_2O_3	0.31	0.44	0.16	0.44	0.00	1.98	0.00	0.00	0.00	4.94	6.34	13.61	0.14	0.14
Al_2O_3	13.23	13.11	16.57	13.92	18.53	29.41	35.44	20.34	20.11	0.14	0.00	0.00	0.00	0.00
FeO_{tot}	6.63	9.51	13.53	12.20	13.78	3.65	1.53	2.41	13.72	85.89	84.77	76.74	29.68	34.28
MnO	0.37	0.10	0.00	0.22	0.20	0.00	0.00	40.76	29.45	0.00	0.00	0.49	15.89	11.48
MgO	21.00	18.13	13.83	16.84	12.53	1.70	0.64	0.00	0.28	0.10	0.00	0.27	0.22	0.00
CaO	0.00	0.00	0.00	0.00	0.00	0.00	0.00	0.40	0.53					
Na_2O	0.00	0.12	0.21	0.00	0.12	0.38	1.93							
K_2O	10.51	10.39	10.54	9.92	10.12	10.79	8.52							
Total	95.15	95.08	95.42	95.03	93.82	94.87	94.37	99.19	100.10	91.33	91.29	91.48	96.70	96.62

1 – phlogopite schist, 2 – amphibolite, 3 – metabasite, 4 – muscovite-biotite schist, 5 – Cr-muscovite-quartz-tourmaline vein, 6 – pegmatite, 7 – banded quartz-tourmaline rock

2.0 wt.% F in mica from amphibolite and quartz-muscovite schist. The H_2O content was calculated from crystal chemistry relations, assuming (F + OH) = 4. The compositions are plotted in Fig. 16, using the Mg/(Mg + Fe) ratio (X_{Mg}) and calculated Al^{VI} content (eastonitic substitution).

The dark mica in phlogopitite and phlogopite-rich rocks has $X_{Mg} = Mg/(Mg + Fe_{total}) = 0.71–0.86$, a low Ti content, and rather high F (F > OH). With regard to Al substitution for ($Mg + Fe^{2+}$) corresponding to 20–50 % eastonite, and because of the fluorine content, this mica can be classified as eastonitic fluorophlogopite. In the present classification of micas, biotite is used as a series (group) name (Rieder et al. 1998), not as a compositional end-member. In the present case, where chemical composition is known, the name phlogopite (fluorophlogopite) should be used.

The dark micas in amphibolites have $X_{mg} = 0.63–0.67$ and 38–65 mol.% eastonite. Dark mica in the quartz-muscovite schists has $X_{mg} = 0.58$ and 79–88 mol.% eastonite (Fig. 16).

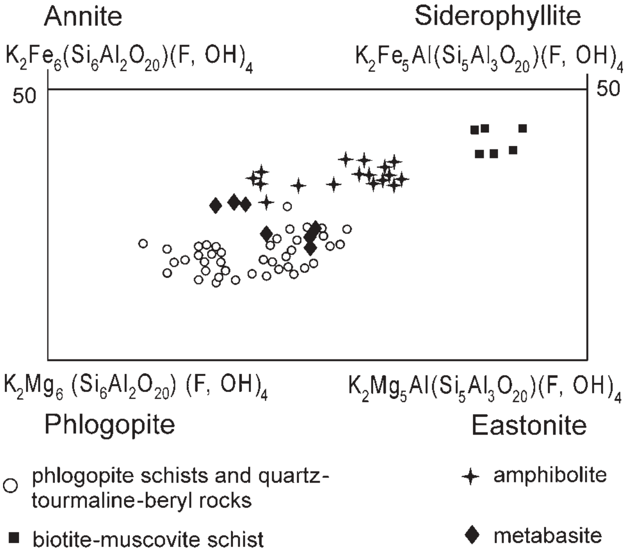


Figure 16. Plot of phlogopite composition from phlogopitites, amphibolites, and metasedimentary schists.

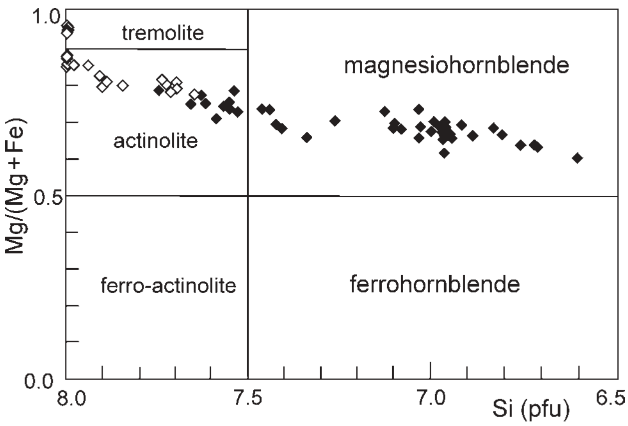


Figure 17. Chemical composition of amphibole from amphibolites (closed symbols) and from metabasites (open symbols) in the diagram of Leake et al. (1997).

Amphibole

Amphibole is a dominant constituent of amphibolite and an important mineral in some metabasites. All amphiboles analysed in this study belong to the group of monoclinic calcic amphiboles characterized by the following site occupancies: $Ca_B > 1.50$, $Ca_A < 0.50$, $Ti < 0.50$, and $(Na + K)_A < 0.50$ apfu, in accordance to the classification of Leake et al. (1997).

Amphibole from the amphibolites shows the following compositional ranges: Si = 6.60–7.75, $Mg/(Mg + Fe_{tot}) = 0.60–0.78$, Ca = 1.68–1.94, $(Na + K)_A < 0.35$ pfu. Octahedral Al exceeds calculated Fe^{3+} in all analyses. These amphiboles frequently contain increased Cr_2O_3, up to 0.68 wt.% (0.077 pfu) but mostly ranging between 0.20 and 0.40 wt.%, low TiO_2 (0.0–0.67 wt.%) and MnO (0.17–0.71 wt.%). We have identified two amphibole groups differing in composition; the first group having 6.8 < Si < 7.1 and a second group with Si approximately between 7.3–7.7 apfu (Fig. 17, Table 8). The amphibole of the first group belongs to magnesiohornblende, while the second group plots within the range of magnesiohornblende to actinolite. Actinolite in the amphibolites of this study has a composition very close to that from some of the metabasites.

Amphibole from the metabasites contains Si = 7.62–8.00, $Mg/(Mg + Fe_{tot}) = 0.78–0.86$, Ca = 1.72–1.86, Na + K = 0.15–0.33 pfu. The concentrations of Cr_2O_3 vary within the range of 0.0–0.47 (mostly 0.2–0.4), TiO_2 = 0.0–0.20, MnO = 0.0–0.32 (all in wt.%). All of these amphiboles are classified as highly magnesian actinolite, with the exception of tremolite in sample FF4 from the Fwaya-Fwaya mine.

Chlorite

Along with talc and actinolite/tremolite, chlorite is an important constituent of metabasites, and a common or minor mineral in amphibolite, phlogopite schist, and muscovite-biotite-quartz schist. In some cases (amphibolites, muscovite-biotite-quartz schists) it represents a retrograde phase. Under the microscope it is apple green, and moderately pleochroic. All chlorites analysed here are moderately to highly magnesian with Mg/(Mg + Fe) > 0.6 and Si = 2.65–3.35 apfu, corresponding to ripidolite-clinochlore-penninite (Fig. 18, Table 8).

Chlorite from the metabasites corresponds to clinochlore or penninite with Mg/(Mg + Fe) = 0.73–0.89, and Si = 2.94–3.34 apfu. It typically contains 0.6–0.9 wt.% Cr_2O_3 (total range 0.30–1.50 wt.%) and constitutes the most important Cr-phase in metabasites besides Cr-magnetite.

The chlorites in the amphibolite and phlogopite schist have a uniform composition corresponding to clinochlore ((Mg/Mg + Fe) = 0.72–0.73, Si = 2.77–3.01 apfu), and up to 0.30 wt.% Cr_2O_3. The chlorite in the muscovite-biotite-quartz schists is classed as ripidolite (Mg/(Mg + Fe) = 0.63–0.66, Si = 2.65–2.71), and is poor in Cr (0.0–0.13 wt.% Cr_2O_3).

Table 8. Chemical composition of hornblende, actinolite, tremolite, chlorite, and talc

Sample	GR1	GR1	FE1	BD4	FB1	FF4	GR5	GR5	FF4	PI1	MB4b	GR5	ME4	BD4
Rock	1	1	1	2	2	2	2	2	2	1	3	2	2	2
Mineral	Hb	Act	Hb	Act	Act	Trm	Act	Chl	Chl	Chl	Chl	Tc	Tc	Tc
SiO_2	47.43	54.28	48.26	57.50	55.51	57.68	54.36	29.27	32.25	27.29	26.63	62.25	60.68	62.26
TiO_2	0.28	0.00	0.20	0.00	0.00	0.00	0.20	0.26	0.16	0.00	0.34	0.00	0.10	0.00
Cr_2O_3	0.00	0.68	0.26	0.00	0.18	0.00	0.30	0.66	1.14	0.24	0.00	0.00	0.10	0.11
Al_2O_3	11.17	2.85	10.70	0.43	0.66	0.09	3.26	18.49	12.83	21.86	22.98	0.17	0.30	0.38
FeO_{tot}	11.74	8.73	11.70	4.56	5.84	2.08	8.16	13.54	7.11	14.21	18.60	5.34	6.31	3.00
MnO	0.67	0.19	0.27	0.13	0.25	0.23	0.20	0.00	0.00	0.17	0.16	0.00	0.03	0.00
MgO	13.12	17.53	13.46	20.77	20.06	22.86	18.08	22.25	30.72	21.82	18.32	26.75	25.17	27.42
CaO	11.21	11.51	10.87	12.06	11.66	12.61	12.00	0.13	0.00	0.00	0.09	0.00	0.00	0.00
Na_2O	1.39	0.59	1.55	0.27	0.19	0.00	0.59	0.00	0.00	0.00	0.00	0.00	0.00	0.00
K_2O	0.18	0.09	0.16	0.07	0.00	0.00	0.05	0.23	0.04	0.00	0.00	0.05	0.00	0.14
H_2O_{calc}	2.07	2.10	2.08	2.14	2.09	2.15	2.12	11.80	12.05	11.85	11.80	4.61	4.49	4.60
Total	99.25	98.56	99.50	97.93	96.44	97.69	99.36	96.63	96.30	97.44	98.92	99.16	97.17	97.90
Si	6.885	7.756	6.965	8.070	7.975	8.039	7.690	2.984	3.212	2.766	2.710	4.048	4.046	4.058
Ti	0.031	0.000	0.022	0.000	0.000	0.000	0.022	0.020	0.012	0.000	0.026	0.000	0.005	0.000
Cr	0.000	0.077	0.030	0.000	0.021	0.000	0.034	0.053	0.090	0.019	0.000	0.000	0.005	0.005
Al	1.910	0.480	1.820	0.071	0.112	0.014	0.544	2.222	1.506	2.611	2.756	0.013	0.023	0.029
Fe^{2+}	1.425	1.043	1.412	0.535	0.701	0.243	0.966	1.154	0.592	1.204	1.583	0.290	0.352	0.163
Mn	0.082	0.023	0.033	0.015	0.030	0.027	0.025	0.000	0.000	0.015	0.014	0.000	0.002	0.000
Mg	2.839	3.734	2.895	4.346	4.295	4.749	3.814	3.383	4.562	3.297	2.780	2.594	2.502	2.664
Ca	1.743	1.762	1.680	1.813	1.794	1.883	1.819	0.014	0.000	0.000	0.009	0.000	0.000	0.000
Na	0.392	0.164	0.433	0.073	0.053	0.000	0.163	0.000	0.000	0.000	0.000	0.000	0.000	0.000
K	0.034	0.017	0.029	0.013	0.000	0.000	0.010	0.030	0.006	0.000	0.000	0.004	0.000	0.012
OH	2.004	2.001	2.002	2.003	2.003	1.999	2.000	8.026	8.005	8.011	8.011	2.000	1.997	2.000
Total	17.345	17.057	17.321	16.939	16.986	16.954	17.086	17.886	17.984	17.924	17.891	8.948	8.933	8.931
XMg	0.666	0.782	0.672	0.890	0.860	0.951	0.798	0.746	0.885	0.733	0.637	0.899	0.877	0.942

1 – amphibolite, 2 – metabasite, 3 – muscovite-biotite schist
Numbers of ions were calculated on the basis 22 O and 4 OH (amphiboles), 10 O and 8 OH (chlorite) and, 10 O and 2 OH (talc).

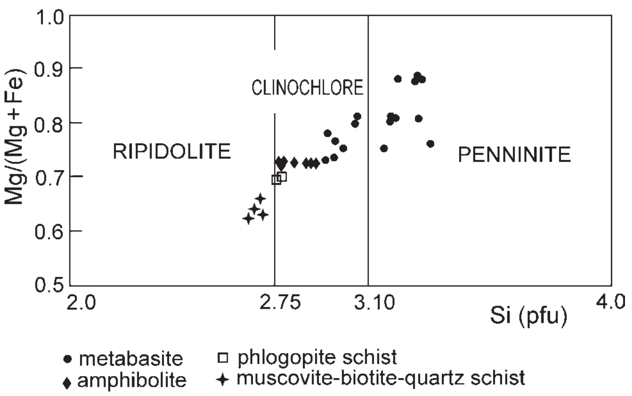


Figure 18. Chemical composition of chlorite in the diagram Si (pfu) vs. Mg/(Mg + Fe_{tot}).

Talc

Talc is abundant in the metabasite assemblage, along with chlorite, actinolite, and opaques. It contains increased FeO (1.97–6.71, typically 4–6 wt.%) at the expense of MgO and thus variable Mg/(Mg + Fe) = 0.88–0.96), and slightly elevated Al_2O_3 (mostly 0.20–0.64 wt. %; Table 8). The concentrations of other minor oxides of Mn, Cr, and Ti are very low (e.g. Cr_2O_3 ranges between 0.0–0.19 wt.%), and are usually undetectable with the microprobe.

Garnet

Spessartine-rich garnet is a minor to accessory component in some pegmatite dikes. Garnet crystals from our field area are largely less than 1 mm in diameter and anhedral, though some pegmatites in Fwaya-Fwaya mine contain garnets up to 5 mm in size. Tourmaline inclusions in garnet in the fresh FF 2 sample indicate the late crystallization of this garnet. Prominent corrosion features on the garnets from kaolinized pegmatite dikes suggest the possible complete dissolution of garnet in some samples, due to strong weathering.

Microprobe analyses, plotted as garnet end-members (Table 7, Fig. 19), show an invariable predominance of spessartine, with clusters at 58–67 and 89 to

93 mol.%. The second important component is almandine (5.8–39 mol.%), but pyrope and grossular contents are typically less than 1 mol.%. No distinct compositional zoning has been noted. The very low iron content in spessartine garnets (Sp 93 mol.%) results in a change of color from red to light beige (sample TW3HM-Twampane mine). These garnet compositions indicate the highly evolved geochemical character of these pegmatites. Notable is the absence of a relatively early garnet containing almandine > spessartine, such as tends to occur in some marginal aplitic/granitic zones of Li-pegmatites elsewhere (Whitworth 1992).

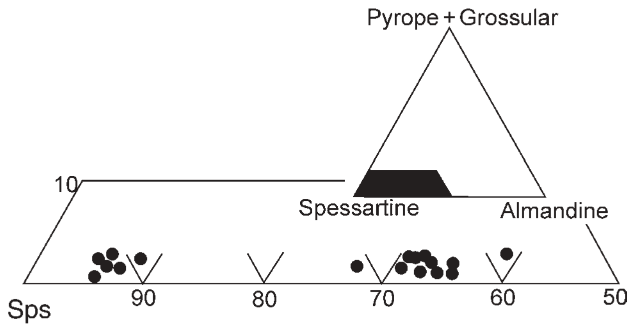


Figure 19. Plot of pegmatitic garnet composition.

Ilmenite

Ilmenite was found as a single opaque phase in some metabasites (KF1 from the Kafubu mine, and FB1 from the Fibolele mine), in some amphibolites (KA9 of the Kamakanga mine, and GE1a of the Gerntina mine), and as a rare accessory in banded quartz-tourmaline rock (KF5 of the Kafubu mine). Ilmenite contains increased Mn (2.16–15.89 wt.% MnO) corresponding to 5–35 mol.% of pyrophanite component (Table 7). High MnO concentrations were found in samples KF1 (12–15.9 wt.%) and KF5 (7.2–11.5 wt.%). Sample PI1 from the Pirala mine contains 2.4–22.5 % MnO; the associated Cr-magnetite contains 3.7–4.0 % Cr_2O_3. The MgO and Cr_2O_3 concentrations in ilmenite are low or below their detection limits (0.0–0.26 wt.% and 0.0–0.35 wt.%, respectively).

Magnetite

Magnetite comprises up to about 4 % of the total volume in the metabasites, and is also present as a rare accessory phase in amphibolites (sample KF10 from the Kafubu mine). It forms euhedral to subhedral crystals from 0.01 mm to about 0.3 mm long, randomly dispersed in the matrix or composing crystal clusters. Magnetite from samples GR5, MB1, FF4, BD4 (from the Grizzly, Mbuwa, Fwaya-Fwaya, and Bedrock mines) contains increased, highly variable Cr_2O_3 concentrations (0.15–13.6 wt.%), though the most common Cr_2O_3 concentrations range between 4 and 7 wt.% (Table 7). Larger magnetite crystals have significantly Cr-richer cores than rims. The contents of other minor oxides are low (TiO_2 = 0.0–0.40 wt.%; Al_2O_3 = 0.0–0.33 wt.%; MnO = 0.0–0.49 wt.%, MgO = 0.0–0.26 wt.%). An inclusion of Ni-bearing magnetite, 80 by 30 microns in size, was found in sample BD4 (3.8–3.9 wt.% NiO). It is notable that this magnetite inclusion contained only 0.12 wt.% Cr_2O_3 compared to the 2.60–13.61 wt.% in the associated and prevailing magnetite. Magnetite found in the amphibolite sample KF10 from the Kafubu mine has Cr_2O_3 concentrations below the detection limit.

Rutile, tantalian rutile, niobian rutile

Rutile is a common accessory mineral occurring in nearly all rock types, with the exception of metabasites. Rutile from the amphibolites (GR1, GR6, KF1, PI1, from the Grizzly, Kafubu, and Pirala mines) contains 0.19–0.72 wt.% Cr_2O_3, 0.45–1.13 wt.% FeO, and there is no detectable Nb or Ta. Rutile from the muscovite-biotite-quartz schist is poor in Cr and Fe. The phlogopite rocks and quartz-tourmaline veins associated with emerald mineralization contain rutile that frequently has increased Cr_2O_3 (1.7–3.4 wt.%), but low FeO (0.28–0.69 wt.%).

Rutile in the pegmatites (TW3HM of the Twampane mine), banded quartz-tourmaline rocks (KF2, KF5-Kafubu mine), and the quartz-tourmaline veins (GA1-Gems of Africa) commonly contain notable concentrations of Nb and Ta (several wt.%), and elevated FeO (1.8–5.0 wt.%). These compositions correspond to tantalian rutile (= strüverite) and niobian rutile (= ilmenorutile). In banded quartz-tourmaline rocks, the highest Fe, Nb, and Ta concentrations are restricted to the rims of grains. Pegmatitic tantalian rutile in sample TW3HM forms short prismatic, black and highly lustrous crystals up to 1.5 mm long, with a red brown color in thin splinters. This specimen exhibits strong multiple compositional zoning associated with variations in Ta, Nb, Ti, and Fe content. Semiquantitative analyses gave (in wt.%): 84.6 TiO_2, 3.7 FeO, 0.3 MnO, and Ta > Nb.

Muscovite

Muscovite, in bladed aggregates up to 20 cm across, occurs in several quartz-tourmaline veins containing only minor tourmaline. Muscovite in books ca. 5 cm long, grouped in aggregates, also occur in some quartz-feldspar-muscovite pegmatites. Table 9 presents minor- and trace-element analyses of coarse muscovite, including three samples from quartz-tourmaline veins (KA 7, KA 11, and GN 2, from the Kamakanga and Gerntina mines), and sample FF5 from a quartz-feldspar-muscovite pegmatite (+ tourmaline and garnet) at the Fwaya-Fwaya mine.

The high abundances of Li, Rb, Be, and Nb in the muscovite of the quartz-tourmaline veins are important, as they reveal a close relationship between the quartz-tourmaline veins and the quartz-feldspar-muscovite pegmatites.

Muscovite is also abundant in muscovite-biotite-quartz schists. This muscovite contains low Fe, Mg, and Ti, but increased Na_2O (1.43–2.00 wt.%). Chromian muscovite from sample CA1 contains 1.08–1.98 wt.% Cr_2O_3, 3.18–4.16 wt.% FeO, 1.69–2.07 wt.% MgO, and lowered Al_2O_3 (28.56–29.41 wt.%); see Table 7.

Table 9. Minor- and trace-element analyses of muscovite from quartz-tourmaline veins and pegmatite (ppm units, Li_2O in wt. %)

Sample	KA7	KA11	GN2	FF5
Li_2O, wt.%	0.195	0.211	0.164	0.149
Be	37.6	59.6	39.7	32.3
Cr	6	35	5	< 2
Ni	73	61	36	28
Cu	8	11	5	5
Zn	334	202	121	432
As	4	5	4	5
Rb	2068	2058	2459	2450
Sr	19	14	16	10
Y	< 1	< 1	< 1	< 1
Zr	< 1	< 1	< 1	< 1
Nb	173	126	106	318
Mo	< 1	< 1	< 1	< 1
Sn	< 2	15	26	5
Pb	16	13	7	4
U	4	7	5	5

Plagioclase

Plagioclase (oligoclase-sodic andesine, 25–38 An) occurs in the amphibolites. The plagioclase of the muscovite-biotite-quartz schists is nearly pure albite (An 3). A vein of medium-grained pinkish pure albite, about 5 cm thick, was found at the Mbuwa mine.

Minor minerals

The alphabetical listing of all minor minerals identified by microprobe analyses, microscopic study, and/or X-ray powder diffraction is summarized in Table 10. It also includes several references to previously published data. This information provides additional important characteristics of the mineralogy of the Kafubu area. The identification of tantalum and niobium minerals is of particular importance, as it proves the rare element typology of local pegmatites. The minerals identified at Kafubu for the first time are marked by an asterisk.

K-Ar age determination

The K-Ar dating of beryl/emerald mineralization was performed using coarse muscovite from a quartz-tourmaline-muscovite vein (Kamakanga mine, sample KA 11) and a coarse muscovite from albitized feldspathic pegmatite dike (Kagem mine, sample FF 5). The analyses, using isotope dilution for ^{40}Ar determination and ICP for K analyses, performed by Activation Laboratories, Ancaster, Ontario, Canada, gave dates of 447.0 ± 8.6 Ma for sample KA 11, and 452.1 ± 16 Ma for sample FF 5 (Table 11). These results show that the age of Be-mineralization is late Pan-African, which corresponds to the observation that the veins and the mineralization post-date the regional metamorphism of the Kafubu area.

The gemmological and mineralogical properties of emerald and beryl

Emerald is a green variety of beryl with the formula $Be_3Al_2(SiO_3)_6$, the colour of which is due to the replacement of aluminium by chromium and ferrous ions. According to the GIA classification only Cr-containing and Cr + V-containing green beryl can be designated as emerald (Sinkankas 1981). Gem-quality emerald is transparent and finely coloured.

Chemical analyses, and the mineralogical and gemmological properties of emerald from the Kafubu area have

Table 10. Minor minerals identified in the Kafubu emerald area

Adularia * $(K,Na)[(Si,Al)_4O_8]$	Hydrothermal, with characteristic rhomb-like crystal morphology and optical zoning; associated with secondary chlorite (after phlogopite) and bertrandite replacing beryl; tourmaline-quartz-beryl vein sample (BD1a – Bedrock mine).
Albite $(Na,Ca)[(Si,Al)_4O_8]$	Monomineral vein 5 cm wide (sample MB5 – Mbuwa mine).
Allanite * $Ca(La,Ce)Fe^{2+}(Al,Fe^{3+})_2$ $[O/OH/SiO_4/Si_2O_7]$	Euhedral crystals up to 150 µm long in metabasite rock (sample PN3 – Pioneer mine). Outer part of crystals is altered to microcrystalline limonitic material with aggregates of cryptocrystalline phosphate containing La, Ce, Nd and Th.
Amethyst * SiO_2	A single vein, < 10 cm wide (sample KF11 – Kafubu mine). This vein is younger than quartz-tourmaline veins associated with emerald mineralization.
Apatite $Ca_5[F/(PO_4)_3]$	Locally up to 5 mm long white crystals and crystal aggregates in phlogopitite and quartz-beryl-phlogopite-tourmaline veins.
Bertrandite * $Be_4^{[4]}[(OH)_2/Si_2O_7]$	7 mm long aggregates of microscopic platy crystals replacing beryl; associated with hydrothermal adularia and secondary chlorite (sample BD1a – Bedrock mine).
Calcite $Ca[CO_3]$	Irregular fillings in tourmaline-amphibole-chlorite-calcite rock with chalcopyrite (sample KF10 – Kafubu mine). It contains minor FeO (1.0–1.1 wt.%), MnO (0.7–0.9 wt.%) and MgO (0.7–0.9 wt.%).
Chalcopyrite * $CuFeS_2$	3 cm long massive accumulation in tourmaline-amphibole-chlorite-calcite rock (sample KF10 – Kafubu mine) associated with metabasites. It also forms euhedral inclusions up to 100 × 40 µm in Cr-muscovite (Cr-muscovite-quartz-tourmaline rock sample CA1 – Chawuma mine).

Table 10, continued

Chromite-Cr-spinels $Fe^{2+}Cr_2O_4$	Tiny euhedral inclusions up to 20 × 10 μm with a prevalence of chromite and gahnite components, enclosed in Cr-muscovite (sample CA1 – Chawuma mine), and in phlogopite rock (sample CT1 – Chantete mine) and phlogopite schist with beryl (sample KF7a – Kafubu mine). The concentration of main oxides (wt.%) ranges as follows (CA1 vs. CT1): Cr_2O_3 = 41.2–41.8 vs. 36.4–37.2; Al_2O_3 = 7.6–8.2 vs. 8.5–9.2; FeO_{tot} = 41.2-41.8 vs. 19.7–22.0; MnO = 0.3–0.6 vs. 2.6–2.9; MgO = 0.6–0.7 vs. 1.2–1.3; ZnO (estimated) = 10 vs. 25 wt%.
Chrysoberyl $BeAl_2O_4$	Minute inclusions in emerald (Graziani et al. 1983).
Columbite-tantalite * $Mn(Nb,Ta)_2O_6$ $Mn(Ta,Nb)_2O_6$	Two different Nb-Ta minerals were identified in kaolinized pegmatite (sample FE6 – Fwaya-Fwaya 10 mine). Manganocolumbite forms equant 0.7 mm long grains with conchoidal fracture and contains Nb > Ta, Mn and almost no Fe; manganotantalite forms euhedral prismatic crystals 0.3 mm long showing Nb = Ta, Mn and no Fe. See also manganotantalite.
Dolomite * $CaMg[CO_3]_2$	Subhedral porphyroblasts and anhedral aggregates up to 1 mm long in some metabasites (samples PI5-Pirala mine; MB1 – Mbuwa mine and FF4 – Fway-Fwaya East mine).
Epidote $Ca_2(Fe^{3+},Al)$ $Al_2[O/OH/SiO_4/Si_2O_7]$	Identified in one pegmatite with garnet (sample FE8HM – Fwaya-Fwaya 10 mine). It contains 8.4–9.7 wt.% FeO_{tot}.
Gahnite * $ZnAl_2O_4$	Rare accessory mineral from pegmatite (sample PN1HM – Pioneer mine). It forms anhedral light greenish-blue grains 0.1–0.4 mm in diameter. EDAX microanalyses gave 64 wt.% Al_2O_3, major Zn and minor Fe.
Hollandite * $(Ba,K)(Mn,Ti,Fe)_8O_{16}$	Opaque material filling cracks and cavities up to 200 × 300 microns long in quartz-tourmaline-beryl vein (sample MB2 – Mbuwa mine). It contains 57.2–61.6 wt.% MnO, 0.45–3.7 wt.% FeO_{tot} and 12.5–15.2 wt.% BaO.
Kyanite $Al^{[6]} Al^{[6]} [O/SiO_4]$	Subhedral grains in heavy fraction from kaolinized pegmatite (sample TW3 – Twampane mine).
Manganotantalite * $Mn(Ta,Nb)_2O_6$	Prismatic euhedral crystals < 1 mm long were also identified in heavy fraction from pegmatite sample PN1HM – Pioneer mine.
Margarite $(Ca,Na)Al_2$ $[(OH)_2/(Si,Al)_4O_{10}]$	Minor inclusions in emerald (Graziani et al. 1983).
Monazite $Ce[PO_4]$	Mostly euhedral, about 10 μm long, inclusions in Cr-muscovite-quartz-tourmaline rock (sample CA1 – Chawuma mine) and banded quartz-tourmaline rock (sample KF5 – Kafubu mine). The following elements were determined: P, Ca, Ce, La, Nd and Th.
Niobian rutile * (= ilmenorutile) $(Ti,Nb,Fe)O_2$	See rutile-major minerals.
Phenakite * $Be_2^{[4]}[SiO_4]$	Glassy pinkish grains up to 10 × 4 mm in size were found enclosed in beryl in the phlogopite schist (sample PN9 – Pioneer mine). Under the microscope, it shows moderately high indices of refraction and first order interference colours. Phenakite includes chlorite flakes and is extremely rich in fluid (gas-liquid) inclusions. Textural relations indicate the sequence: phenakite-tourmaline-beryl. Microprobe analysis determined only SiO_2 content 54.5 wt.%, while all other analysed elements were below the detection limit. BeO content calculated to 100 % is 45.4 wt.% and it fits well with a theoretical formula.
Plumbomicrolite *$(Pb,Na,Ca,)_2(Ta,Nb)_2$ $(O,OH)_7$	Brownish-yellow crystals and crystal fragments up to 1 mm long, with a good cleavage, were separated from kaolinized pegmatite (sample PI3 – Pirala mine). The mineral was identified by X-ray powder diffraction and EDAX microprobe. The complex Ta oxide contains also Pb, U, Nb and Ti.
Pseudorutile * $Fe_2^{3+}Ti_3^{4+}O_9$	Identified in metabasite rock (sample KF1 – Kafubu mine). It contains (wt.%) 56.8 TiO_2, 34.2 Fe_2O_3, 1.1 MnO and 0.27 Cr_2O_3. Marginal leaching of Mn and a part of Fe from ilmenite-pyrophanite formed the mineral.
Pyrite FeS_2	Found as small inclusions in Cr-muscovite-quartz-tourmaline rock (sample CA1 – Chawuma mine) and tourmaline-amphibole-chlorite-calcite rock, together with chalcopyrite (sample KF10 – Kafubu mine).
Tantalian rutile * (=strüverite) $(Ti,Ta,Nb,Fe)O_2$	See rutile-major minerals
Titanite $CaTi[O/SiO_4]$	Rare mineral, identified as one inclusion (40 × 15 microns) in tourmaline from Cr-muscovite-quartz-tourmaline rock (sample CA1 – Chawuma mine) and in several amphibolite samples (e.g. sample KA9 – Kamakanga Old Pit). Titanite from the first mentioned sample shows a very high Al_2O_3 (8.17–9.84 wt.%), increased FeO (1.17–1.27 wt.%) and Cr_2O_3 (0.45–0.80 wt.%); most probably also high F and (OH). Titanite from sample KA9 displays a "common" composition with a low Al_2O_3 content (1.66–1.98 wt.%).
Vermiculite * ~ $Mg_2(Mg,Fe^{3+},Al)$ $[(OH)_2/$ $(Si,Al)_4O_{10}]$. $Mg_{0.35}(H_2O)_4$	EDAX analyses indicate a small-scale alteration of phlogopite to vermiculite (sample PN9 – Pioneer mine).
Violarite * (or pentlandite) $FeNi_2S_4$	Found as a rare euhedral inclusions (300 × 400 μm) intergrown in chalcopyrite (sample KF10 – Kafubu mine). Ni strongly prevails over Co and Fe. The habit of inclusion suggests a cubic symmetry of mineral.
Xenotime * $Y[PO_4]$	Found as unique 5 × 15 μm sized euhedral inclusion in phlogopite rock (sample KA12 – Kamakanga Old Pit). Besides Y contains minor Yb.

* minor minerals identified for the first time in the Kafubu area

been given by Wood and Nassau (1968), Hickman (1972), Campbell (1973), Bank (1974), Schmetzer et al. (1974), Schmetzer and Bank (1981), Hänni (1982), Koivula (1982, 1984), Graziani et al. (1983, 1984), Gübelin and Koivula (1986), Schwarz and Henn (1992), Moroz et al. (1998), Milisenda et al. (1999), Moroz and Eliezri (1999), Dereppe et al. (2000), and Calligaro et al. (2000). Only in the studies of Hickman (1972) and Milisenda et al. (1999) are the precise locality data for the analyzed samples given; otherwise, the source localities are stated only as Zambia or Kitwe, the town nearest to the Kafubu emerald area.

Chemical properties

The beryl and emerald from individual mines in the Kafubu area are characterized by generally low to moderate Cr_2O_3 content, varying between 0.11–0.77 wt.%, and elevated contents of MgO (1.55–2.64 wt.%) and FeO_{tot} (0.76–1.88 wt.%). The average concentrations show significant variation corresponding to the color zones of individual samples, as well as to individual localities. The direct correlation between the color intensity of emerald crystals and chromium content can be observed.

Previously published compositional data of the Zambian emeralds by other authors are summarised in Table 12. Except for the data of Hickman (1972) and the BeO contents presented by Milisenda et al. (1999), all other values were determined as spot measurements by electron microprobe. Data for vanadium contents are given by Milisenda et al. (1999) for emeralds from the Fwaya-Fwaya mine, in the central part of the Kafubu area.

Table 11. K-Ar muscovite age determination

Sample	K wt.%	$^{40}Ar_{rad}$ nl/g	% $^{40}Ar_{air}$	Age Ma
FF5 Muscovite pegmatite	8.66	169.65	4.2	452.1 ± 16
KA11 Quartz-tourmaline vein with muscovite	8.84	170.97	2.9	447.0 ± 8.6

Physical and optical properties

There exists much previous data on the standard gemmological properties of emeralds from the Kafubu area (Table 13). This includes data by Campbell (1973) on the approximate values of an unspecified number of Zambian emeralds, Graziani et al. (1983) on a single sample, and the approximate values of an unspecified number of representative samples of the individual grades by Milisenda et al. (1999).

UV-VIS spectra

Polarised spectra were obtained by using a Unicam UV540 spectrometer at the Gemmological Laboratory, National Museum of Natural History, Leiden, The Netherlands. One sample from the Kamakanga mine (sample no. RGM 421703) was selected for obtaining representative spectra (Fig. 20). This sample is a medium vivid green, transparent emerald crystal (length approximately 1 cm) in a matrix of black phlogopite. This crystal was polished on both sides for analytical purposes. Semi-quantitative analyses (EDXRF microprobe, Leiden) of this crystal gave 0.6 wt.% Cr_2O_3, 1.8 wt.% FeO_{tot}, 2.9 wt.% MgO and 2.8 wt.% Na_2O.

The ordinary ray gives a spectrum with a peak at 371 nm, bands at 435 and 609 nm, peaks at 637 and 681 nm, and a band at 860 nm. The extraordinary ray gives a spectrum with a peak at 370 nm, bands at 420 and 652 nm, with additional peaks at 631, 663 and 685 nm.

The bands at 435 and 609, and at 420 and 652 nm, and the peak at 685 nm, indicate the presence of chromium, which causes the mineral's green colour (Wood and Nassau 1968; Schmetzer et al. 1974). Additional weaker peaks at 631, 637, and 663 are also caused by the

Table 12. Chemical composition of Zambian emeralds (in wt.%), published by other authors

	1	2	3	4	5	6	7	8	9	10	11
SiO_2	62.79	62.75	61.91	61.42	62.07	63.81	63.80	63.91	58.92–65.72	62.23	64.9
TiO_2	–	–	–	–	–	–	–	–	–	–	–
Cr_2O_3	0.37	0.55	0.25	0.12	0.10	0.31	0.40	0.08	0.23–0.53	0.33	–
V_2O_3	0.03	0.05	0.02	0.04	0.02	0.02	0.00	–	–	–	–
Al_2O_3	12.08	11.24	12.23	11.59	11.98	15.07	14.60	18.88	13.63–15.26	15.41	14.7
FeO_{tot}	1.07	1.35	0.96	1.01	1.17	1.03	0.90	0.69	0.47–0.97	0.11	–
MnO	–	–	–	–	–	–	–	0.08	–	0.02	–
MgO	2.28	2.90	2.07	2.58	2.30	2.04	2.30	0.83	1.84–2.34	0.76	2.3
CaO	0.06	0.07	0.03	0.05	0.04	0.03	0.00	0.96	–	0.31	0.05
Na_2O	1.77	1.99	1.71	1.88	1.85	1.86	1.90	1.45	0.96–1.65	2.63	1.9
K_2O	0.08	0.06	0.06	0.07	0.07	0.04	0.00	0.01	–	2.89	0.06
BeO_{calc}	13.96	13.96	13.96	13.96	13.96	–	–	13.70	–	11.90	14.2

Localities: 1–5 Kagem Mining Ltd., Fwaya-Fwaya mine (Milisenda et al. 1999); 6 – Kamakanga mine (Schwarz and Henn 1992); 7 – locality not stated (Hänni 1982); 8 – locality Kitwe District, Zambia (Graziani et al. 1983); 9 – locality Kitwe, Zambia, average value of 3 samples (Moroz et al. 1998); 10 – Miku mine (Hickman 1972), 11 – locality not stated, average value of 11 samples (Calligaro et al. 2000).

presence of Cr^{3+}. The shift of absorption from 435 to 420 nm, and from 609 to 652 nm, causes an absorption low at 512 nm for the ordinary ray, producing a yellowish green colour, and a shift towards a low at 498 nm for the extraordinary ray, producing a bluish green colour.

The peak at 370 nm and the band at 860 nm show the presence of iron in both divalent and trivalent states. The band at 860 nm indicates the presence of Fe^{2+}, whereas the peak at 371 nm proves the presence of Fe^{3+}. This non-destructive test only gives qualitative spectra. The exact Fe^{2+}/Fe^{3+} ratio cannot be measured by this method.

Table 13. Physical and optical properties of emerald (beryl) from the Kafubu area

Colour	Range from whitish to dark green. Colour is predominantly unevenly distributed, colour zoning is often present. Stones are mostly pale in colour, however small grain size may show a fine colour.		
Clarity	Moderately to heavily fractured, many small inclusions.		
Refractive indices	Campbell (1973)	n_e = 1.583;	n_o = 1.590
	Graziani et al. (1983)	n_e = 1.580 ± 0.004	n_o = 1.586 ± 0.003
	Milisenda et al. (1999)	n_e = 1.581–1.589	n_o = 1.589–1.597
Birefringence	Campbell (1973)	+n = –0.007	
	Graziani et al. (1983)	+n = –0.006	
	Milisenda et al. (1999)	+n = –0.008	
Specific gravity	Campbell (1973)	2.75	
	Graziani et al. (1983)	2.794	
	Milisenda et al. (1999)	2.69–2.77	
Pleochroism	Distinct dichroism, yellowish green (n_o) and bluish green (n_e).		
Fluorescence	Inert to long-wave and short-wave ultraviolet radiation.		
Reaction to Chelsea filter	The majority of stones show green, a few stones either show green or pink/red through the filter.		

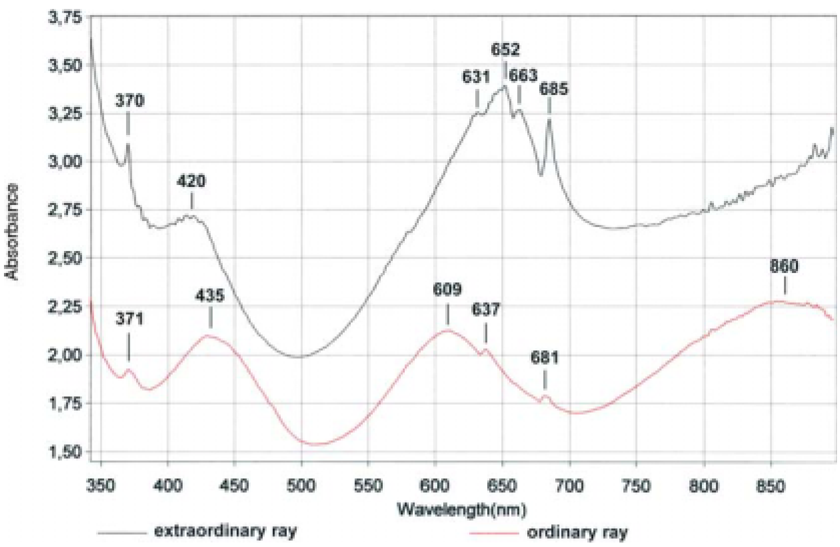


Figure 20. Polarised absorption spectra of emerald (sample RGM 421703) from Kamakanga mine. The FeO_{tot}/Cr_2O_3 ratio is 2.87.

Solid inclusions

Solid inclusions have been described by Campbell (1973), Koivula (1982, 1984), Graziani et al. (1984), Gübelin and Koivula (1986), Milisenda et al. (1999), and Moroz and Eliezri (1999). Milisenda et al. (1999) described phlogopite/biotite platelets as the most characteristic mineral inclusions in emeralds from the central part of the Kafubu area (at the Fwaya-Fwaya mine). They occur with rod-like mineral inclusions, identified as actinolite-tremolite, together with oriented square to rectangular-shaped fluid inclusions, i.e. negative crystals filled with liquid and gaseous phases. Moroz and Eliezri (1999) recognized mineral inclusions such as phlogopite (the most common), glauconite, talc, apatite, quartz, and Fe-Mn and Fe-Cr oxides in five samples of green and green-blue emeralds from the "Kitwe area". Graziani et al. (1983) further identified inclusions of apatite, quartz, chrysoberyl, margarite, muscovite and rutile (or brookite) in one sample from the "Kitwe area".

In sample MB2 (from the Mbuwa mine), which is from a quartz-emerald-tourmaline vein in the phlogopitized metabasite, some reddish orange crystals enclosed in the emerald crystal were identified as niobian rutile (= ilmenorutile) (Fig. 21). The mineral has the appearance of rutile, which has been previously described by various authors (e.g. Graziani et al. 1984; Gübelin and Koivula 1986), but the reddish orange colour suggests the presence of Fe^{3+}, Nb, and/or Ta. A qualitative microprobe analysis confirmed the abundance of Nb and Ti, and lesser amounts of Ta and Fe. This is the first proven occurrence of niobian rutile (= ilmenorutile) as an inclusion in the Zambian emeralds.

Fluid inclusions

Fluid inclusions were studied in 12 samples from various types of the quartz-tourmaline ± beryl veins. This section presents a summary of the data obtained, as a more detailed paper on fluid inclusions is currently in preparation. A microthermometric study was carried out using a Linkam THMSG 600 heating-freezing stage, mounted on an Olympus BX-50 microscope (magnification up to 800×). The inclusions were classified according to Roedder's (1984) criteria of primary and secondary origins. Salinity (as wt.% NaCl eq.) was calculated using the equations of Bodnar (1993), Diamond (1992), or Sterner et al. (1988), for aqueous, aqueous-carbonic, and aqueous halite-bearing inclusions, respectively. Isochores were constructed using the equations of Zhang and Frantz (1987) for H_2O-NaCl, Bakker (1999) for

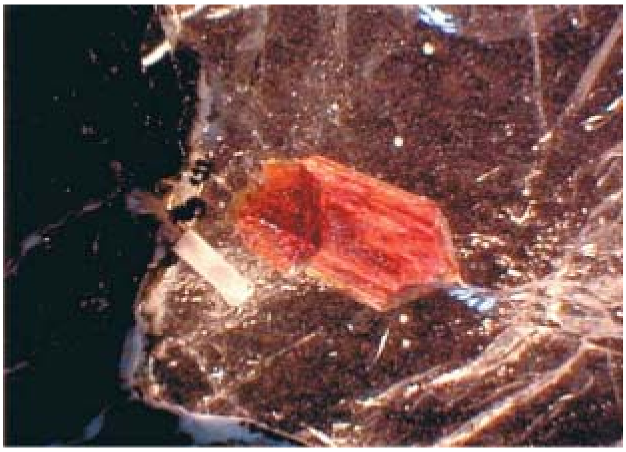


Figure 21. Niobian rutile (= ilmenorutile) crystal in emerald from Mbuwa mine. Oblique illumination, length of niobian rutile (ilmenorutile) crystal is 1.3 mm.

H_2O-CO_2-NaCl, and Bowers and Helgeson (1983) for H_2O-CO_2. The admixture of N_2 or CH_4 in the gaseous phase of the inclusions was estimated according to data of Thiery et al. (1994).

Ambiguous primary inclusions were only identified in some beryl crystals (Fig. 22 a, b, e). The primary inclusions in tourmaline are scarce, and the primary character of the inclusions in quartz is questionable, as most of them seem to be pseudosecondary (Fig. 22 c, d, f) rather than primary. Several generations (usually up to three) of secondary inclusions are quite common in all the samples examined in this study (Fig. 22h).

Three general types of fluids were recognized: aqueous-only, aqueous-carbonic, and carbonic. The first two types can be further subdivided with respect to their salinity into low, moderate, and high-salinity subgroups. The carbonic fluids were identified only in two samples, and are clearly of secondary origin. The aqueous-only and aqueous-carbonic fluids were found in all samples of all genetic types, the second type being significantly more common in quartz than in tourmaline.

The following fluid inclusion types were identified in our samples: 1. two or three phase, liquid-rich H_2O-CO_2 inclusions; 2. two or three phase, vapor-rich H_2O-CO_2 inclusions; 3. one phase liquid-rich CO_2 inclusions; 4. multiphase liquid-rich H_2O-CO_2 inclusions, with 1–2 solid translucent phases (one of which is usually cubic); 5. two phase liquid-rich H_2O inclusions; 6. multiphase liquid-rich H_2O inclusions, with 1–2 solid translucent phases (one of which is usually cubic); and 7. monophase liquid H_2O inclusions.

The early fluids in quartz are always of the aqueous-carbonic type, while the late ones are of the aqueous-only type. In contrast, all inclusions in beryl and tourmaline are usually aqueous-only. However, a few beryl samples with extremely rare aqueous-carbonic inclusions of uncertain origin were also identified. The aqueous-carbonic inclusions in tourmaline were all secondary.

The aqueous-carbonic inclusions homogenize mostly into liquid state. The highest observed total homogenization temperatures (Th-tot, Fig. 23 a) correspond to 420–410 °C (quartz) and 330°C (beryl). The inclusions frequently underwent decrepitation between 2 and 20 °C, either before or after the homogenization of the entire inclusion. The homogenization temperatures of H_2O-only fluids (Fig. 23 b) display four well-shaped peaks at 370–350 °C, 300–280 °C, 230–210 °C, and 160–130 °C. They are believed to represent four separate fluid fluxes. Primary and pseudosecondary aqueous-only inclusions in beryl and tourmaline homogenized mostly at 230–220 °C, while several measurements are randomly scattered up to 320 °C (tourmaline) and 370 °C (beryl).

The salinity of the aqueous phase (of H_2O-only and H_2O-CO_2 fluids) is estimated as 0–1, 5–8, 15–17, 23–25 and 34–35 wt.% NaCl eq. (Fig. 23c). The most common first melting temperatures (from –57 to –47 °C) indicate the presence of a H_2O-NaCl-$CaCl_2$ complex system.

The CO_2-phases of fluid inclusions homogenize mostly from +26 to +31°C, to both liquid and vapor. The solid CO_2 melts mostly from –56.6 to –56.7 °C, and less frequently from –57.4 to –57.6 °C. The maximum total $CO_2 \pm CH_4 \pm N_2$ content of the aqueous-carbonic fluids is estimated at 25 mol.%, and decreases with time to about 4–3 mol.%. The N_2 or CH_4 admixture in the gaseous phase is generally very low (0–2 mol.%), and is higher only in exceptional circumstances (sample KA-7: 10 mol.% of N_2, or 3 mol.% of CH_4).

Possible pressure-temperature (P-T) trapping conditions for the fluid inclusions in these samples are summarized in Fig. 24. The measured homogenization temperatures define only minimum trapping conditions from a homogeneous fluid.

The trapping conditions of fluid inclusions are constrained by two limits: the metamorphic equilibration temperatures of the amphibolites (590–630 °C), and the fluid inclusion homogenization data of sample KA14 (ca. 200 MPa and 300 °C – the field of "late mineralization stage", type 3 of quartz-tourmaline veins). The data for the rest of the samples lie between these two limits, and the temperature range of quartz-tourmaline veins is around 400–500 °C.

The highest homogenization (i.e. minimum trapping) conditions, at 400–450 MPa and 360–390 °C, were recorded in quartz of several samples (MA3a, ME3, ME5). These isochores define the "early mineralization stage." However, most of quartz veins containing tourmaline and beryl crystallized at lower pressures of the "main mineralization stage" (ca. 200–400 MPa). The fluid inclusion data thus indicate three separate P-T stages of the supposed evolution of quartz-tourmaline veins. In contrast to the fluid inclusion study, the field data do not allow the division of quartz-tourmaline veins to "early" and "main" mineralization stage.

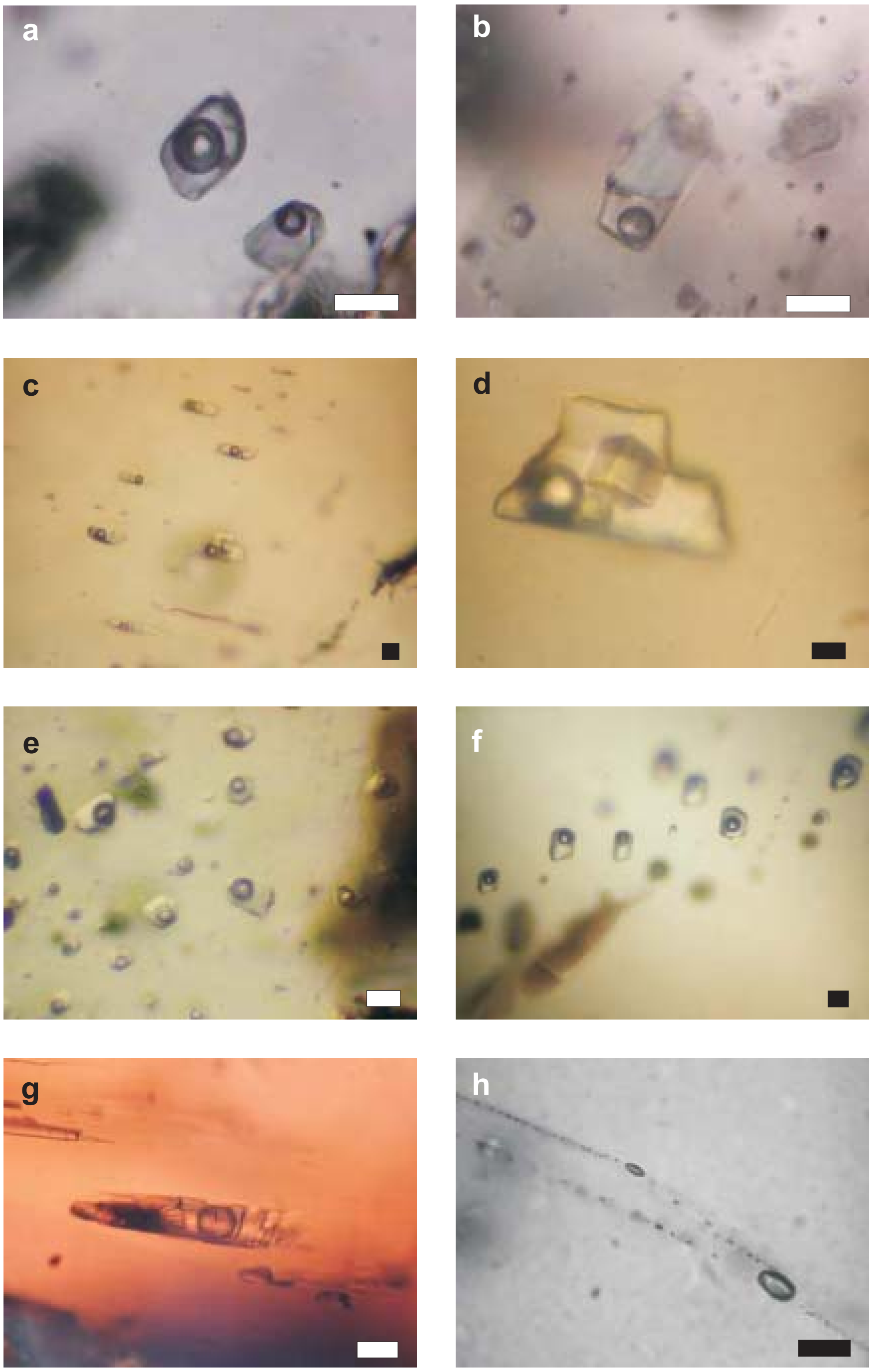


Figure 22. Microphotos of selected fluid inclusions (scale bar is 20 µm): a – Sample ME5 – liquid rich fluid inclusion of supposed primary origin in beryl; three-phase aqueous-carbonic (in centre) and two-phase aqueous-only. b – Sample ME5 – two-phase liquid-rich aqueous primary inclusions in beryl. One of them is attached to an unidentified solid phase inclusion. c – Sample CA2 – pseudosecondary or secondary multiphase aqueous inclusions in quartz. The size of both-vapor bubble and cubic daughter crystals is constant in all inclusions. d – Detail of a multiphase inclusion from photo c. Inclusion contains vapour bubble, large cubic crystal (NaCl) and small translucent grain, which does not dissolve on heating. e – Sample TW5/1 – group of primary three-phase aqueous-carbonic inclusions in beryl. f – Sample KA4 – trail of pseudosecondary aqueous-carbonic inclusions in quartz. g – Sample ME3 – tubular (primary?) aqueous inclusion in tourmaline. Note the presence of pin-like aggregates of black solid phases. h – Sample MA3A – trail of secondary carbonic inclusions.

Discussion

Country rocks

Alteration and metamorphism have obliterated the diagnostic igneous textures in the metamorphosed basic rocks. The present mineral assemblage of the metabasites (talc-chlorite ± actinolite ± magnetite) is completely of metamorphic origin, and the same origin is indicated for the accessory minerals chromian magnetite and ilmenite. Chemical analyses of these rocks show that they correspond to the present criteria for komatiites: $MgO > 18$ wt.%, $TiO_2 < 1$ wt.%, and $Na_2O + K_2O < 2$ wt.% (Le Bas, 2000). Their chalcophile element ratios are also consistent with komatiite or komatiite to Mg-rich basalt precursors.

The rare earth elements have been determined in three metabasite samples (talc-chlorite ± actinolite ± magnetite), four amphibolite samples, and three metasedimentary quartz-muscovite-phlogopite schist samples. The REE distribution pattern for the talc-chlorite ± actinolite ± magnetite rocks is different from that of peridotite and related volcanic rocks of upper mantle derivation. The pattern shows a highly evolved REE distribution, very similar to those of other rock types analyzed. This evolved pattern includes significant enrichment in the light REEs and a prominent negative Europium anomaly, which is larger than in any other rock type ana-

lyzed from the Kafubu area. We have considered the following processes in the interest of explaining these relations:

1. a) A slightly anomalous enrichment of allanite in the original basic volcanics is indicated by relics of euhedral allanite crystals (metabasite sample PN3) and by limonite + microcrystalline REE-rich phosphate pseudomorphs after an original REE-rich mineral.
   b) Removal of plagioclase from respective magma batches during fractional crystallization may be responsible for the prominent negative Eu anomaly.
2. Hydrothermal alteration, possibly in a saline environment, may have caused the mobility, fractionation, and enrichment of REEs in the volcano-sedimentary sequence containing the horizon of basic magnesian, possibly volcaniclastic rocks. Such an environment may induce the efficient mobilization of REEs through chemical complexing (Möller 1998).

The addition of continental detrital material, with an evolved REE assemblage is unlikely, as it would result in increased alkali element contents (such as Na and K), while analyses show the metabasites to contain persistently low abundances of these elements.

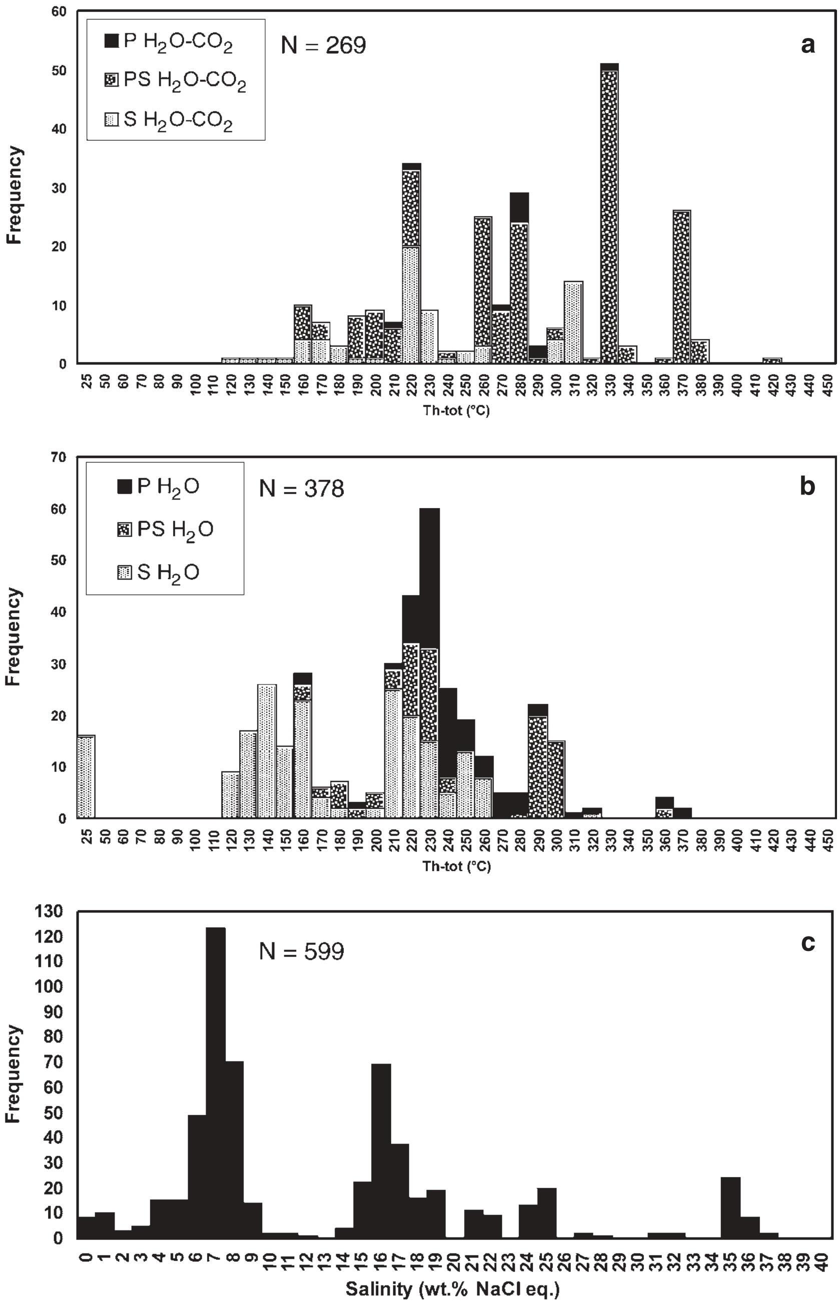


Figure 23. Summary histograms of selected microthermometric data (not discriminated with respect to the hosting mineral; P – primary, PS – pseudosecondary, S – secondary inclusions). a – Total homogenization temperatures of aqueous-carbonic inclusions. b – Total homogenization temperatures of aqueous-only inclusions. c – Salinity of aqueous-carbonic and aqueous-only inclusions (not differentiated with respect to P, PS or S types).

Banded quartz-tourmaline rocks

Our analytical data do not support the opinion presented by Milisenda et al. (1999) of a possible role for evaporitic environment with reference to stratiform and finely banded quartz-tourmaline rocks. Namely, no dolomite, magnesite, or other chemogenic metasediments indicating an evaporitic depositional environment have been found in the local Muva sequence. Our data suggest that the banded quartz-tourmaline rocks were formed by the tourmalinization of fine-grained quartz-muscovite-phlogopite schists from fluids related to fertile granite and pegmatites. This idea is supported by the relatively high Nb content (accompanied by significant Ta, detected by microprobe EDAX spectra) in the banded tourmaline rock (sample KF2 of the Kafubu mine), and by the zoning of Nb and Ta contents in niobian rutile, which indicate that these elements were enriched due to granite- or pegmatite-related mineralization. A hypothetical Nb- or Ta-rich detrital component in the precursors of the tourmaline-rich rocks may be thus excluded.

In contrast to the tourmaline-rich rocks, some evaporitic characteristics may be preserved in the metasediments and metamorphosed basic volcanic rocks. These characteristics include: 1. relatively high Na/Ca and Mg/Fe ratios in metasedimentary schists; and, 2. a similarity in the REE patterns of the metasedimentary schists and the associated metamorphosed basic rocks.

Alternatively, some compositional features of the country rocks, such as high Na/Ca ratio in metasedimentary schists and REE patterns in metavolcanic rocks, might have been caused by the alteration of these rocks by hydrothermal fluids related to the mineralization pro-

cess. However, we do not have evidence to suggest that the activity of such fluids is solely responsible for the geochemical patterns in the country rocks discussed.

Phlogopitites, emeralds, and rare-element mineralization

A specific feature of the Kafubu area is the presence of abundant quartz-tourmaline veins, and K, F, Be, Li, and Rb enrichment in the associated phlogopite zones at the contacts with the magnesian metabasite. These materials seem to have been deposited from fluids that were the apical forerunners of an advancing front of abundant pegmatite intrusions. Due to the strong kaolinization of the pegmatites and their country rocks, it was not possible to sample fresh phlogopitites around pegmatites.

The comparison of oxide/element abundances in phlogopitites with those in Mg-rich metabasic rocks shows that the transformation of metabasic rocks to phlogopitite involves the major import of K, Al, F, Li, and Rb, plus some prominent localized enrichments of beryllium and boron, and the removal of Ca, some Si, and water. Phlogopitization is thus accompanied by enrichment in pegmatitic components. Cr and Ni behave as components that became somewhat diluted during the process by which the protolith metabasite became altered into phlogopitite.

The phlogopitite zones around the quartz-tourmaline veins and the quartz-feldspar pegmatites indicate significant lithium enrichment, with concentrations in the range of 0.12 to 0.74 wt.% Li_2O in the phlogopitites. Given the large volumes of phlogopitites, the quantity of imported Li is very significant. The situation with Rb is similar, as this element is present in concentrations between 1725 to around 2900 ppm. We did not obtain analyses for Cs, but Calligaro et al. (2000) reported an average content of 1150 ± 540 (1σ) ppm Cs in 11 Zambian emerald samples. This Cs content is more than twice the highest value for Cs reported for emeralds from 13 other worldwide sources.

According to present documentation, the “Kafubu pegmatite field” is approximately 2 km wide and 10 km long, trending NE-SW. It bears the highest quality emerald mineralization in the Kafubu area, and is seems to be structurally controlled by the dominant antiform. It roughly corresponds with the final phase of the Pan-African (Lufilian) orogeny – a weak orogenic phase with faulting (Milisenda et al. 1999), associated with the structural ENE-WSW trend.

In situations with adverse bedrock exposure conditions, such as in the Kafubu area, it is necessary to consider similar cases of rare-element mineralization/metasomatism (Li-Rb-Cs-Be-F-B) on a regional scale, related to fertile granites or pegmatites.

Breaks and Jones (1991) have detailed the relations of extensive syn-magmatic metasomatism, genetically related to the Ghost Lake Batholith of NW Ontario, and the post-magmatic metasomatism manifested at selvedges of rare-element pegmatite dikes. The lithium-rich amphibole, holmquistite, is a typomorphic indicator of these rare element mineralizations wherever they are superimposed onto

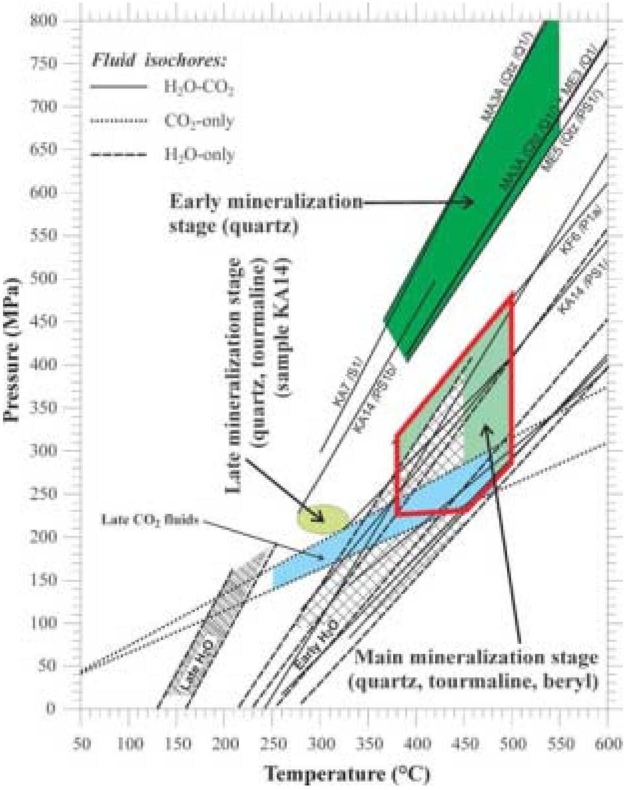


Figure 24. Reconstruction of pressure-temperature conditions of the final homogenization and trapping conditions of the inclusions. The coloured fields represent the most probable trapping conditions of the early, main, and late mineralization stages. Some of the isochores are labelled by sample name, host mineral, and inclusion type.

basic metavolcanic country rock. The mineralization relationships indicate an early phase of fluid discharge into the amphibolitic country rocks. These fluids could have originated from granitic melts representing precursors to the chemically evolved material of the pegmatitic granite dikes. The apparent ingress of metasomatic fluids, guided by a ductile shear zone, was traced for a minimum of 2.5 km in the Ghost Lake Batholith, and the occurrence of holmquistite is documented for a distance of 3.5 km from the nearest lithian pegmatite dike. Field evidence indicates that this period of exomorphism occurred prior to the solidification of the potassic pegmatite, which subsequently intruded the dravite-phlogopite-actinolite ± holmquistite sub-units of the early metasomatic zone. Exocontact metasomatic zones around lithian pegmatite dikes also show enrichment in rare elements, but holmquistite is confined to a distance of several metres around the pegmatite contact.

An extensive metasomatized zone, 800 m wide and 5 km long, in a gabbro-anorthosite layered intrusion in NW Russia was studied by Gordienko et al. (1975) with the use of numerous boreholes. The mineralized zones, exhibiting a regular metasomatic zoning sequence, attain the highest rare-element enrichment in biotite-holmquistite-chlorite gneisses and holmquistite-chlorite gneisses with biotite and epidote (Li_2O max. 1.2 wt.%, Cs_2O 0.04 wt.%, Rb_2O 0.10 wt.%). The temperature of mineralization is estimated at 540–350 °C. The mineralization is clearly related to a

dike swarm of the rare-element-rich spodumene pegmatites, occurring higher in the structural sequence. However, individual pegmatite dikes show their own small-scale metasomatized zones (2–4 meters wide) in the gabbro-anorthosite country rock. The metasomatized rocks around the pegmatite dikes are identical in composition with the large-scale metasomatized zones (up to 5 km long). This example clearly shows that fluids of the same composition caused both types of metasomatized zones: that of a small-scale around pegmatite dikes, as well as on a regional scale. This indicates that the rare-element mineralization in pegmatites and in the large-scale metasomatized zones relates to the same abyssal source – a fertile granite.

The results of a petrochemical study of rare alkali-metal metasomatites show that silica, potassium, and rare alkali elements were introduced into the system during the formation of the metasomatites, whereas calcium and some magnesium and iron were gradually removed. In the process of metasomatism, a metasomatic column develops with a sequence of mineral parageneses from the rear zone (monomineral quartz, such as in the quartz-tourmaline veins in the Kafubu area), through various assemblages of micas, chlorite, and amphiboles (Krivovichev 1988). The zoning of the metasomatic column is explained in terms of the acidity-alkalinity of the mineral-forming solutions. The directional change in the properties of the solutions is caused either by gradual neutralization of an originally acid solution, or by a gradual temperature decrease and an associated change in acidity, resulting in neutral and slightly alkaline solutions. Holmquistite crystallization in place of biotite/phlogopite is dependent on the Li/K ratio. Relatively high potassium potentials result in the crystallization of dark micas enriched in Li, Rb, and Cs, in place of the amphibole holmquistite, as is the case in the Kafubu area.

As such, the quartz-tourmaline veins at Kafubu can be interpreted as the rear part of a metasomatic column, with the neighbouring phlogopite zone representing an intermediate zone bordering the metabasite protolith. The complete absence of feldspars in quartz-tourmaline veins at Kafubu indicates that the acidity of these solutions was somewhat higher than those of plagioclase- or albite-bearing quartz veins in other schist type emerald deposits (Barton and Young 2002).

It is suggested that this mineralization was caused by the extreme fractionation of rare elements from fertile granites and related hydrothermal activity (e.g. London 1986). It is probable that high contents of fluorine (2.6 to 4.7 wt.% in phlogopitite zones) and boron (in the exceptionally abundant tourmaline) at Kafubu functioned as solidus/liquidus depressants during the evolution of late fractions of the fertile granite and pegmatites, and assisted in the channeling of a number of pegmatitic rare elements into hydrous fluids. Experimental studies of granite system with elevated contents of fluorine and boron point to the separation of F- and B-enriched fluids, in part as hydrosaline melts (high-temperature brines) (London 1986; Veksler et al. 2002). Barton and Young (2002) discuss the connection between F entry from solution into the newly formed mica of phlogopite zones as a mechanism triggering the precipitation of Be-minerals.

The fractionated character of phlogopitites around quartz-tourmaline veins, and of the pegmatite suite at Kafubu, allows the exclusion of other alternative modes of formation, such as generation through anatectic (nearly in-situ?) derived melts (Milisenda et al. 1999). Numerous examples of phlogopitite zones (at places with significant emerald mineralization) around discordant quartz-tourmaline veins and discordant pegmatite dikes indicate that the model of stratiform evaporitic mineralization, as advocated by Milisenda et al. (1999), is not generally applicable. The efficiency of the evaporite model in explaining the highly differentiated chemistry of the pegmatite minerals, such as the Ta > Nb oxides and spessartine-rich garnet, is also questionable. Since many pegmatites exhibit a strong albitization (sample FF2 of the Fwaya-Fwaya mine), potassium released by the albitization of K-feldspar, according to the reaction K-feldspar + $Na^+ \rightarrow$ albite + K^+, is probably an important source of the potassium involved in the formation of phlogopitite zones around pegmatites.

Dereppe et al. (2000) used an ANN (artificial neural networks) procedure, based on microprobe chemical data, to classify more than 450 emerald samples from various worldwide deposits into five categories. The emeralds from the Miku-Kafubu localities fall into the category of deposits related to granitic pegmatite intrusions and hydrothermal veins in mafic/ultramafic rocks. Similarly, internal inclusions of niobian rutile crystals in emeralds, such as that identified in sample MB2 from Mbuwa mine, can only be found in beryl related to a pegmatite. Also the high Cs concentrations in Kafubu emeralds indicate an origin related to rare-element-enriched fertile granite and pegmatites.

Fluids inclusions and pressure-temperature conditions

The P-T conditions of the regional metamorphism of the Muva Supergroup in the Kafubu area, and of the emerald mineralization process, have been approximated. The mineral assemblages in the quartz-muscovite-biotite schists and metabasites are compatible with amphibolite facies. With reference to the rare presence of kyanite in metasedimentary schists (Hickman 1973), amphibole-plagioclase thermometry for several samples (following Holland and Blundy 1994) gives a narrow equilibration temperature interval of 590–630 °C for pressures of 400–600 MPa. This estimate can be considered as valid for the Muva Supergroup complex in the Kafubu area.

Fluid inclusion studies of quartz from quartz-tourmaline veins associated with beryl/emerald mineralization suggest the presence of a homogeneous fluid phase. The highest minimum trapping conditions correspond to ca. 400–500 MPa and 360–390 °C. However, the most common interval of quartz veins with tourmaline and beryl lies at lower P-T conditions around 200–400 MPa and 350–400 °C. The youngest, rarely occurring vein type (free of beryl/emerald) formed at ca. 200 MPa and 300 °C.

Graziani et al. (1983) estimated the P-T conditions of the crystallization of an emerald sample "from Kitwe" (0.08 wt.% Cr_2O_3) at 430–650 °C and < 400 MPa using the inclusion assemblage of chrysoberyl + beryl + margarite + muscovite + quartz. If this emerald crystal is an original porphyroblast that formed in the mica schist, as the description by Graziani et al. (1983) suggests, it is possible that paragonite-bearing muscovite and margarite could be older minerals passively inherited from the enclosing schist. In this case, the upper temperature limit (650 °C) would be too high. The available information indicates that the emerald mineralization and pegmatite intrusion post-date regional metamorphism. Temperatures of 390 and 590 °C can bracket the probable crystallization temperature of the Kafubu emeralds. However, the upper temperature limit is probably too high, as it represents a lower limit of regional metamorphism indicated from the study of amphibolites.

Gemmology

The polarised spectrum of emeralds from the Kamakanga mine is very similar to those from the Kagem Mine, shown by Milisenda et al. (1999). Their emerald contains Cr_2O_3 = 0.55 wt.% and FeO_{tot} = 1.35 wt.%, with a FeO/Cr_2O_3 ratio of 2.45. Our emerald showed just a little more of both components, with a FeO/Cr_2O_3 ratio of 2.87. The presence of more iron (especially Fe^{3+}) is indicated by asymmetrical bands at 420 and 435 nm. The presence of Fe^{3+} is characteristic of emeralds from Zambia, but also of Brazilian emeralds, such as those from the commercially important Belmont mine, Itabira district, Minas Gerais. Thus, the UV/VIS spectrum can be used as a tool for narrowing down the possible countries of origin of a cut emerald of unknown source.

Recommendations for future emerald exploration

Emerald mineralization of economic quantity and good gem-quality in the Kufubu region is almost entirely confined to the locally developed phlogopite reaction zones along the contacts between the metabasic host rocks and quartz-tourmaline veins penetrating these rocks. The proximity of quartz-feldspar pegmatites is another important factor that allows emerald to be formed.

The metabasic rocks hosting the emerald mineralization are discontinuous and have been fragmented by tectonism. In places where the best gem-quality emeralds occur, predominantly in the form of crystal aggregates, the reaction rim along the contact between metabasite host rocks and quartz-tourmaline veins is marked by newly formed phlogopite schist. Rarely, some individual good-quality stones may be found in the quartz-tourmaline veins, or very exceptionally in less altered host rocks. In the past, the exploitation of loose emeralds in residual weathering products and in local alluvial deposits next to the Kamakanga Old Pit was also profitable.

The metabasic rocks display great variability in magnetic susceptibility, from 0.31 to 90.7 (10^{-3} SI units). They can be subdivided into low (0.31–0.88) and high (5.2–90.7) magnetic susceptibility classes. The ground magnetic method used for the mapping of metabasic rocks as host-environments for quartz-tourmaline veins and pegmatites, is not always effective. Even fairly rich deposits may be missed when magnetometry is used as the only method. On the other hand, this method is the least expensive way to outline magnetized bodies of metabasic rocks with possible emerald mineralization. The combination of ground magnetic profiles coupled with a reasonable degree of exploration pitting and trenching (and somewhat expensive drilling), in combination with structural-tectonic research of already opened deposits, would seem to be the best option for prospecting emerald mineralization in this flat and thickly covered area.

In spite of the high variability of chromium and nickel contents in the metabasites (even within one locality), these elements may be used as pathfinders for metabasic rocks hidden near the surface soil cover. The emerald-related phlogopite schist shows generally high contents of chromium (4670–275 ppm, average 1556 ppm) and nickel (1266–177 ppm, average 646 ppm). A regular and closely-spaced grid of geochemical sampling for Cr, Ni and Be elements is highly recommended.

Tourmaline mineralization is commonly widespread and intense throughout the area, but locally developed accumulations of tourmaline or quartz-tourmaline veins invading metabasic rocks are the best places to find emeralds. Where the quartz-tourmaline veins are absent, the metabasic rocks are barren of beryl mineralization. The most favourable zones with potential emerald segments ("ore-shoots") are located at the intersections of subvertical and flat lying veins/veinlets inside the metabasic rocks, and in the close vicinity of intersections of steeply dipping granitic pegmatite dikes with flat lying tourmaline veins ("armpits").

Some quartz-feldspar pegmatite dikes (± tourmaline) contain large crystals of common beryl. However, no good-quality emeralds have been observed within the pegmatite dikes.

At present, the emerald mineralization has only been explored and mined to depths of 50–60 m (e.g. the deepest Kamakanga, Grizzly and Kagem mines). There are no data on emerald mineralization in the deeper parts of recently mined deposits or under recently worked mining floors. However, the continuation of the mineralization to deeper levels is promising, especially in places where favourable structural and lithological criteria coincide. Future underground mining will probably reveal many new emerald accumulations. We may also expect that new and large deposits of good-quality emeralds will be discovered in the future, and the Zambian Kafubu emerald field will be among the largest producers of emerald gemstones during the next few decades.

A better understanding of all possible controls of emerald mineralization should also contribute to more effective exploration and mining activities. This aspect will become even more important in the near future, as emerald workings will gradually shift to underground mining.

Conclusions

This study provides the first quantitative geochemical, petrological, and mineralogical data on the major rock types of the Kafubu emerald deposits. A full report, including maps, exact GPS coordinates of the main mines, pits, and samples, and all geochemical and mineralogical analyses, has been given in Seifert et al. 2002.

The highly magnesian metabasites hosting the mineralization are identified as metamorphosed komatiites. These rocks, with high chromium contents in the range of 3000–4000 ppm, yielded the chromium necessary for crystallization of emeralds. The main chromium sources in these rocks are chromian magnetite, chlorite, and actinolite. Associated amphibolites of andesitic and basaltic-andesitic composition, as well as some basic rocks of transitional composition, are usually too low in chromium to have served as a source of this element. The positive identification of Cr-rich rocks is, however, hardly possible without chemical analyses.

Quartz-tourmaline veins, accompanied by emerald-bearing phlogopite schists, are related to the metasomatic hydrothermal activity of fertile (hidden) granite and to the quartz-feldspar pegmatite dikes. The formation of phlogopite schists from metabasite was associated with the introduction of ca. 8–10 wt.% K_2O, 3–4 wt.% fluorine, significant Li, Rb, and enrichment of beryllium. The quartz-feldspar pegmatites of the Kafubu area belong to the rare-element pegmatites of the LCT family (i.e. Li-Cs-Ta), for which beryllium enrichment is common. Present data on the pegmatite occurrence in active mines and exploration pits, and their extrapolation to the surrounding area, points to the existence of a single, major pegmatite field – the "Kafubu pegmatite field".

Rather high activities of fluorine (up to 4 wt.% F in phlogopite schists) and boron (in exceptionally abundant tourmaline) probably functioned as solidus/liquidus depressants during the evolution of mineralizing fluids and their separation from the parent granite. These fluids deposited quartz-tourmaline veins, and altered the adjacent metabasites into the emerald- bearing phlogopite schists. Thus, it appears that the classical explanation for the origin of emerald in schist-related deposits still stands. The volcanosedimentary country rocks are generally low in beryllium, except in places where this element was introduced by quartz-tourmaline veins or pegmatites.

The following minerals have been newly identified in the Kafubu emerald area: adularia, allanite, amethyst, bertrandite, chalcopyrite, columbite-tantalite, dolomite, elbaite, gahnite, hollandite, manganotantalite, niobian rutile (= ilmenorutile), phenakite, plumbomicrolite, pseudorutile, tantalian rutile (= strüverite), vermiculite, violarite, and xenotime.

The identification of tantalum and niobium minerals in the pegmatites and banded quartz-tourmaline rocks of the Kafubu emerald area, and of the high contents of several pegmatitic elements (F, B, Be, Li, Rb) in the emerald-bearing phlogopitites, are of prime importance for the classification of the Kafubu pegmatites in the LCT group.

The time interval of 452–447 Ma from the $^{40}K/^{40}Ar$ dating of muscovite from a muscovite pegmatite and a quartz-tourmaline-muscovite vein accompanying the emerald mineralization allow the conclusion that the age of Be-mineralization is late Pan-African. This corresponds to the geological observation that the quartz-tourmaline veins and pegmatite dikes, together with the associated Be-mineralization, post-date the regional metamorphism of the Kafubu area.

The beryl and emerald samples from the Kafubu area range in colour intensity from whitish to dark green. Colour is unevenly distributed and is often zoned. Individial crystals have many inclusions and are on average moderately fractured. The emeralds show distinct dichroism, are inert to long- and short-wave ultraviolet radiation, and commonly show green under the Chelsea filter.

The UV-VIS spectra of the ordinary ray for emerald give values with a peak at 371 nm, bands at 435 and 609, peaks at 637 and 681 nm, and a band at 860 nm, while the extraordinary ray gives values with a peak at 370 nm, bands at 420 and 652 nm, with additional peaks at 631, 663, and 685 nm. The bands at 435 and 609, 420 and 652 nm, and at 685 nm indicate the presence of chromium. The peak at 370 nm and the band at 860 nm show the presence of iron, in both divalent and trivalent states.

Data on fluid inclusions in beryl, tourmaline, and quartz for the Kafubu emerald area are provided here for the first time. Three types of fluids were recognized: aqueous-only, aqueous-carbonic, and carbonic. Ambiguous primary inclusions were identified in some beryl crystals, scarce primary inclusions in tourmaline, and pseudosecondary inclusions in quartz. Several generations of secondary inclusions are common in all minerals considered here. Possible pressure-temperature trapping conditions of the representative fluid inclusions are shown. Fluid inclusion studies of quartz from quartz-tourmaline veins associated with beryl/emerald mineralization suggest the presence of a homogeneous fluid phase. The highest minimum trapping conditions correspond to ca. 400–500 MPa and 360–390 °C. The most common interval of quartz veins with tourmaline and beryl, however, lies at slightly lower conditions, at ca. 200–400 MPa and 350–400 °C. The youngest, rarely occurring vein type (free of beryl/emerald) formed at ca. 200 MPa and 300 °C.

Our field survey and laboratory analyses, together with structural research of the emerald mineralization (Tembo et. al. 2000), unambiguously demonstrate that the potential for new emerald occurrences in the Kafubu area still remains very high.

Acknowledgements. Funding for this project was granted to the Republic of Zambia by the Czech Government within the Foreign Assistance Programme for the years 2001–2003. The project was carried out at the request of the Ministry of Mines and Minerals Development during May–July 2001, as a joint project between the Geological Survey Department of Zambia and the Czech Geological Survey.

The authors are grateful to D. Mulela, M. P., Ch. Ngóna, geologist of Kamakanga Corp., Mr. Raul, the owner of Kamakanga Corp. and J. G. Dey, senior geologist of Kagem mining Ltd, and especially to D. K. Lombe, the senior geophysicist, Geological Survey Department,

Lusaka, for their generous support during the fieldwork. We thank P. Černý, Winnipeg, for valuable consultation on pegmatite problematics. A. Cheilletz, Vandoeuvre-les Nancy, and M. Novák, Brno, provided a critical review and discussion of this paper. The help of V. Janoušek, Czech Geological Survey, in plotting the geochemical data in Figs. 6 through 8 and 10 is acknowledged.

References

Bakker R. J. (1999): Adaptation of the Bowers and Helgeson (1983) equation of state to the H_2O-CO_2-CH_4-N_2-NaCl system. Chem. Geol. 154, 225–236.

Bank H. (1974): The emerald occurrence of Miku, Zambia. J. Gemmology 14, 8–15.

Barnes S-J., Boyd R., Korneliussen A., Nilsson L-P., Often M., Pedersen R. B., Robins B. (1988): The use of mantle normalization and metal ratios in discriminating between the effects of partial melting, crystal fractionation and sulphide segregation on platinum-group elements, gold, nickel and copper: examples from Norway. In: Prichard H. M., Potts P. J., Bowles J. F. W. and Cribb S. S. (eds) Geo-platinum 87. Elsevier, London, 113–143.

Barton M. D., Young S. (2002): Non-pegmatitic deposits of beryllium: mineralogy, geology, phase equilibria and origin. In: Grew E. S.: Beryllium, mineralogy, petrology and geochemistry. Rev. Mineral. Geochem. 50, 591–691.

Bodnar R. J. (1993): Revised equation and table for determinig the freezing point depression of H_2O-NaCl solutions. Geochim. Cosmochim. Acta 57, 683–684.

Bone Z. (1988): The geological setting of tourmalinite at Rum Jungle, N. T., Australia – genetic and economic implications. Miner. Deposita 23, 34–41.

Bowers T. S., Helgeson H. C. (1983): Calculation of the thermodynamic and geochemical consequences of nonideal mixing in the system H_2O-CO_2-NaCl on phase relations in geologic systems: Equation of state for H_2O-CO_2-NaCl fluids at high pressures and temperatures. Geochim. Cosmochim. Acta 47, 1247–1275.

Boynton W. V. (1984): Cosmochemistry of the rare earth elements: meteorite studies. In: Henderson P. (ed.) Rare Earth Element Geochemistry. Elsevier, Amsterdam, 63–114.

Breaks F. W., Jones D. A. (1991): Granite-related mineralization of the Dryden Area, Superior Province of Northwestern Ontario; Geological Association of Canada, Mineralogical Association of Canada, Society of Economic Geologists, Joint Annual Meeting, Toronto 1991, Field trip B7; Guidebook.

Cahen L., Delhal J., Deutsch S., Groegler S., Pasteels P. (1970a): The age of the Roan Antelope and Mufulira granites (Copperbelt of Zambia). Ann. Mus. roy. Afr. Centr., 8°, Sci. géol. 65, 15–42.

Cahen L., Delhal J., Ledent, D. (1970b): On the age and petrogenesis of the microcline-bearing pegmatite veins at Roan Antelope and Musoshi (Copperbelt of Zambia and S-E. Katanga). Ann. Mus. roy. Afr. Centr., 8°, Sci. géol. 65, 43–68.

Cahen L., Snelling N. J. (1966): The geochronology of Equatorial Africa. North-Holland Publ. Co., Amsterdam.

Calligaro T., Dran J. C., Poirot J. P., Querré G., Salomon J., Zwaan J. C. (2000): PIXE/PIGE characterisation of emeralds using an external micro-beam. Nuclear Instruments and Methods in Physics Research B 161–163, 769–774.

Campbell I. C. C. (1973): Emeralds reputed to be of Zambian origin. J. Gemmology 13, 169–179.

Černý P. (1991): Rare element granitic pegmatites. Part 1. Anatomy and internal evolution of pegmatite deposits. Geosci. Can. 18, 49–67.

Černý P. (2002): Mineralogy of beryllium in granitic pegmatites. In: Grew E. S.: Beryllium, mineralogy, petrology and geochemistry. Rev. Mineral. Geochem. 50, 405–444.

Cox K. G., Bell J. D., Pankhurst R. J. (1979): The interpretation of igneous rocks. George Allen & Unwin, London.

Daly M. C., Unrug R. (1983): The Muva Supergroup in Zambia – a craton to mobile belt sedimentary sequences. Transactions Geol. Soc. South Africa 85, 155–165.

Dereppe J. M., Moreaux C., Chauvaux B., Schwarz D. (2000): Classification of emeralds by artificial neural networks. J. Gemmology 27, 93–105.

Diamond L. W. (1992): Stability of CO_2 clathrate hydrate + CO_2 liquid + CO_2 vapour + aqueous KCl-NaCl solutions: Experimental determination and application to salinity estimates of fluid inclusions. Geochim. Cosmochim. Acta 56, 273–280.

Fersmann A. E. (1929): Geochemische Migration der Elemente: Abh. Prakt. Geologie Bergwirtschaftlehre 18, 1, 74–116.

Gordienko V. V., Syritso L. F., Krivovichev V. G. (1975): New type of rare-metal metasomatites after mafic rocks and trends of distribution of Cs, Li and Rb in them. Dokl. Akad. Nauk SSSR, Geochemistry 224, 1, 198–200 (in Russian).

Grauch R. I. (1989): Rare-earth elements in metamorphic rocks. In: Lipin B. R., McKay G. A. (eds) Geochemistry and mineralogy of the rare earth elements. Rev. Min. 21, 147–167.

Graziani G., Guebelin E., Lucchesi S. (1983): The genesis of an emerald from the Kitwe District, Zambia. Neues Jb. Miner., Monat. 1983, 175–186.

Graziani G., Gübelin E., Lucchesi S. (1984): Report on the investigation of an emerald from the Kitwe District, Zambia. The Australian Gemmologist 15, 7, 227–234.

Grundmann G., Morteani G. (1982): Die Geologie des Smaragdvorkommens im Habachtal (Land Salzburg, Österreich). Archiv. Lagerstättenforsch. Geol. Bundensanst. Wien 2, 71–107.

Grundmann G., Morteani G. (1987): Multistage emerald formation in regional metamorphism: Case studies from Gravelotte, South Africa and Habachtal, Austria [abs.]: Terra Cognita 7, 292.

Grundmann G., Morteani G. (1989): Emerald mineralization during regional metamorphism: Habachtal (Austria) and Leysdorp (Transvaal South Africa) deposits. Econ. Geol. 84, 1835–1849.

Gübelin E., Koivula, J. I. (1986): Photoatlas of Inclusions in Gemstones. ABC Edition, Zürich.

Hänni H. (1982): A contribution to the separability of natural and synthetic emeralds. J. Gemmology 18, 138–144.

Herron M. M. (1988): Geochemical classification of terrigenous sands and shales from core or log data. J. Sediment. Petrol. 58, 820–829.

Hickman A. C. J. (1972): The Miku emerald deposit. Geol. Surv. Zambia, Economic Rep. 27.

Hickman A. C. J. (1973): The geology of the Luanshya area. Rep. Geol. Surv. Zambia 46.

Holland T. J. B. and Blundy J. D. (1994): Non-ideal interactions in calcic amphiboles and their bearing on amphibole-plagioclase thermometry. Contrib. Mineral. Petrol. 116, 433–447.

Irvine T. N., Barragar W. R. A. (1971): A guide to the chemical classification of the common volcanic rocks. Canad. J. Earth Sci. 8, 523–548.

Koivula J. I. (1982): Tourmaline as an inclusion in Zambian emeralds. Gems & Gemology 18, 225–227.

Koivula J. I. (1984): Mineral Inclusions in Zambian Emeralds. The Australian Gemmologist 15, 7, 235–239.

Krivovichev V. G. (1988): Mineral parageneses and analysis of mineral equilibria in rare alkali-metal metasomatic rocks of pegmatite fields. International Geology Review 30, 71–82.

Lams B. M., Dilles J. H., Snee L. W. (1996): Emerald mineralization and metasomatism of amphibolite, Khaltaro granitic pegmatite-hydrothermal vein system, Haramosh Mountains, Northern Pakistan. Can. Mineral. 34, 1253–1286.

Leake B. E., Woolley A. R., Arps C. E. S., Birch W. D., Gilbert M. C., Grice J. D., Hawthorne F. C., Kato A., Kisch H. J., Krivovichev V. G., Linthout K., Laird J., Mandarino J., Maresch W. V., Nickel E. H., Rock N. M. S., Schumacher J. C., Smith D. C., Stephenson N. C. N., Ungaretti L., Whittaker E. J. W., Youzhi G. (1997): Nomenclature of amphiboles: Report of the Subcommittee on Amphiboles of the International Mineralogical Association Commission on New Minerals and Mineral Names. Mineral. Mag. 61, 295–321.

Le Bas M. J. (2000): IUGS reclassification of the high-Mg and picritic volcanic rocks. J. Petrol. 41, 1467–1470.

Lombe D. K. (1999–2000): Geophysical reports on different plots in the Kafubu area. Unpublished reports, Geological Survey Department, Mining Records, Lusaka.

London D. (1986): Magmatic-hydrothermal transition in the Tanco rare-element pegmatite: Evidence from fluid inclusions and phase-equilibrium experiments. Am. Mineral. 71, 376–396.

Milisenda C. C., Malango V., Taupitz K. C. (1999): Edelsteine aus Sambia – Teil 1: Smaragd. Zeitschr. Deutsch. Gemmolog. Gesellsch. 48, 9–28.

Möller P. (1998): Rare earth elements and yttrium fractionation caused by fluid migration. In: Novák M., Rosenbaum J. (eds) Challenges to chemical geology. Refereed Papers from MAEGS-10. Czech Geological Survey. Prague, 9–32.

Moroz I., Panczer G., Roth M. (1998): Laser-induced luminiscence of emeralds from different sources. J. Gemmology 26, 316–320.

Moroz I. I., Eliezri I. Z. (1999): Mineral inclusions in emeralds from different sources. J. Gemmology 26, 6, 357–363.

Morteani G., Grundmann G. (1977): The emerald porphyroblasts in the penninic rocks of the central Tauern Window. Neues Jb. Mineral., Mitt. 11, 509–516.

Nwe Y. Y., Grundmann G. (1990): Evolution of metamorphic fluids in shear zones: The record from the emeralds of Habachtal, Tauern Window, Austria. Lithos 25, 281–304.

Plimer I. R. (1986): Tourmalinites from the Golden Dyke Dome, Northern Australia. Miner. Deposita 21, 263–270.

Rieder M., Cavazzini G., D'Yakonov Y. S., Frank-Kamenetskii V. A., Gottardi G., Guggenheim S., Koval P. V., Muller G., Neiva A. M. R., Radoslovich E. W., Robert J. L., Sassi F. P., Takeda H., Weiss Z., Wones D. R., Wones D. R. (1998): Nomenclature of the micas. Clay. Clay Miner. 46, 586–595.

Roedder E. (1984): Fluid inclusions. Reviews in Mineralogy, Vol. 12, Mineralogical Society of America, 646 pp.

Schmetzer K., Bank H. (1981): An unusual pleochroism in Zambian emeralds. J. Gemmology 17, 443–445.

Schmetzer K., Berdesinski W., Bank H. (1974): Über die Mineralart Beryll, ihre Farben und Absorptionsspektren. Zeitschr. Deutsch. Gemmolog. Gesellsch. 23, 1, 5–39.

Schwarz D., Henn U. (1992): Emeralds from Madagascar. J. Gemmology 23, 140–149.

Seifert A. V., Vrána S., Žáček V., eds (2002): Lithological, geochemical and petrological research of beryl mineralization in the Kafubu Area, Zambia. Report, Record Office, File Report no. 2/2002. Prague.

Selway J. B., Černý P., Hawthorne F. C., Novák M. (2000): The Tanco pegmatite at Bernic lake, Manitoba. XIV. Internal tourmaline. Can. Mineral. 38, 877–891.

Sinkankas J. (1981): Emerald and other beryls. Chilton Book Co., Pennsylvania.

Slack J. F., Herriman N., Barnes R. G., Plimer I. R. (1984): Stratiform tourmalinites in metamorphic terranes and their geologic significance. Geology 12, 713–716.

Sliwa A. S., Nguluwe C. A. (1984): Geological setting of Zambian emerald deposits. Precambrian Res. 25, 213–228.

Sterner S. M., Hall D. L., Bodnar R. (1988): Synthetic fluid inclusions V.: Solubility relations in the system NaCl-KCl-H_2O under vapour-saturated conditions. Geochim. Cosmochim. Acta 52, 989–1005.

Tembo F., Kambani S., Katongo C., Simasiku S. (2000): Draft report on the geological and structural control of emerald mineralisation in the Ndola Rural Area, Zambia. Report, University of Zambia, School of Mines. Lusaka.

Thiery R., Van den Kerkhof A. M., Dubessy J. (1994): vX properties of CH_4-CO_2 and CO_2-N_2 fluid Inclusions: modeling for $T < 31$ °C and $P < 400$ bars. Eur. J. Mineral. 6, 753–771.

Veksler I. V., Thomas R., Schmidt C. (2002): Experimental evidence of three coexisting immiscible fluids in synthetic granitic pegmatite. Am. Mineral. 87, 775–779.

Whitworth M. P. (1992): Petrogenetic implications of garnets associated with lithium pegmatites from SE Ireland. Mineral. Mag. 56, 75–83.

Wilson M. (1989): Igneous petrogenesis. Harper Collins Academic, London.

Wood D. L., Nassau K. (1968): The characterization of beryl and emerald by visible and infrared absorption spectroscopy. Am. Mineral. 53, 777–799.

Zhang Y. G., Frantz J. D. (1987): Determination of the homogenization temperatures and densities of supercritical fluids in the system NaCl-KCl-$CaCl_2$-H_2O using synthetic fluid inclusions. Chem. Geol. 64, 335–350.

Zwaan J. C., Touret, J. L. R. (2000): Emeralds in Greenstone belts: the case of Sandawana, Zimbabwe. Münchner Geol. Hefte, A28, 245–258.